

HYDROXYPROPYL- β -CYCLODEXTRIN MODIFIED NICKEL FERRITE NANOCOMPOSITES FOR REMOVAL OF PHARMACEUTICAL POLLUTANTS

Thesis

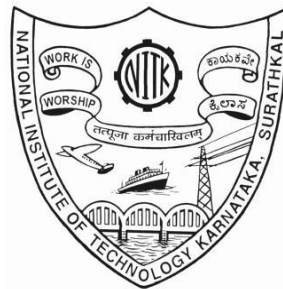
Submitted in fulfillment of the requirements for the degree of

DOCTOR OF PHILOSOPHY

By

Smitha C K

(Reg No: 155143CH15F10)



**DEPARTMENT OF CHEMICAL ENGINEERING
NATIONAL INSTITUTE OF TECHNOLOGY KARNATAKA,
SURATHKAL, MANGALORE - 575 025
OCTOBER, 2022**

DECLARATION

I hereby *declare* that the Research Thesis entitled “**Hydroxypropyl- β -Cyclodextrin Modified Nickel Ferrite Nanocomposites for Removal of Pharmaceutical Pollutants**” which is being submitted to the **National Institute of Technology Karnataka, Surathkal** in partial fulfillment of the requirements for the award of the Degree of **Doctor of Philosophy** in Chemical Engineering is a *bonafide report of the research work carried out by me*. The material contained in this Research Synopsis has not been submitted to any University or Institution for the award of any degree.



Smitha C K

Reg. No. 155143CH15F10


Department of Chemical Engineering

Place: NITK, Surathkal

Date:03-10-2022

CERTIFICATE

This is to *certify* that the Research Thesis entitled “**Hydroxypropyl- β -Cyclodextrin Modified Nickel Ferrite Nanocomposites for the Removal of Pharmaceutical Pollutants**” submitted by **Smitha C K (Register Number: 155143CH15F10)** as the record of the research work carried out by her, *is accepted as the Research Synopsis submission* in partial fulfilment of the requirements for the award of degree of **Doctor of Philosophy**.



Research Guide

Dr. Raj Mohan B

Professor

Department of Chemical Engineering

NITK, Surathkal



Chairman-DRPC

Dr. P.E. Jagadeesh Babu

Associate Professor

Department of Chemical Engineering

NITK, Surathkal

Head of the Department

विभागाध्यक्ष

Department of Chemical Engineering

रासायनिक अभियांत्रिकी विभाग

National Institute of Technology Karnataka - Surathkal

राष्ट्रीय प्रौद्योगिकी संस्थान कर्नाटक, सुरात्कल

PO Srinivasnagar, Mangalore - 575025 Karnataka

पी.ओ. श्रीनिवासनगर, मंगलौर - ५७५०२५, कर्नाटक

ACKNOWLEDGEMENTS

I would like to thank God, the Almighty for showering his blessings throughout my research work to complete my research successfully. Being part of the prestigious institution like NITK has been an honour, and my dream of achieving a PhD here has me beaming with pride and joy.

My research supervisor has been the most important person throughout my research career in NITK. It is a genuine pleasure to express my deep sense of gratitude to mentor and guide, Dr Raj Mohan B, Professor, Department of Chemical Engineering. His dedication and keen interest in research, above all his overwhelming attitude of helping his students had been solely and mainly responsible for completing my research work. His meticulous scrutiny, scholarly advice and scientific approach has propelled me to accomplish my task to a great extent.

I would like to thank my Research Progress Assessment Committee (RPAC) members Dr. Uday Bhat, Professor, Metallurgy Department, Dr. Hariprasad Dasari, Associate Professor, Chemical Department for their insightful and valuable suggestions that has helped in the progress of my work.

I express my sincere gratitude to the Head of the Department of Chemical Engineering Dr. P.E. JagadeeshBabu and former Head of the Department Dr. Prasanna B.D and Dr. Harimahalingam. I also express my whole hearted gratitude towards Prof Karnam Umamaheshwara Rao, Director of NITK for research aid throughout this research career in NITK.

I am also grateful of Dr Hari Prasad for the TGA facility, IIT Bombay for TEM facility, Manipal Institute of pharmacy for zeta potential analysis, Mangalore University for FESEM and EDS analysis and STIC Cochin for XRD analysis.

I am deeply thankful to the non-teaching staff Mrs Shashikala, Mr Sadashiva, Mrs Thrithila Shetty, Mrs Bhavyashree, Ms Vijetha Kotian, Mrs Sandhya, Mr Harish, Mr Suresh, Mr Ramesh and all other non-teaching staff for all the help they have rendered.

I also indebted to my dearest friends Dr. Rashmi B S, Dr. Smruthi Prabhu, Ms Deekshitha Kulal for helping me in every possible way. I am also thankful to my colleagues Ms. Thivani Senathiraja, Mr. Sai Abhishek Lolla and Ms Yushmitha Sahay for their hard work, dedication and enthusiasm. I also thank Mrs Vrushali Kadam, Ms Deepti, Mrs Indumathi,

Dr. Anjana Anantharaman, Dr. Pragadeesh of Chemical Engineering Department for their help at the time of need.

I dedicate all my achievements to my mother Mrs. Shakunthala K, my first guru who always believed in me and supported me. My father Mr. Chandrashekar K who always motivated me to aim higher; My brother Mr. Sharath C.K who always has supported me in my career and in my hardships. Finally, my husband Mr. Rithesh Pilar for patiently waiting throughout my PhD research till its completion. Finally, I thank the Lord Ganesha and Hanuman for giving me the strength to overcome the hurdles.

SMITHA C K

ABSTRACT

The growth of the pharmaceutical companies has been a boon to the mankind in myriad ways. However, the consequences due to the excess usage of these pharmaceutical compounds in our day-to-day life have resulted in irreplaceable damage to the ecosystem. Researchers have used nanocomposite-based systems for the removal of a wide range of pharmaceutical pollutants from the aqueous systems. Among them the magnetic based silica system has gained momentum due to its ease of synthesis and wide applicability. Nickel ferrite-based silica nanocomposites attached to cysteine and nickel ferrite-based silica nanocomposites attached to aminosilanes were both optimised for their size and morphology. Cysteine coated and amine coated nanocomposites revealed a particle size of 130-150 nm and 50- 100 nm. The physiochemical properties of the nanocomposites were evaluated using different characterization techniques such as TEM, FESEM, XRD, FTIR and TGA. The adsorption studies were performed on both the nanocomposites which revealed a higher adsorption potential of 97.01%, 94.12% and 70.13% for IBF, ACE and STR respectively for aminosilane coated nanocomposite. The nanocomposites revealed a good removal efficiency of ~90% up to 4 cycles with reduction in removal efficiency during the 5th cycle. Hence, aminosilane coated nanocomposites were further grafted with hydroxypropyl- β -cyclodextrin to determine the removal efficiency post grafting. The hydroxypropyl- β -cyclodextrin grafted nanocomposites (14 mg /L) revealed a very good removal efficiency of 98.01 %, 98.89 %, 98.3 % for IBF, ACE and STR respectively. The nanocomposites also showed good reusability of ~92% for up to 5 cycles thus exhibiting higher pollutant removal in comparison to aminosilane coated nickel ferrite-based silica nanocomposites. The adsorption kinetics for the adsorption seemed to follow pseudo second order reaction kinetics. Also, the Langmuir model of adsorption seemed to fit well with the experimental data confirmation monolayer adsorption process.

Keywords: *Adsorption, Nanocomposites, Pharmaceuticals, Reusability*

TABLE OF CONTENTS

CHAPTER 1 INTRODUCTION

1.2 Scope of the present work & objectives	9
1.2.1 Research gaps.....	9
1.2.2 Aim	9
1.2.3 Objectives	10
1.3 Organization of thesis	10

CHAPTER 2 LITERATURE REVIEW..... 12

2.1 Pharmaceutical pollution	12
2.2 Ferrite nanoparticles and their applications	13
2.3 Prominence of nickel ferrite nanoparticles	14
2.4 Synthesis of nickel ferrite nanoparticles	15
2.5 Magnetic silica composites	31
2.6 Cyclodextrins	35

CHAPTER 3 MATERIALS AND METHODS..... 42

3.1 Materials	42
3.2 Sample Characterization	42
3.3 Methodology	43
3.3.1 Synthesis of Nickel Ferrite nanoparticles	43
3.3.2 Preparation of GPTS coated nickel ferrite nanoparticles.....	44
3.3.3 Grafting of L-cysteine onto NFO@ SiO ₂ @GPTS nanoparticle	44
3.3.4 Synthesis of APTS coated NiFe ₂ O ₄ composites	45
3.3.5 Ninhydrin Test	46
3.3.6 Grafting of 2-hydroxypropyl-β-cyclodextrin (HPCD) to NFO@SiO ₂ @APTS.....	47
3.4 Adsorption of Acetaminophen, Ibuprofen and Streptomycin by NFO@SiO ₂ @GPTS	47
3.4.1 Batch adsorption experiments.....	47
3.4.2 Adsorption of Acetaminophen, Ibuprofen and Streptomycin by NFO@SiO ₂ @APTS. (Batch adsorption Experiments).....	48
3.4.3 Adsorption of Acetaminophen, Ibuprofen and Streptomycin by NFO@SiO ₂ @APTS@HPCD. (Batch adsorption Experiments)	48

3.4.4 Adsorption isotherm.....	48
3.4.5 Regeneration of the adsorbent NFO@SiO ₂ @GPTS.....	49
3.4.6 Regeneration of the adsorbent NFO@SiO ₂ @APTS.....	49
3.4.7 Regeneration of the adsorbent NFO@SiO ₂ @ APTS-HPCD.....	50
CHAPTER 4 RESULTS AND DISCUSSION.....	51
4.1 X-Ray Diffraction analysis	51
Subsection 4.1.1 Optimization of the size distribution of nanoparticles	51
4.2 Transmission Electron Microscopy analysis	56
4.3 Field Emission Scanning Electron Microscopy analysis	58
4.4 FTIR analysis	61
4.5 TGA analysis	65
4.6 VSM analysis	68
4.7 Dynamic light scattering	72
4.8 Ninhydrin test	72
4.9 Adsorption studies of NFO@SiO ₂ @GPTS-Cys for removal of IBF	73
4.9.1 Effect of pH on sorption capacity	73
4.9.2 Effect of Cysteine concentration on adsorption.....	74
4.9.3 Effect of nanomaterial dosage	75
4.9.4 Effect of Ibuprofen concentration.....	76
4.9.5 Adsorption isotherm.....	77
4.9.6 Adsorption kinetics	78
4.10 Reusability of the NFO@SiO ₂ @GPTS@Cys nanomaterial.....	79
4.11 Mechanism of IBF removal	79
4.12 Adsorption studies of NFO@SiO ₂ @APTS for removal of IBF, ACE and STR.....	80
4.12.1 Influence of pH on pharmaceutical uptake	80
4.12.2 Effect of nanocomposite dosage	82
4.12.3 Effect of pharmaceutical concentration	83
4.12.4 Adsorption kinetics and isotherms.....	84
4.12.5 Reusability	88
4.13. Adsorption studies of NFO@SiO ₂ @APTS-HPCD for removal of IBF, ACE and STR	89
4.13.1 Influence of pH on pharmaceutical adsorption.....	89
4.13.2 Effect of adsorbent dosage against the pharmaceutical adsorption	91

4.13.3 Effect of pharmaceutical concentration on adsorption efficiency	92
4.13.4 Adsorption kinetics and isotherms.....	93
4.13.5 Reusability	97
CHAPTER 5 CONCLUSION.....	98
5.1 Summary and significant findings	98
5.2 Future scope of work	103
REFERENCES.....	105
LIST OF PUBLICATIONS AND CONFERNCES	129
BIODATA.....	130

LIST OF FIGURES

Figure No.	TITLE	Page no.
1	Schematic representation of the experimental set up of the co-precipitation method	43
1.1	Schematic representation of L-cysteine onto NFO@SiO ₂ @GPTS nanoparticles	45
1.2	Schematic representation of the synthesis of NFO@SiO ₂ @APTS	46
4.1	XRD graphs of nickel ferrite nanoparticles for different ratios (1:1, 1:2, 1:2.5)	53
4.2	XRD patterns of NFO@SiO ₂ @GPTS-Cys nanocomposite	54
4.3	XRD patterns of NFO@SiO ₂ @APTS nanocomposite	55
4.4	XRD patterns of NFO@SiO ₂ @APTS-HPCD nanocomposite	56
4.5	a) TEM image of nickel ferrite nanoparticles at 20 nm scale (8 -16 nm); b) SAED pattern of nickel ferrite nanoparticles; c) lattice fringes of nickel ferrite nanoparticles at 2 nm scale.	57
4.6	TEM- HRTEM images of NiFe ₂ O ₄ nanoparticles (a) 100 nm scale (b) 2 nm scale (c) Corresponding SAED pattern and (d) NiFe ₂ O ₄ @SiO ₂ @GPTS@Cys nanomaterial at 20 nm scale	58
4.7	FESEM analysis performed at 40kX magnification at 1 μm scale of different APTS coating concentrations (a) 20 μL (b)40 μL and (c)60 μL (d) EDX analysis of NFO@SiO ₂ (e)NFO@SiO ₂ @APTS (60 μL)	60
4.8	FESEM analysis performed at 30kX magnification at 1 μm scale of different concentrations of maleic anhydride (a) 1 mmol (b) 2 mmol and (c) 3 mmol (d) EDX analysis of NiFe ₂ O ₄ @SiO ₂ (e)NiFe ₂ O ₄ @SiO ₂ @APTS (60 μL)	61
4.9	FTIR spectrum of nickel ferrite nanoparticles	62
4.10	FTIR spectrum of (a)NFO@SiO ₂ @GPTS@Cys (b) NFO@SiO ₂ @GPTS (c) NFO	63
4.11	FTIR analysis of the NFO@SiO ₂ @APTS nanocomposite	64

4.12	FTIR analysis of the NFO@SiO ₂ @APTS-HPCD nanocomposite	65
4.13	Thermogravimetric analysis curve of nickel ferrite nanoparticles	66
4.14	TGA analysis of NiFe ₂ O ₄ @SiO ₂ @GPTS-Cys from 40 °C to 860 °C.	67
4.15	TGA analysis of the composite from 40 °C to 860 °C of the APTS coated NFO@SiO ₂ nanocomposite.	67
4.16	TGA analysis of the composite from 40 °C to 860 °C of the HPCD coated NiFe ₂ O ₄ @SiO ₂ @APTS nanocomposite	69
4.17	Hysteresis loop of the as-prepared nickel ferrite nanoparticles	70
4.18	VSM analysis of NFO@SiO ₂ @GPTS and of NFO@SiO ₂ @GPTS@Cys	70
4.19	VSM magnetisation curve of NFO nanoparticles and NFO@SiO ₂ @APTS composite.	71
4.20	VSM magnetisation curve of NFO@SiO ₂ @APTS-HPCD nanocomposite.	71
4.21	(a) Zeta potential of NFO@SiO ₂ @GPTS@Cys at pH 6.0 and (b) average particle size	72
4.22	a) Absorbance peak observed at 570 nm (b) Ninhydrin colorimetric assay conformation	73
4.23	Effect of pH on the initial concentration of ibuprofen (50 mg L ⁻¹) and dosage 10 mg of the catalyst loading	74
4.24	Effect of Cysteine concentration (3,5,7 and 9 mmol) on the initial concentration of ibuprofen (50mg L ⁻¹) and dosage 10 mg of the catalyst loading	75
4.25	Effect of nanomaterial dosage (10, 30, 50 mg) for an initial concentration of 50 mgL ⁻¹	76
4.26	Effect of IBF concentration (50-300 mg L ⁻¹) for the nanomaterial dosage of 30 mg and pH 6.0	77
4.27	(a) Langmuir adsorption model (b) Freundlich adsorption model for IBF sorption onto NFO@SiO ₂ @GPTS@Cys	78
4.28	Pseudo-Second order kinetics (a) maximum adsorption capacity (b) of IBF sorption onto NFO@SiO ₂ @GPTS@Cys	78

4.29	Reusability of the NFO@SiO ₂ @GPTS@Cys nanomaterial for 3 cycles at pH 6.0; nanomaterial dosage 30 mg; time 30 min	79
4.30	Plausible mechanism for the removal of IBF	80
4.31	Effect of pH on the adsorptive removal of (a) Ibuprofen, (b) acetaminophen (c) streptomycin	82
4.32	Effect of nanocomposite dosage on the adsorption of (a) IBF, (b) ACE, and (c) STR	83
4.33	Effect of pharmaceutical concentration (12 mg L ⁻¹) on the nanocomposite (a) IBF, (b) ACE, and (c) STR	84
4.34	Pseudo second order kinetics of the experimental data for a) IBF b) ACE and c) STR	85
4.35	Langmuir adsorption isotherm of the experimental data for a) IBF b) ACE and (c) STR and (d) maximum adsorption capacity.	86
4.36	Freundlich adsorption isotherm of the experimental data for a) IBF b) ACE and c) STR	87
4.37	Schematic representation of the adsorption mechanism of NFO@SiO ₂ @APTS nanocomposite to (a) IBF, (b) ACE, and (c) STR	88
4.38	Regeneration capacity up to four cycles	89
4.39	Effect of pH on the adsorptive removal of (a) Ibuprofen (pH 5.0), (b) acetaminophen (pH 7.0) (c) streptomycin (pH 7.0)	91
4.40	Effect of nanocomposite dosage on the adsorption of (a) IBF, (b) ACE, and (c) STR	92
4.41	Effect of pharmaceutical concentration (10 mg L ⁻¹) on the nanocomposite (a)IBF, (b) ACE, and (c) STR	93
4.42	Pseudo second order kinetics of the experimental data for a) IBF b) ACE and c) STR	99
4.43	Langmuir adsorption isotherm of the experimental data for a) IBF b) ACE and c) STR and (d) maximum adsorption capacity	95
4.44	Freundlich adsorption isotherm of the experimental data for a) IBF b) ACE and c) STR	96

4.45	Schematic representation of the adsorption mechanism of NFO@SiO ₂ @APTS nanocomposite to (a) IBF, (b) ACE, and (c) STR	97
4.46	Regeneration capacity up to four cycles.	98

LIST OF TABLES

Table No.	TITLE	Page no.
1	Structure of pharmaceuticals of interest in this work	18
2	Overview of different synthesis methods of nickel ferrite nanoparticles	17
3	Synthesis of Nickel ferrite nanoparticles using co-precipitation method	28
4	Overview of silica modified magnetic composites used for various applications	33
5	Overview of cyclodextrin modified nanocomposites used for various applications	37
6	Optimization of nickel ferrite nanoparticle synthesis	44
7	Optimization of synthesis of NFO@SiO ₂ @APTS	46
8	The lattice constants and crystallite size of varied ratios of surfactant concentrations.	52
9	Adsorption kinetics and adsorption isotherm parameters	83
10	Adsorption kinetics and adsorption isotherm parameters	87
11	Adsorption kinetics and adsorption isotherm parameters	97

LIST OF ABBREVIATIONS

Abbreviations	Full form
EDS	Energy Dispersive Spectroscopy
DLS	Dynamic Light Scattering
FTIR	Fourier Transform Infrared Spectroscopy
FESEM	Field Emission Scanning Electron Microscopy
TEM	Transmission Electron Microscopy
TGA	Thermo Gravimetric Analysis
VSM	Vibrating Sample Magnetometer
XRD	X-Ray Diffraction

NOMENCLATURE

Notation	Description (units)
C	Concentration of the pharmaceuticals (mg/L)
h	Hours (h)
mg L ⁻¹	Milligram per litre
q	Amount adsorbed per gram of the adsorbent
t	Time (min)
T	Temperature (°C)
V	Volume (L)
µg L ⁻¹	Microgram per Litre
ng L ⁻¹	Nanogram per Litre

CHAPTER 1

INTRODUCTION

Water, a primordial element responsible for the emanation of the universe, has been worshipped for its life healing properties. However, with time the uninhibited human interference with the ecosystem has resulted in the depreciation of the natural functioning the aquatic ecosystem worldwide. The anthropogenic activities, such as the release of effluents from industries, domestic and hospital runoffs, agriculture, and urbanization, has led to the exploitation of these natural resources. Thus, driving all the aquatic species to the brink of extinction and also causing potential health hazards on all the species in the biosphere.

The word "Emerging Pollutants" (EPs) have been in the limelight for more than a decade, and homo sapiens play an integral part in releasing these pollutants into the environment. As defined by the Environmental Protection Agency (EPA), the EPs are substances that have no regulatory standards and cause a significant impact that are lethal to the ecosystem(Deblonde et al. 2011).These EPs could be persistently present in the environment and are only recently detected, or they could be new pollutants that are formed due to the disposal of existing chemicals (Geissen et al. 2015).However, in both cases, they cause a detrimental impact on the environment. The Environmental Quality Standard (EQS) has enlisted a list of 33 priority hazardous pollutants that encompasses pesticides, biocides, endocrine disruptors and industrial chemicals, among which pharmaceutical pollutants have been gaining attention from the past few decades(Jones et al. 2015).

Pharmaceutical pollutants are also known as persistent organic pollutants (POP) that fall under this category, made the water sources vulnerable to anomalies. These EP's have been infiltrating into water cycle, through the influents and effluents of wastewater treatment plants (WWTPs) (Kolpin et al. 2002; Glassmeyer et al. 2005), surface runoffs (Benotti et al. 2009; Ferrell and Grimes, 2014) and drinking water purifying systems (Synder et al. 2007; Benotti et al. 2009). The associated lifestyle diseases like cardiovascular diseases and diabetes are due to the direct effect of urbanization, which has led to corresponding changes in the consumption of pharmaceuticals (Mohapatra et al.

2016). Thus, water streams containing a wide range of living species have begun to coexist with pollution and become part of the food-web worldwide.

Among these various pharmaceutical and personal care products (PPCP's), synthetic hormones, pesticides, beta-blockers, antimicrobials, diuretics and other transformation products persistently present in our day-to-day life (Halden 2010). Further, if PPCP's present in trace concentrations in ambient waters/ or administered when not required, they arguably pose a considerable threat to the aquatic flora and fauna and human health (Ebele et al. 2017). These compounds cause potential toxic effects on the ecosystem when present at elevated levels. Although wastewater treatment plants remove a wide range of conventional pollutants, the detection and treatment of PPCP's are limited due to various reasons. Some of the main reasons for the inability of detection and treatment are i) Failure in identifying and isolating the emerging pharmaceutical pollutants ii) Conventionally no techniques are available to precisely identify and remove from the environment. iii) Even at lower concentrations, their impact on the environment is alarming. (Kumar et al. 2005).

Wastewater treatment by conventional biological treatment were also not effective in degrading PPCPs. On the other hand, radiation technology was a promising alternative for the degradation of these PPCPs; however, it suffered significant drawbacks such as high cost and safety concerns and precautions for radioisotope usage. Even though the pollution due to pharmaceuticals have been reported decades earlier, its only in the recent years researchers have started to detect and quantify trace concentrations of pharmaceuticals using advanced technology. The characteristic features, occurrence, permissible limit and the impact on flora and fauna are briefly discussed as follows.

Non-Steroidal anti-inflammatory drugs (NSAIDs) and analgesics are the most often prescribed over the counter Drugs (OTC) (Koffeman et al. 2014). India ranks third and thirteenth globally for pharmaceutical production and consumption, respectively (Mutiyaar et al. 2018). The increased usage of bioactive compounds has elevated the concentration to a detectable range. The persistence and resistance to degradation allow infiltration of these drugs back into the drinking waters due to their high mobility in the aquatic environment (Behera et al. 2012). Ibuprofen (IBF) is the first member of the propionic acid derivative non-steroidal anti-inflammatory drug frequently prescribed OTC drug, which has been found persistently in the ground and surface waters (Kunkel et al. 2008). The World Health Organisation (WHO) has added IBF to the essential drugs list in 2010 due to their high

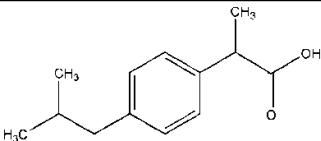
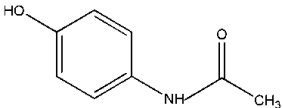
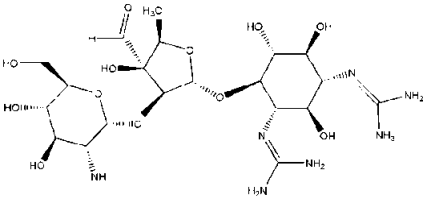
consumption rate which has in turn increased the concentration and toxicity in aqueous water systems (Chopra and Kumar 2020). For instance, the concentrations of IBF in Indian waters were found to be 200 ng L^{-1} (Shanmugam et al. 2014). In the city of Barcelona, the presence of NSAIDs was found upto $1 \text{ } \mu\text{g L}^{-1}$ in which the main contributor was the analgesic ibuprofen with 988 ng L^{-1} (López-Serna et al. 2013). Further, (Subedi et al. 2015) reported $2.32 \text{ } \mu\text{g L}^{-1}$ of Ibuprofen along with other bioactive compounds in Coum River that flows through Chennai. As a result of this persistent presence in water, the significant increase in the concentration of $\geq 1 \text{ } \mu\text{g L}^{-1}$ can cause perturbation in the reproductive system of the fish as reported by (Ji et al. 2013). IBF was also observed to cause endocrine disruption in *Mytilus galloprovincialis* at a concentration of 250 ng L^{-1} followed by other complications such as antioxidative stress, increased activity of catalase, superoxidase dismutase within 7 days of exposure (Gonzalez-Rey and Bebianno 2012)

Paracetamol or acetaminophen (ACE) is another most commonly consumed drug worldwide used to relieve pain (Allegaert et al. 2019). It is also used during pregnancy as it does not show any significant side effects. The regular oral dose for adults is 500 -1000 mg; however, the permissible limit for daily dose is 4000 mg (Rannug et al. 1995). It has been classified as "harmful to the aquatic organisms" based on the EC_{50} values (Žur et al. 2018). The direct disposal of these compounds from households and effluent discharge from municipal/ industrial wastewater treatment plants has resulted in alleviated concentrations of pharmaceuticals in surface water systems (Cooper et al. 2008; Nikolaou et al. 2007). The presence of acetaminophen in elevated levels is also observed in the soil and groundwaters due to the excessive usage of the drug for controlling tree snakes (Andreozzi et al. 2003). This persistent presence of ACE in the aqueous systems has been known to cause hepatotoxicity and nephrotoxicity in aquatic animals. In plants, the chronic exposure of ACE has resulted in growth inhibition and inhibition of antioxidant, which has affected metabolic activities (Daniel et al. 2019; Khan et al. 2018). ACE has been known to inhibit cyclooxygenase (COX) activity. When organisms like Zebrafish were exposed to these COX inhibitors, it caused detrimental effects on the growth of the organism and increased the mortality rate at $10\text{-}100 \text{ } \mu\text{g L}^{-1}$ (David and Pancharatna 2009). They are highly mobile and accumulate in the aquatic environment from ng to $\mu\text{g /L}$ in surface waters of India (Chinnaiyan et al. 2018) (de Oliveira et al. 2017). Hence the removal of ACE from the aqueous systems is mandatory.

The antibiotic consumption in India has increased from 3.2 to 6.5 billion tonnes from 2000 to 2015 (Klein et al. 2018). Streptomycin is an aminoglycosidic antibiotic containing amino sugar, guanidino-substituted cyclohexane with three hydroxyl functional groups linked by glycosidic bonds (Qian et al. 2012). It is used to treat gram-positive, gram-negative bacteria and also used as a second-line therapeutic for humans (Jadhav et al. 2013; Liu et al. 2011). The ubiquitous natures of antibiotics (streptomycin and erythromycin) pose detrimental effects on the growth of individual species. At deficient levels of antibiotics, they lead to physical and behavioural changes in micro invertebrates like *Daphnia Magna* and dysbiosis in Zebrafish embryos (Flaherty and Dodson 2005; Pindling et al. 2018).

Further, streptomycin is one of the six pharmaceutical compounds classified as "Highly toxic" for aquatic organisms (Petrie et al. 2015). The rise of these antibiotics' concentrations in our water sources has led to a upheave of antibiotic-resistant bacteria, which could further make the species susceptible to rare diseases (Kraemer et al. 2019). Thus, the removal of these persistent compounds from marine habitat is the need of the hour. Researchers have delved into this aspect from the past decade and are trying to address this grave challenge using various nanomaterials. The following table shows the structure and properties of the pharmaceuticals of interest in Table 1.

Table 1: Structure of pharmaceuticals of interest in this work.

Name	Molecular formula	Structure	Molecular weight (g mol ⁻¹)
Ibuprofen	C ₁₃ H ₁₈ O ₂		206
Paracetamol	C ₈ H ₉ NO ₂		151
Streptomycin	C ₂₁ H ₃₉ N ₇ O ₁₂		581

Researchers worldwide are trying to explore simple and effective techniques to curb the elevated levels of pharmaceutical compounds. Many technologies have been developed for water remediation, such as coagulation (Norte et al. 2018), precipitation (Sun et al. 2017), degradation (Kumar et al. 2018), so on so forth. (Kruglova et al. 2016) used a large laboratory-scale wastewater treatment plant for the removal of four emerging micropollutants ibuprofen (IBF), diclofenac, estrone and 17α -ethinylestradiol. They observed that the membrane bioreactor exhibited higher removal potential than the conventional activated sludge sequential reactor. The degradation of pharmaceutical compounds using nanoparticles, for instance, IBF degradation, produced intermediates, and these intermediates were also present in the wastewater plant effluents (Ferrando-Climent et al. 2012). Hence, removal of these pollutants by adsorption has been adopted as the surface functional groups can be tuned to access a wide variety of pollutants and application for large scale treatment process.

In recent days, adsorption through nanoparticles/nanocomposites with stronger adsorption capacities, higher kinetics and cost-effectiveness have been explored. Modifying the surface functional groups of these nanoparticles with silica, silane, chitosan, and lignocellulosic fibres (Huang et al. 2017; Zhou et al. 2016a) can be used to remove the targeted organic pollutants and pharmaceutical compounds. From ancient times silica-based materials have played a vital role in pottery, ceramics, and advanced technologies in the recent times such as fibre optic technology, superhydrophobic surfaces (Wu et al. 2012; Tian and Guo 2017; Yu et al. 2019). The intriguing properties of nanoscale materials have revolutionized modern technological industries. The organic compounds have endowed the polymer nanocomposites with augmented properties alongside the metal oxide/ metal nanoparticles. The application of functionalized silica-coated nanoparticles has currently gained eminence due to reactive surface groups (silanol or Si-OH). Thus, increasing the versatility of the nanocomposites. Also, considerable efforts towards the synthesis of tailored morphologies in recent years. For instance, cholesterol oxidase, when bound to magnetic silica composites, retained 50% of its activity compared to its free form (Šulek et al. 2010a). Currently, silica composites significantly contribute to environmental applications and remediation of contaminated water sources (Maiti et al. 2019). Thus, materials with higher stability will pave the way for an efficient remediation process.

Organosilanes are also known as monomeric forms of silicon chemicals often used as coupling agents and adhesion promoters (Pape 2011). The unique nature of silane

chemistry of both inorganic and organic reactivity in one molecular structure provides a hydrophobic nature to the nanoparticles, improves the stability and prevents agglomeration (Dey 2012). Among the common silanes used so far, such as aminopropyltriethoxysilane (APTS), mercaptopropyltrimethoxysilane (MPTS) (Villa et al. 2016); aminopropyltriethoxysilane has shown its potential with its highly reactive amine group and its multifunctional nature (Smith and Chen 2008). Aminopropyltriethoxysilane (APTS) or aminopropyltrimethoxysilane (APTMS) has found its utility in the production of functionalized thin films of silica coatings on nanoparticles for various applications (He et al. 2004). APTS has also been frequently used to produce the aminosilane ($\text{SiO}_2\text{-NH}_2$) coating to enhance protein and cell adhesion, rabbit mesenchymal stem cell (MSC) labelling (Sapsford and Ligler 2004; Zhang et al. 2010). Recently these aminosilane coated nanocomposites for the removal of dyes (Gemeay et al. 2020), cyanate (Ranjan et al. 2017), heavy metals and bacterial treatment (Sahoo et al. 2020), and so on. Aminosilane coated nanocomposites have been proven to be a potential candidate for targeted drug delivery so far (Dhavale et al. 2018a). However, very few reports have been found on removing pharmaceutical pollutants using aminosilane coated magnetic nanocomposites. Further, magnetic nanoparticles coated with organo-silanes have been gaining attention to their ease of functionalization and ability to form complexes with various functional groups (Cui et al. 2010; Mohammad-Beigi et al. 2011).

Cyclodextrins are macrocyclic oligosaccharides composed of 6 to 8 glucopyranose monomers connected by 1-4-glucosidic linkages. It was first discovered by Villers in 1881 and identified by Schardinger in 1903 (Zhou and Ritter 2010). Cyclodextrin composites have benchmarked activated carbon, which was once the most opted material for water remediation. In a similar work by Ling et al. (2017) where they investigated the removal capacity of porous cyclodextrin polymers and coconut shell activated carbon. They inferred that the uptake efficiency of the cyclodextrin polymer is more selective uptake and not affected by natural organic matter. Cyclodextrins (CDs) are oligosaccharides that are naturally occurring comprising of six, seven, or eight glucose subunits and are linked by α -(1, 4) glycosidic bonds. These cyclodextrins have a torus shaped structure and are classified as α -, β -, and γ -CD, respectively. The semi polar nature of the cyclodextrin cavity gives it a higher energy in comparison to the walls of the cyclodextrin cage, hence it gets filled with water molecules when placed in an aqueous system. It has been suggested that a large contribution to the complexation of guest species in solution results in the expulsion of

these high-energy water molecules from the cavity as part of an overall hydrophobic effect (Crini 2003). During the inclusion complex formation, no covalent bonds are broken. The main driving force of complex formation is the release of enthalpy-rich water molecules from the cavity. Water molecules are displaced by more hydrophobic guest molecules present in the solution to attain an apolar–apolar association and decrease of cyclodextrin ring strain resulting in a more stable lower energy state (Schneiderman and Stalcup 2000).

Attention has recently been focused on cyclodextrin based polymeric materials in a wide variety of applications due to their unique sorption properties (Alsbaiee et al. 2015). The hydrophobic nature of the cyclodextrins enables it to form complexes with a wide range of apolar organic molecules. Recently, a number of insoluble cyclodextrin polymer or co-polymers have been widely used for various application such as contaminants removal from wastewater, protein refolding, drug delivery etc. (Badruddoza et al. 2010; Freitas et al. 2012). β -Cyclodextrins as adsorbents has been gaining momentum due to its low toxicity and ability to form complexes through intermolecular hydrogen bonds (del Valle 2004). The naturally occurring cyclodextrins suffers from certain drawbacks, on the other hand the cyclodextrin derivatives have proven to be advantageous (Liu et al. 2020). However, these cyclodextrins alone when used as adsorbents can be separated only by high-speed centrifugation, thus limiting its usage in practical applications. The usage of magnetic nanoparticles prevails over this limitation by providing a promising alternative method to separate powder adsorbents from the solution effectively (Badruddoza et al. 2011).

Functionalized magnetic nanocomposites have been successful in the adsorption of a wide range of pollutants such as, heavy metals, dyes (Mehmood et al. 2021). The surface of the magnetic nanoparticles can be tuned by polymers (Santos et al. 2021) , organic and inorganic molecules/compounds (Srinivasan and Huang 2008). As mentioned earlier coating SiO₂ onto the magnetic nanoparticles enables the fabrication of multifunctional nanoparticles (Ge et al. 2008). The silica coated magnetic nanoparticles when grafted with cyclodextrins paved a new direction for the nanocomposites by enhancing the dispersibility, superior stability and chemical tunability (Liu et al. 2009; Jiang et al. 2018). On a similar front, Sinha and Jana, (2021) synthesized γ -cyclodextrin functionalized graphene nanocomposite which was observed to exhibit 100 % removal efficiency against microcystin-LR.

Fe₃O₄ nanoparticles functionalized β-cyclodextrin synthesized by Badruddoza et al. (2013) was able to successfully exhibit a maximum adsorption capacity of 64.50, 27.70 and 13.20 mg g⁻¹ towards Pb²⁺, Cd²⁺ and Ni²⁺ respectively. (Chen et al. 2019) developed a PEI linked β-cyclodextrin coated magnetic nano adsorbent that was able to simultaneously able to remove methyl orange and Pb (II) from wastewater up to 83.9 % and 73.4 % respectively. Kitaoka and Hayashi, (2002) synthesized epichlorohydrin cross-linked β-cyclodextrin which was able of remove 98 % of bisphenol-A from the aqueous systems. Fe₃O₄@SiO₂-PGMA-CD was successful in the removal of Cu²⁺ ions up to 79.5 % and bisphenol-A up to 41.6% as reported by (Wang et al. 2014). It was also observed that cyclodextrin grafted magnetic nanocomposites exhibited good recyclability up to five to seven cycles. For instance, the Fe₃O₄@β-CD show excellent removal efficiency of 97.3-100 % against methylene blue and the removal efficiency was maintained at 86 % even after seven cycles. Helal et al. (2018) synthesized succinyl-β-cyclodextrin coated APTES @maghemite nanoparticles, wherein the said nanoparticles exhibited a maximum adsorption capacity of 286 mg. These nanoparticles were determined to be stable up to 10 cycles with a removal efficiency of 91 %. Lately, the upsurge of pharmaceutical residues in aqueous systems has driven researchers to develop nanostructures that eliminate pharmaceutical residues. In this regard, Ghosh et al. (2013) synthesized aminated β-cyclodextrin functionalized Fe₃O₄ nanoparticles which exhibited maximum adsorption capacity of 1.304, 1.074 and 0.899 mg/g of CBZ, NAP and BPA respectively. Recently, Fenyvesi et al. (2020) were successful in achieving ~85% efficiency for 5 μg/L of Diclofenac and Ibuprofen with β-CD cross lined epichlorohydrin. Thus, in light of the excellent potential of cyclodextrin modified absorbents towards the removal a wide range of pollutants including pharmaceutical residues from wastewater.

Removal of pharmaceuticals from aqueous has been investigated using different kinds of nanomaterials. Recently, cyclodextrin coated nanocomposites have been reported to be highly effective for the removal of these pharmaceutical residues with good recoverability. Inclusion of magnetic nanoparticles to these nanocomposites has avoided the usage of centrifugation and filtration by facilitating removal by an external magnet. However, nickel ferrite based cyclodextrin nanocomposite have not been assessed yet. Thus, in light of the advantages of magnetic cyclodextrin nanocomposites as reported by the previous literatures the current work focuses on synthesizing nickel ferrite nanoparticles and further coated with silanes evaluate the adsorptive potential of coated nanoparticles

towards the target pharmaceuticals viz. ibuprofen, acetaminophen and streptomycin. Further, grafted with hydroxypropyl- β -cyclodextrin and the adsorption capacities of these against the above-mentioned target pharmaceuticals is determined.

1.2. Scope of the present work & objectives

1.2.1. Research gaps

Hydroxypropyl- β -Cyclodextrin and nickel ferrite nanoparticles, be it in their natural form or as a composite, have proved their potential in water treatment and drug delivery. HP- β -CD is the most versatile excipient in cyclic oligosaccharides, which acts as an excellent stabilizing agent by forming complexes with drugs and hormones. Recently the rise of emerging pollutants like pharmaceuticals has become a looming threat to the biosphere. Although researchers are working on providing an effective method for the removal of the same, literature has been limited to the removal of various other organic pollutants and a few papers on the removal of pharmaceuticals. In the present scenario, there is a need to develop magnetic cyclodextrin composite that has the potential to remove pharmaceutical compounds that are exceedingly posing a threat to the habitat due to frequent use. Also, the fundamental structure and properties have to be determined based on previous literature to develop this hybrid composite.

The aminosilane coated onto the nickel ferrite nanoparticles plays a crucial role in amplifying the properties of the cyclodextrin composite. Moreover, cyclodextrins coated onto other metal oxide nanoparticles or as crosslinked structures suffer the disadvantage of having to be centrifuged while repeating the adsorption cycle. Whereas, the magnetic cyclodextrins could be separated easily post adsorption and will be used effectively for multiple adsorption cycles. Hence, a simple and efficient technique for the synthesis of these composites can overcome these challenges. Thus, enhancing the properties of the resultant composites.

1.2.2. Aim

Synthesis of 2-hydroxypropyl- β -cyclodextrin modified nickel ferrite/silica nanocomposites and to investigate their properties using various characterization techniques and use them for potential applications.

1.2.3. Objectives

- II. Synthesize and characterize 3-aminopropyltrimethoxysilane (APTS) coated nanocomposites.
 - a) Study effect of concentration of APTS on morphology and properties.
 - b) Study the impact of time on the coating of APTS onto the surface of the magnetic silica composites.
 - c) To optimize parameters during the synthesis of nanocomposites, i.e., APTS loading and polymerization time.

- III. Application of synthesized NFO@SiO₂@APTS nanocomposites, for the removal of Ibuprofen, paracetamol, and streptomycin.

- IV. Comparison of the removal efficiency of Glycidylxypropyltrimethoxysilane (GPTS) NFO@SiO₂@GPTS-Cys and NFO@SiO₂@APTS, for the removal of Ibuprofen, paracetamol, and streptomycin.

- V. Synthesize and characterize NFO@SiO₂@APTS-HPCD nanocomposites.
 - a) Study effect of pH on NFO@SiO₂@APTS-HPCD nanocomposite formation.
 - b) Study effect of concentration and time.
 - c) To optimize parameters during the synthesis of nanocomposites, i.e., HP-β-CD loading and polymerization time.

- VI. Determine the efficiency of NFO@SiO₂@APTS-HPCD nanocomposites for the removal of Ibuprofen, paracetamol, and streptomycin.

1.3. Organization of the thesis

The thesis focuses on the synthesis of hydroxypropyl-β-cyclodextrin grafted nickel ferrite nanocomposites. The surface of the nickel ferrite nanoparticles was initially functionalized with silane for effective attachment of the cyclodextrin onto the nanoparticles. The nanocomposites synthesized were used for removal of the target pharmaceutical pollutants viz., Ibuprofen, acetaminophen and streptomycin. The removal efficiency of the

nanocomposites before and after cyclodextrin was analyzed. It was observed that former showed higher efficiency in comparison to the silane coated nanocomposite.

The current research work is organized into five chapters as follows:

Chapter 1 highlights the prime sources and causes of water pollution. It also highlights the contribution of pharmaceutical pollutants towards detrimental effects on the living species. It also focuses on the various techniques involved in water treatment and the eminence of nanotechnology in improving the same. Further, it elucidates the significance of magnetic, silica nanocomposites in various applications and the need for opting these for water remediation. Further, the chapter also emphasizes the eminent role of cyclodextrin in water remediation. It also outlines the main objectives of the current work and concludes with the scope of the work.

Chapter 2 comprises of an overview of the synthesis of nickel ferrite nanoparticles. An archive on various silica based magnetic nanocomposites involved in removal of pollutants. Also provides a review on the cyclodextrin based nanocomposites and its significance. Further, it sheds light on the use of cyclodextrin based nanocomposites for the removal of pharmaceutical pollutants.

Chapter 3 describes the materials and methodology used to achieve the required nanocomposite in the research work. The section includes the synthesis of nickel ferrite nanoparticles, followed by the coating of silanes and grafting of cyclodextrins. It also contains tuning the necessary parameters and methodology required for the application of these nanocomposites for the adsorption of the pharmaceutical pollutants. It also contains the methodology followed in batch adsorptions studies and kinetics for the removal of acetaminophen, ibuprofen and streptomycin.

Chapter 4 encompasses the complete results and discussion of the synthesis and characterization of the nickel ferrite nanoparticles. Further, the parameters varied for the coating of silanes and grafting of cyclodextrins. The chapter also includes the various parameters affecting the adsorption efficiency of the silane coated nanocomposites followed the cyclodextrin grafted nanocomposites. The regeneration capacity of the nanocomposites is also determined.

Chapter 5 provides a summary of the research work followed by implications of the obtained results. It also sheds light on the possible scope for future work.

CHAPTER 2

LITERATURE REVIEW

2.1. Pharmaceutical pollution

The era before the 19th century was marked by the use of natural compounds for therapeutics such as crude plant extracts, herbicides etc. However, with the advancement of medicine towards the end of the 19th century, the world witnessed various synthetic therapeutic compounds such as aspirin, naphthalene, etc. The consumption of these compounds has increased two-folds in the last 20 years, resulting in the exacerbation of pharmaceutical pollution in water resources over time. Furthermore, over time, the water sources containing this subtoxic concentration should have led to inadvertent effects on the ecosystem and its species (Lapworth et al. 2012).

Analgesics such as ibuprofen are the third most popularly consumed globally and enlisted in essential drugs list 2010 of world health organization (WHO) (Marchlewicz et al. 2015). A study conducted by (Heberer 2002) revealed that Ibuprofen, Ketoprofen and Diclofenac were present at $\mu\text{g L}^{-1}$ in groundwater used for drinking in Berlin, Germany. The recycling of treated water in a medium-sized Mediterranean parchent showed a high levels of acetaminophen concentrations up to 250 ng L^{-1} (Rabiet et al. 2006). Ibuprofen and four other NSAID's were present between 2 ng L^{-1} to 18 ng L^{-1} in rivers of Madrid region in Spain. Another survey conducted in Barcelona, Spain, revealed that higher levels of ibuprofen in aquifers than in wastewater treatment influents and effluents, indicating that the initial untreated waste waters of this region could have been source for Ibuprofen for its presence in aquifers (Teijon et al. 2010).

Acetaminophen, another widely used analgesic, acts as an endocrine disrupter at chronic levels. The high solubility and hydrophilicity of acetaminophen aids in its bioaccumulation into aquatic environment. In freshwater fishes like *Rhamdia quelen*, acetaminophen decreased testosterone levels and increased estrogen levels at concentrations above 2.5 ng L^{-1} (Guiloski et al. 2017). At concentrations of 500 ng L^{-1} of acetaminophen significant alterations were observed in the embryo production and

fecundity in zebrafish like *Danio rerio* (Galus et al. 2013). Acetaminophen was also said to decrease the reproductive capacity of *Diopatra neapolitana*, at concentrations of 25 $\mu\text{g L}^{-1}$ (Freitas et al. 2015). Further chronic exposure of these compounds i.e., 1.2 mg L^{-1} and 1.7 mg L^{-1} resulted in increased mortality rates in *Daphnia magna* (Nunes et al. 2014).

A study conducted by (Carballa et al. 2004) where they reported the removal efficiency of ibuprofen to be 70% by WWTP's, however the treatment was not effective in removing recalcitrant and trace levels of the compounds. Many such reports also analyzed the ubiquity of the pharmaceuticals where they observed that the trace concentrations of these pharmaceuticals go undetected by the conventional treatment methods (Ba et al. 2014). A study conducted by (Shraim et al. 2017) in the municipal wastewater of Saudi Arabia were analyzed before and after treatment by the wastewater treatment plants. It was observed that the pharmaceutical that were present in the influents showed no significant variation post treatment process, indicating the release of these compounds into the water sources. In this regard, plethora of nanotechnology was explored for removal of a wide range of pollutants from the aqueous systems.

Many researchers have been exploring the potential of nanoparticles to remove pharmaceuticals from aqueous systems for more than a decade. The intriguing properties of the metal oxide nanoparticles were found to have exceptional adsorptive potential compared to the conventional wastewater treatment methods. In this regard, various metal oxide nanoparticles such as zinc oxide (El-Maraghy et al. 2020), iron oxide (Parashar et al. 2020), graphene oxide (Khan et al. 2017) and different types of nanocomposites (Levard et al. 2021; Medhat Bojnourd and Pakizeh 2018; Rocha et al. 2021) have been used till date for the removal of these harmful pharmaceutical pollutants.

2.2. Ferrite nanoparticles and their applications

The potential of the iron oxide based magnetic nanoparticles have been explored from memory devices (Chalasanani and Vasudevan 2012) to the environmental remediation such as heavy metal adsorption (Dave and Chopda 2014) till date. Although they exhibit fast sorption kinetics, depending on the environmental conditions the iron oxide nanoparticles are subject to phase changes into other oxides and show low stability at low pH (Parsons et al. 2009). MFe_2O_4 nanoparticles have been gaining lot of interest due to their stronger magnetic features, larger surface area and higher resistance to chemical oxidation compared to iron oxide nanoparticles such as Fe_2O_4 , Fe_2O_3 , etc. (Ramimoghadam et al. 2014). Ferrites

are a large class of oxides with remarkable magnetic properties and used for various applications since last ~50 years (Goldman 2005). These applications are based upon the very basic properties of ferrites: a significant saturation magnetization, a high electrical resistivity, low electrical losses, and a very good chemical stability. Ferrites can be obtained in three different crystal systems by many methods, and the feasibility to prepare a virtually unlimited number of solid solutions unveils the means to tailor their properties for many applications.

Ferrites are important class of conventional oxides that vary in their crystal structure. They are classified based on their crystal structure and magnetic ordering as spinel, garnet, hexa and orthoferrite (Buschow 2008). Spinel ferrites have gained recognition due to their physiochemical properties and simple composition when compared to other ferrites. The structure elucidation of the ferrites dates back to 1915 where Bragg and Nishikawa studied the structure of naturally occurring mineral $MgAl_2O_4$. Due to the transition of their electronic, optical, magnetic and catalytic properties from their bulk counterparts these ferrites are regarded as one of the most important inorganic materials. The spinel ferrites have a general structural formula $A^{2+}B_2^{3+}O_4^{2-}$ and have been used for wide range of applications including catalysis (Kharisov et al. 2009). Remarkable electrical and magnetic properties of ferrites depend upon the nature of the ions, their charges and their distribution among tetrahedral (A) and octahedral (B) sites (Kurtan et al. 2015).

2.3. Prominence of nickel ferrite nanoparticles.

Nickel ferrite ($NiFe_2O_4$) nanoparticles are known as one of the most important nanocrystalline spinel ferrites (Kale et al. 2004). The academic community has extensively explored the novel properties and applications of nickel ferrite nanoparticles since the 80's. Their utility has been witnessed in a wide range of applications such as sensors, magnetic resonance imaging (MRI) enhancement, catalysis, drug delivery and high-density data storage (Sugimoto 1999; Zhang and Jiao 2015).

The nickel ferrite in its bulk form exhibit ferrimagnetism that originates from the anti-parallel alignment between Fe^{3+} sub-lattice at the tetrahedral sites and Ni^{2+} sublattice at the octahedral site (Kumari et al. 2016). Whereas, $NiFe_2O_4$ nanoparticles exhibit an inverse spinel form of a cubic structure where Fe^{2+} and Ni^{2+} ions get concentrated at tetrahedral sites and the rest (Fe^{2+} , Ni^{2+} and O^{2-}) at the octahedral sites. This particular has a

characteristic antiparallel spin of the magnetic moments which is responsible for the ferromagnetic behaviour (Giannakopoulou et al. 2002).

Nickel ferrite is one of the versatile and technologically important soft ferrite materials because of its typical ferromagnetic properties, low conductivity and thus lower eddy current losses, high electrochemical stability, catalytic behaviour, abundance in nature, etc. (Gunjakar et al. 2008). The Nickel ferrite nanoparticle exhibits an inverse spinel structure with Ni^{+2} in octahedral sites ($\text{Ni}(\text{O}_h)$) and Fe^{+3} equally distributed in between tetrahedral ($\text{Fe}(\text{T}_d)$) and octahedral sites ($\text{Fe}(\text{O}_h)$) of the $\text{O}^2\text{-fcc}$ cell (Naseri et. Al 2011). This ferrite is an inverse spinel in which eight units of NiFe_2O_4 go into a unit cell of the spinel structure. Half of the ferric ions preferentially fill the tetrahedral sites (A-sites) and the others occupy the octahedral sites (B-sites) (Goldman, 1993).

NiFe_2O_4 have also been studied for their hydrogen storage properties by Wan et al. (2015) and was found to adsorb 2.06 wt % H_2 within 3 hours near room temperature under H_2 pressure of 4 MPa. Recently ferrite nanoparticles have been used for hyperthermia treatments due to their low inherent toxicity and physiochemical stability. Lasheras et al. (2016b) had synthesized monodispersed NiFe_2O_4 nanoparticles of 8-12 nm to improve the response in magnetic hyperthermia treatments as convenient MRI contrast agents and observed to be innocuous at concentrations upto 0.5 mg/mL. Pollutants that undergo oxidation and bear negative charge can be easily bound to magnetic nanoparticles. As this binding is initiated due to the charge the pollutants get along with the nanoparticles and further when subjected to magnetic field, they are get separated rapidly and efficiently from the medium/environment (Kakhki 2015).

2.4. Synthesis of nickel ferrite nanoparticles

The supreme structural, magnetic and other properties of nickel ferrite are determined by preparation methods and its occupancy at tetrahedral and octahedral sites. A large number of methods have been employed to prepare nickel ferrite nanoparticle such as sonochemical method (Shafi et al. 1997) solid-state reaction (Yattinahalli, Kaparkar, Ayachit 2013), hydro-thermal (Nejati and Zabihi 2012), decomposition (Lasheras et al. 2016), sol-gel (Chen and He 2001) and co-precipitation (Rodrigues et al. 2015).

Choosing an apt method is considered to be the indispensable facet to obtain ferrites of high quality. Chemical co-precipitation method is widely operated based on the ease and reproducibility. The pros of the above method being tuning of the size by controlling the

surfactant to the metal ion ratio, homogeneity, cost effective, less time consumption and easy scalability for industrial applications. The table below gives an overview of the various synthesis methods utilized for the synthesis of nickel ferrite nanoparticles (Table 2).

Table 2: Overview of different synthesis methods of nickel ferrite nanoparticles

Sl. No	Synthesis method	Modification	Characteristics	Application	Reference
1	Thermal plasma (TP) & Co-precipitation (CP)	NiFe ₂ O ₄	Particle size 34 nm (TP) and 28 nm (CP)	NFOFP - antibacterial activity against <i>E. Coli</i>	(Bhosale et al. 2018)
2	Pechini's	NiFe ₂ O ₄	Indirect (1.6eV) and direct (1.1eV), Particle size 11-120 nm.	NFOCP agglomerated- no activity. Hydrogen production of (317.7 mmol H ₂ /g) > TiO ₂ P25 (68 mmol H ₂ /g) under visible light	(Dominguez-Arvizu et al. 2017)
3	Sol-Gel	NiFe ₂ O ₄ with Citric acid monohydrate as surfactant	Particle 42-315 nm for 750°C to 950°C	-	(Parishani et al. 2017)

4	Thermal decomposition method	NiFe ₂ O ₄	Particle size 4.5 nm – 26 nm	-	(Jankovský et al. 2017)
5	Sol-Gel auto combustion with honey as surfactant	NiFe ₂ O ₄	Particle size from 20 nm to 163 nm for 800°C – 1100°C; Ms =32.3 -49.9 emu/g	-	(Yadav et al. 2017)
6	Sol-gel	NiFe ₂ O ₄	E _g =2.85eV, Particle size 40-50 nm. Ms- 30 emu/g	-	(Akbar Hoseini and Khademolhoseini 2016)
7	Hydrothermal	NiFe ₂ O ₄	Particle size 5-9 nm, Ms= 34emu/g	-	(Kumari et al. 2016)
8	Sol-gel	NiFe ₂ O ₄ / SiO ₂ nanocomposite	TEM diameter of the composites calcined at 1000°C showed particles of size 10nm.	-	(Stoia et al. 2016)
9	Microwave assisted	NiFe ₂ O ₄	Particle size 50±10nm	Removal efficiency of 91% of As(III)	(Karakas et al. 2016)

combustion method									
10	Thermal decomposition method	NiFe ₂ O ₄	TEM diameter of particles of size 8-12nm	Nontoxic contrast agents	0.5mg/mL as MRI contrast agents	at	(Lasheras et al. 2016)		
11	Thermal decomposition (polyol method)	NiFe ₂ O ₄ capped with oleylamine	TEM diameter of the particles ~6.4nm	-	-	-	(Kurtan et al. 2015)		
12	Controlled self-assembly	NiFe ₂ O ₄ with lauric acid as stabilizer	TEM diameter of the particles 5-8nm	-	-	-	(Kumari et al. 2016)		
13	Co-precipitation /Hydrothermal method	NiFe ₂ O ₄	TEM diameter of the particles ~12nm	-	-	-	(Karaagac et al. 2016)		
14	Solvothermal method	NiFe ₂ O ₄ microspheres	TEM diameter of the particles 150-200nm	Wave absorbance	27.8 dB	-	(Jiao et al. 2016)		
15	Ultrasonication	NiFe ₂ O ₄	Crystallite size of 45nm	Band gap	3.7eV	-	(Khushboo et al. 2016)		
16	Sol -gel	NiFe ₂ O ₄	Particle size 14-26nm	-	-	-	(Argish et al. 2015)		

17	Microwave assisted	NiFe ₂ O ₄ with citric acid as chelating agent	Average crystalline size of 26.38nm	-	(Carpenter et al. 2015)
18	NiFe ₂ O ₄	Sol-gel	Particle size=113.3 nm; Eg= 5.5 eV		(Sen et al. 2015)
19	Co- precipitation and Hydrothermal	NiFe ₂ O ₄	TEM reveals particle size 20-30nm	-	(Tejabhiram et al. 2014)
20	Solvothermal method	NiFe ₂ O ₄ with oleylamine as capping agent and CTAB	TEM revealed diameter of the coated particles to be 9-11.7nm	Higher relaxivity (278.9 s ⁻¹ mM ⁻¹ in an NMR spectrometer at 11.7 T)	(Menelaou et al. 2014)
21	Colloidal technique	NiFe ₂ O ₄	TEM particle diameter of 50 nm	Adsorption capacity of EBT upto 32.41 mg/g.	(Moeinpour et al. 2014)
22	Polymeric precursor method	NiFe ₂ O ₄	Average crystallite size 78 nm	Pb-99% removal, 1h, pH-9 at room temperature	(Andal Buvanewari 2014)

23	Sol-gel method	NiFe ₂ O ₄ with citric acid as reducing agent and SDS as surfactant	SEM revealed homogenous particles of diameter ≤ 60 nm	revealed The maximum dye adsorption capacity	(Mahmoodi 2013)
				0.50 mg/g BB41, 0.41 mg/g BG4 and 0.25 mg/g BR18 for NFN and	
				111 mg/g BB41, 17 mg/g BG4 and 44 mg/g BR18 for NFN-SDS	
24	Hydrothermal method	NiFe ₂ O ₄ with PEG as surfactant	SEM revealed spherical particles of more than 100nm	Heavy metal removal efficiency	(Sezgin et al. 2013)
				Cu(II)-92.55%, Ni(II)-36.56%, and Zn(II)-99.91%,	
25	Flotation extraction	NiFe ₂ O ₄ with SDS as surfactant	TEM diameter of 2 – 6 nm	- nanoparticles, calcined at 600°C	(Mirgorod et al. 2013)

26	Co-precipitation	NiFe ₂ O ₄	Average crystallite size - 44.68 nm, calcined at 800°C for 4 hours	-	(S.S. Yattinahalli, S. B. Kaparkar, H. H. Ayachit 2013)
27	Electrochemical synthesis	NiFe ₂ O ₄	TEM diameter of nanoparticles 5-45 nm	Catalyst for oxidation of glucose, oxidation potential 0.76 eV, current density 0.56 mA/cm ²	(Galindo et al. 2012)
28	Hydrothermal method	NiFe ₂ O ₄	with surfactants glycerol and SDS	TEM diameter of the nanoparticles with surfactant 10-15 nm and without 50-60nm.	(Nejati and Zabih 2012)
29	Sol-gel combustion methd	auto NiFe ₂ O ₄	with oleic acid as surfactant	TEM showed spherical nanoparticles of size 28nm	(Sivakumar et al. 2012)
30	Sol-gel combustion method and high frequency	self- NiFe ₂ O ₄	with self- glycine as self- combustion agent	TEM diameter of the particles for self- combustion 25-40 nm and plasma assisted	(Zalite et al. 2012)

	plasma chemical synthesis.		have particles of 10-100nm.		
31	Hydrothermal	NiFe ₂ O ₄ with glycerol or SDS as surfactant	Particle size=10-15 nm; Ms= 39.60 emu/g	-	(Nejati and Zabihi 2012)
32	Hydrothermal	NiFe ₂ O ₄	Particle size	55 µg of Histagged	(Chun et al. 2011)
			Ms=41.3 emu/g	sGFP removed by 500 µg of NiFe ₂ O ₄ in 2 hours	
33	Sol-Gel auto combustion	NiFe ₂ O ₄ with citric acid as surfactant	Particle size – 30 nm; Ms=47.3 – 51.3 emu/g	-	(Sivakumar et al. 2011a)
34	Sol-gel method	NiFe ₂ O ₄ with egg white as capping agent	3D porous structure Calcined at 400°C	Adsorption of Methylene blue (138.50mg/g), Fuschin Red (1.61mg/g), Methyl Violet (19.06mg/g), Cu(II) (55.83mg/g), Cr(VI) (36.95mg/g)	(Hou et al. 2011)

		and Ni(II) (37.02mg/g).		
35	Sol-gel and autocombustion method	NiFe ₂ O ₄ with citric acid as chelating agent	TEM diameter of nanoparticles 28nm	(Sivakumar et al. 2011b)
36	Sol-gel and autocombustion method	NiFe ₂ O ₄ with PVP as capping agent	TEM diameter of nanoparticles are upto 8nm.	(Sivakumar et al. 2011b)
37	Thermal treatment method	NiFe ₂ O ₄ with PVP as capping agent	TEM diameter of the particles 7-47nm when calcined from 623-823K.	(Naseri et al. 2011)
38	Sol-gel	NiFe ₂ O ₄ with PLGA as capping agent	NiFe ₂ O ₄ was less toxic compared to CoFe ₂ O ₄ at concentration of 5-15%.	(Astamulu et al.2010)
39	Sol-Gel auto combustion	NiFe ₂ O ₄ with Octanoic acid as capping agent	Particle size- 25±5 nm; M _s =23.12emu/g	(Salavati-Niasari et al. 2009)

40	Sol-gel/ hydrothermal method	NiFe ₂ O ₄ glycolic acid chelating agent	with as particles for hydrothermal and 27 nm particles for sol-gel method	TEM diameter of 9 nm	-	(Srivastava et al. 2009a)
41	Sol-gel	NiFe ₂ O ₄ glycolic acid chelating agent	with as nanoparticles 27±2 nm conductivity 5.0eV	FESEM diameter of	The Optical	(Srivastava et al. 2009b)
42	Solvothermal method	NiFe ₂ O ₄	TEM diameter of ferrite nanospheres 130-240 nm		-	(Wang et al. 2009)
43	Soft chemistry route	NiFe ₂ O ₄	TEM diameter increased from 30-70nm with increase in calcination 300-800°C		-	(Jiang and Yang 2007)
44	Reverse Micelle	NiFe ₂ O ₄ /TiO ₂	TEM diameter spherical nanoparticles of 10-15 nm		Antimicrobial activity	(Rawat et al. 2007)
45	Sol-gel method	NiFe ₂ O ₄	Grain size of 15 nm		-	(George et al. 2006)

46	Polyol method	NiFe ₂ O ₄ with oleic acid as capping agent	TEM diameter 150±50 nm	-	(Yin et al. 2005)
47	Co-precipitation / hydrothermal method	NiFe ₂ O ₄	TEM diameter varied with aging time 2-4nm, and 10-13nm for 9 hours	-	(Nam et al. 2004)
48	Reverse micelle	NiFe ₂ O ₄	TEM diameter 5-8nm, spherical nanoparticles	-	(Kale et al. 2004)
49	Sol -gel	NiFe ₂ O ₄	TEM diameter 5-30nm, calcined at 300°C for 2hours	-	(Chen and He 2001)
50	Co-precipitation/ ball milling	NiFe ₂ O ₄	TEM diameter 10nm, spherical nanoparticles, calcined 650°C for 2 hours gave 50nm size particles	-	(Shi et al. 1999)

Although these methods provide promising applications, the co-precipitation route provides a uniform nanoparticles distribution matrix using simple experimentation at optimum operational temperatures. In the present investigation, an endeavour has been made to prepare the NiFe_2O_4 nanoparticles by the co-precipitation method. The table below represents the synthesis of nickel ferrite nanoparticles using the co-precipitation method (Table 3)

Table 3: Synthesis of Nickel ferrite nanoparticles using co-precipitation method

Sl. No	Material	Method	Characteristics	Surfactants	Application	Reference
1	NiFe ₂ O ₄	Co-precipitation	Particle size =28 nm;	-	-	(Sagadevan et al. 2018)
2	NiFe ₂ O ₄	Co-precipitation	Particle size= 12-42 nm for 700°C – 1000°C	-	-	(Pottker et al. 2018)
3	NiFe ₂ O ₄	Co-precipitation	Eg=2.66 eV, Particle size- 15- 18 nm	-	Methylene Blue -99% degradation	(Annie Vinosha et al. 2017)
4	NiFe ₂ O ₄	Co-precipitation	Particle size 250-400 nm	-	-	(Tahir et al. 2017)
5	NiFe ₂ O ₄	Co-precipitation	Particle size= 20±3 nm; Ms=26 emu/g	-	Removal of dipyrone 30.4mg/g (pH 6) and 25.0mg/g (pH 4)	(Springer et al. 2016)
6	NiFe ₂ O ₄	Co-precipitation	Particle size = 11±5 nm; Ms = 23.54 emu/g	Citric acid	Dry magnetic liposomes showed increased fluorescent	(Rodrigues et al. 2015)

emission in cell
membrane

7	NiFe ₂ O ₄	Co-precipitation	Particle size 161 nm	-	(Yattinahalli et al. 2014)
8	NiFe ₂ O ₄	Co-precipitation	Particle size 8-20 nm for 250- 550 °C; Ms= 20.1 emu/g – 35.5 emu/g	Oleic acid	(Joshi et al. 2014)
9	NiFe ₂ O ₄	Co-precipitation	Eg = 3.98eV, particle size – 40 nm	-	(Asokarajan et al. 2013)
10	NiFe ₂ O ₄	Co-precipitation	Average crystallite size - 44.68nm, calcined at 800°C for 4 hours	-	(S.S. Yattinahalli, S. B. Kaparkar, H. H. Ayachit 2013)
11	NiFe ₂ O ₄	Co-precipitation	Particle sizes to be 32.96, 54.85 and 82.12 nm for different ratios of iron and nickel	Oleic acid	(Ong et al. 2012)

12	Ag/ NiFe ₂ O ₄	Modified Co- precipitation	-	-	Degradation of toluene 96.28% in 12 hours	(Zhu et al. 2010)
13	NiFe ₂ O ₄	Co-precipitation	Particle size 8 -28 nm (600°C – 1000°C)	Oleic acid	-	(Maaz et al. 2009)

Ms = 9-40.5 emu/g

Nanoparticles with exceptional functionalities have been obtained till date with the combination of alkylamines with carboxylic acids or thiols (Adegoke et al. 2018). Oleic acid and oleylamine have been one of the commonly used surfactants over the past decade has been advocated for the synthesis of magnetic nanoparticles such as magnetite, FeMo and FePt (Klokkenburg et al. 2004; Sun et al. 2004). According to a report by Harris et al. (2015) where they studied the interaction of the surfactants oleic acid (surfactant) and oleylamine (co-surfactant) it was observed that a surfactant double layer is formed with the oleic acid molecules which has three binding motifs is found close to the nanoparticle core and the oleylamine molecules which has single binding motifs forming an outer layer. Hence, restricting the growth of nanoparticles during the synthesis procedure. Recent findings by (Mourdikoudis et al. 2022) also stated the use of oleylamine and oleic acid for the synthesis of ferrite nanoparticles where these surfactants act as stabilizer and reductant for producing nanoparticles of the size range of 10 nm.

Octylamine has also proven to be a very good candidate to maintain the stability of the nanoparticles (Bomila et al. 2018). The hydrophobic nature of this versatile organic compound has played an important role in assembly of organic and inorganic phases in silica synthesis (Mosquera et al. 2010). So far there are no reports studying the effect of octylamine on the synthesis of nickel ferrite nanoparticles. Thus, in this work an attempt is made to synthesize nickel ferrite nanoparticles using the combination oleic and octylamine to study their effect on the size of the nanoparticles.

2.5. Magnetic silica composites

Silica functions as an ideal shell for magnetic composites and have proven their potential in biomedical applications (Dabagh and Dini 2019; Li et al. 2019b). Additionally, the ease of succedent functionalization by tailoring the surface of silica has also paved the way for target specific applications. For instance, (Sheng et al. 2016) evaluated the amine-functionalized magnetic nanospheres ($\text{Fe}_3\text{O}_4@\text{SiO}_2@\text{EDPS}$) towards DNA separation where they observed an increase in the DNA binding capacity in the presence of amine groups (210.22 $\mu\text{g}/\text{mg}$), when compared to SiO_2 , coated spheres alone (138.44 $\mu\text{g}/\text{mg}$). In a similar work, (Iqbal et al. 2017) investigated the catalytic activity of $\text{NFO}@\text{SiO}_2$ in the S-arylation reaction and obtained a high yield of 84% in the presence of the catalyst. Further, (Hong et al. 2015) fabricated nickel ferrite embedded nanofibrous silica

membranes and observed that the membranes had excellent flexibility and magneto responsivity.

The foremost concern in our day-to-day life is water pollution. In the last decade, several notable contributions of this composite towards water remediation have shed light on its versatile nature. Although silica-coated composites have shown high stability and reproducibility, the maximum adsorption capacity is significantly lower as compared to the tailored silica surface. As the silica surface has abundant hydroxyl groups, it can be tuned by amino silanes (Liu et al. 2004) or decorated with metals like Ag (Blanco-Esqueda et al. 2015; Kooti et al. 2015) reported that streptomycin conjugated magnetic silica microspheres showed an enhanced antibacterial property. Silica coated magnetic spheres showed a maximum adsorption capacity of 50.54 mg/g of Congo red, as reported by (Wang et al. 2016). (Freitas et al. 2017) reported the maximum removal of methylene blue to be 73%.

Similarly, glutamic acid cross-linked with magnetic silica/chitosan spheres exhibited maximum removal of methylene blue (180.1 mg/g), crystal violet (375.4 mg/g) and cation light yellow (217.3 mg/g). Whereas, it showed lower adsorption of methylene blue (28.8 mg/g), crystal violet (76.8 mg/g), and cation light yellow (17.6 mg/g) for silica-coated magnetic spheres (Yan et al. 2013). In another work dithiocarbamate was grafted to aminosilane functionalized iron oxide nanoparticles to determine its Hg(II) removal efficiency. It was observed that the modified nanoparticles attained 99.8% of Hg(II) removal for an initial concentration of 50 $\mu\text{g L}^{-1}$ (Figueira et al. 2011). Thus, it can be concluded that modification of the magnetic silica spheres further increases its adsorption capacity. The list of modified silica magnetic composites used for various applications is depicted in Table 4.

Table 4. Overview of silica modified magnetic composites used for various applications

SI No:	Nanocomposite	Application	Reference
1.	MMIP	High binding capacity of 70 & 32 mg/g of erythromycin and ciprofloxacin	(Kuhn et al. 2020)
2.	Fe ₃ O ₄ @mSiO ₂ -NH ₂	Fe ³⁺ : 20.66 mg/g	(Meng et al. 2018)
3.	CoFe ₂ O ₄ @SiO ₂ -NH ₂	Cd(II): 99.96%; Cu(II): 88.05%; Pb(II): 90.79 %	(Ren et al. 2017)
4.	Fe ₃ O ₄ @ SBA-15-NH ₂	Pb ²⁺ :243.9 mg/g	(Wang et al. 2015a)
5.	Ph-N ₃ -HNS	Ciprofloxacin: 11.75 mg/g	(Gao et al. 2015)
6.	CoFe ₂ O ₄ /SiO ₂ /Ag/streptomycin	Antibacterial activity	(Kooti et al. 2015)
7.	Fe ₃ O ₄ @SiO ₂ @ZnO-Ag	100% Rhodamine B degradation in 90 mins	(Wang et al. 2015a)
8.	Fe ₃ O ₄ @chitosan@Ag	Removal 99.5% of 8 dyes	(Ramalingam et al. 2015)
9.	Fe ₃ O ₄ @SiO ₂ @meso- SiO ₂ -NH ₂	Pb ²⁺ :289.7 mg/g; Cu ²⁺ :196.5 mg/g; Cd ²⁺ :154.2 mg/g	(Yuan et al. 2014)
10.	Fe ₃ O ₄ @SiO ₂ @TiO ₂ -Ag	Degradation of Rhodamine up to 99%	(Chi et al. 2013)
11.	Fe ₃ O ₄ @SiO ₂ -NH ₂	Pb ²⁺ :17.65 mg/g	(Mahdavi et al. 2013)

12. ATEs@MS Pt(IV): 140 mg/g (Dobrowolski et al. 2013)
13. Fe₃O₄@SiO₂/HPG-COOH Removal of methyl violet: 95 %; Rhodamine 6G: 90% (Zhou et al. 2010)
14. Fe₃O₄@SiO₂-NH₂ Cu(II):0.47 mmol/g ; Pb(II): 0.37 mmol/g), Cd(II): 0.20 mmol/g (Wang et al. 2010)

2.6. Cyclodextrins (CD)

Cyclodextrins were ventured back in 1881 by Villers and identified by Schardinger in 1903. Since then, these oligosaccharides have proved their potential as a drug carrier (Marco et al. 2017) to the removal of pollutants from soil (Wang et al. 2019) and water (Sikder et al. 2014; Zhou et al. 2019). These cyclodextrins are macrocyclic oligosaccharides that are composed of 6 to 8 glucopyranose monomers connected by 1-4-glucosidic linkages. The unique features of a cyclodextrin include a hydrophobic cavity, a large number of functional groups, the ability to incorporate a wide range of molecules, as shown in Table 5. These unique features make it a plausible candidate for pollutant adsorption from wastewaters. Three principal oligosaccharides found in cyclodextrins viz. α -cyclodextrin, β -cyclodextrin, γ -cyclodextrin (Saenger et al. 1998). These cyclodextrins are crystalline, homogenous, and non-hygroscopic molecules having a torus-like macro ring shape. Among them, α -cyclodextrin and γ -cyclodextrin are not suitable for many drugs as a carrier and are expensive. Whereas, β -cyclodextrin has been employed in many therapeutic applications due to its availability and compatibility for a wide range of guest molecules (Marques Fernandes et al. 2003).

β -cyclodextrins frequently showed their potential as an adsorbent with a wide range of organic compounds ranging from 200 g/mol to 800 g/mol (Cheng et al. 2014). The application of silica-based cyclodextrin composites towards the removal of organic pollutants dates back in 2002, where (Phan et al. (2002) investigated the removal of p-nitrophenol, pentachlorophenol, and (2,4-dichloro phenoxy) acetic acid. Methacryloyl- β -cyclodextrin@silica composites showed 100% removal for both p-nitrophenol, pentachlorophenol and 95% for (2,4-dichloro phenoxy) acetic acid. The inclusion complex formation with β -cyclodextrin has been studied for various compounds among which a similar work was reported by El-Kemary et al. (2011). Here they studied the complex formation of β -cyclodextrin, methyl- β -cyclodextrin, and hydroxypropyl- β -cyclodextrin. They observed that paracetamol formed better inclusion complexes with methyl- β -cyclodextrin and hydroxypropyl- β -cyclodextrin. Cyclodextrins were also cross-linked with molecules and used as a filter for the removal of micropollutants. For instance, (Wang et al. 2017) observed the removal rate of β -CD cross-linked with 4,4-difluorodiphenylsulfone (DFPS) was able to remove BPA, BPS, 2-NO, 2,4-DCP ~ 99% except for 20% of Propranolol hydrochloride (PR) which was due to lower binding interaction between β -CD

and PR. In recent times due to the increase in pollutants, the removal of emerging pollutants using cyclodextrin nanocomposites is on the rise.

In a similar work by Bhattarai et al. (2014) where they synthesized β -CD composites with two types of cross-linking agents hexamethylene diisocyanate (HMDI) and epichlorohydrin (EPI) and copolymers (glycidoxypopyl trimethoxysilane (GPTS) and aminopropyl triethoxysilane (APTS) and determined that they showed that the former cross-linker (HMDI) showed higher adsorption efficiency of more than 90% for 17 β -estradiol, PFOA, and BPA. However, the main drawback of the cross-linking agents like (HMDI), and EPI is their toxicity (Krabicová et al. 2020). In a similar study, the removal of polyaromatic hydrocarbons investigated by (Topuz and Uyar 2017), wherein they observed that the addition of cyclodextrin increased the adsorption of polyaromatic hydrocarbons by two-fold, i.e., from 0.3 to 1.6 mg/g. Recently, Gómez-Morte et al. (2021) synthesized a EPI- β -CD polymer which exhibited 77 % removal of Ibuprofen from aqueous systems. Further, in the presence of pulsed light the polymer was able to remove up to 91 % with the aid of EPI- β -CD polymer.

Table 5: Overview of cyclodextrin modified nanocomposites used for various applications

Sl no:	Nanocomposite	Application	Reference
1	β -CD-EBT-CD	100% removal of Coomassie brilliant blue G 250 (CBB-G250) and Alizarin red S (ARS)	(Chang et al. 2020)
2	THF- β -CD	BPA, Chloroxylenol (PCMX), and Carbamepazine (CBZ) was 98.1%, 90.8% and 65.0%	(Zhou et al. 2019)
3	SiO ₂ @Ag@EDA- β -CD and SiO ₂ @Ag@cysteiny- β -CD	2.15 μ g (7.40%) and 1.57 μ g (5.48%) of DOX,	(Kang et al. 2019)
4	Ag@ Fe ₃ O ₄ @Ag-HS- β -CD	Detection of butyl benzyl phthalate (BBP) up to 5x 10 ⁻⁸ M	(Li et al. 2019a)
5	β -CD/Au-FeNPs	The detection limit of Cr ⁶⁺ : 2.5nM	(Amanulla et al. 2018)
6	β -CD/GPTMS/GO	Removal of Cu ²⁺ :44.795 mg/g	(Yu et al. 2017)
7	Fe ₃ O ₄ @NH ₂ -TsO- β -CD	Uptake of 78.8mg/g of methylene blue and release of 73%	(Zhou et al. 2016c)
8	Fe ₃ O ₄ @CM- β -CD	Removal of As (III): 85%	(Zeinali et al. 2016)

9	β -CD cross-linked with THF	Removal of bisphenol A(BPA) up to 99%	(Alsaiee et al. 2016)
10	$\text{SiO}_2@Au@Ag@CD$	Detection of PCB up to 1 μM	(Lu et al. 2014)
11	β -CD/zeolite derivatives with GPTS as the linker	Removal of methyl orange: 64%	(Mallard et al. 2015)
12	GO- β -CD	Removal of fuchsin acid: 85.2%	(Wang et al. 2015b)
13	β -CD cross-linked with EDTA	The removal of Cu (II) :(96.06%); MB:37.91%	(Repo et al. 2015)
14	$\text{Fe}_3\text{O}_4@$ Triazinyl- β -CD	Maximum adsorption capacity 105.38 mg/g -Pb ²⁺ , 58.44 mg/g - Cu ²⁺ , 51.30 mg/g -Zn ²⁺ , 33.33 mg/g -Co ²⁺	(Abdolmaleki et al. 2015)
15	$\text{Fe}_3\text{O}_4@$ β -CD	70% degradation of BPA 90.1% removal of methyl green	(Kumar et al. 2018)
16	Fe_3O_4 - β -CD-IL	Able to detect Bisphenol A at very low electrochemical potential	(Sinniah et al. 2015)

17	β -CD cross-linked with EPI	The maximum adsorption capacity of the regenerated beads was 4.5 μ mol/g	(Jurecska et al. 2014)
18	Ag@ β -CD	Removal of Melamine: 80.50%	(John Xavier et al. 2014)
19	Fe ₃ O ₄ @TS- β -CD	Recovery of 5-hydroxy-3-indole acetic acid: 97 \pm 4%	(Gaber Ahmed et al. 2014)
20	Fe ₃ O ₄ @GO- β -CD	Removal of Rhodamine 6G: 90%	(Liu et al. 2014)
21	Fe ₃ O ₄ @ β -CD-NH ₂	Removal of MB:90%	(Li et al. 2014)
22	Fe ₃ O ₄ @-CM- β -CD	Removal of Pb ²⁺ , Cd ²⁺ & Ni ²⁺ :64.50, 27.70 and 13.20 mg/g,	(Badruddoza et al. 2013b)
23	Fe ₃ O ₄ @TiO ₂ -CMCD	Removal of Bisphenol A-90%	(Vasudevan et al. 2012)
24	Au@ β -CD	The detection limit up to 20 μ mol/L	(Aswathy et al. 2012)
25	Fe ₃ O ₄ @SiO ₂ -CM- β -CD	Removal of L-Trp > L-Phe > L-Tyr	(Ghosh et al. 2011)

26	Mono-6-deoxy-6-(3-butylimidazolium)- β -cyclodextrin iodide- ionic liquid complexes	80% removal of p-Nitrophenol and 2,4,6-trichlorophenol, 100% removal of Cr^{6+}	(Mahlambi et al. 2010)
27	Ag-Per-6-thio- β -CD	The detection limit of pyrocatechol, hydroquinone, and resorcinol was 5×10^{-5} M	(Chen et al. 2010)
28	CM- β -CD cross-linked with EPI	Maximum adsorption capacity 53.2 mg -Basic Violet 10, 42.4 mg -Basic blue 3, 35.8 mg- Basic Violet 3	(Crini 2008)

The literature so far reports the utility of cyclodextrins for the removal of wide range of pollutants. However, reports on the usage of cyclodextrins for the removal of pharmaceutical pollutants are very few. (Xiao et al. 2011) explored the potential of this multifaceted oligosaccharides (CD's) for the removal of levofloxacin, aspirin and acetaminophen. They observed that among the three cyclodextrins, α , β and γ . The β -cyclodextrin had higher binding capacity with the target pharmaceuticals. Thus, higher adsorption capacity was exhibited by the β -cyclodextrins. Fluorescein β -CD was successful in the detection of $50 \mu\text{g mL}^{-1}$ of diclofenac in aqueous system (Xiao et al. 2015). Similar reports were also obtained by citric acid cross linked cyclodextrins (25 mg) and it was reported to exhibit $\sim 85\%$ efficiency for 10 ppm of the progesterone (Moulahcene et al. 2015). Recently, Yadav et al. (2021) developed $\text{Fe}_3\text{O}_4/\text{CD}/\text{AC}/\text{SA}$ polymer gel bead which exhibited maximum removal efficiency of 98.21 % (MV), 97.5 % (BG) , 97.5 % (NOX, CPX) and 96.8 % (Cu(II)). These beads also exhibited good regeneration capacity up to four cycles.

The fast sorption kinetics and good regeneration capacity of the CD's and cyclodextrin based nanocomposites has propelled the researches to utilize the potential of cyclodextrins in removal of pollutants from aqueous systems (Cova et al. 2021). Thus, it is evident from the previous literatures that cyclodextrin based nanomaterials can provide effective removal of pharmaceutical pollutants. Further magnetic based composites exalt the efficiency of the removal process by providing the ease of separation post adsorption. Thus, combining both these counterparts the current work was focused on developing a magnetic cyclodextrin composite in which hydroxypropyl- β -cyclodextrin shall combine with APTS coated $\text{SiO}_2@\text{NiFe}_2\text{O}_4$ nanoparticles. The two moieties will serve as nanocomposite for the removal of selective pharmaceuticals compounds.

CHAPTER 3

MATERIALS AND METHODS

The materials required for the synthesis and characterization of functionalized nickel ferrite nanoparticles and methods adopted to remove the pharmaceuticals from aqueous phase is illustrated in this chapter. All the chemicals used in the experiments are of analytical grade and procured from internationally recognized manufacturers.

3.1. Materials

3-aminopropyltrimethoxysilane (97%), 3-Glycidyloxypropyltrimethoxysilane (98%), octylamine (97%), Tetraethyl orthosilicate (98%), 4-acetaminophen ($\geq 90\%$), Streptomycin sulfate ($\geq 99.9\%$), Maleic anhydride (99%), 2-hydroxypropyl beta-cyclodextrin ($\geq 98\%$), Di-methyl sulphoxide (99.9%) were purchased from Sigma Aldrich. Sodium hydroxide (98%) and Oleic acid (98%) were purchased from Spectrum Chemicals. L-cysteine (Cys) was purchased from Lobacheme. The rest of the chemicals, such as Nickel Chloride heptahydrate (98%), Ferric Chloride Hexahydrate (99%), Ibuprofen ($\geq 98\%$), were purchased from Molychem, Medlisc, and TCL Chemicals respectively. Toluene ($\geq 99.9\%$) and ethanol ($\geq 99\%$) were purchased from Merck. Stock solutions (50 mg L^{-1}) of IBF, ACE, and STR were prepared in standard flasks using deionized water, and the calibration curve was plotted. All experiments were conducted in triplicates to achieve concordance.

3.2. Sample Characterization

The particle size and morphology of aminosilane coated nickel ferrite nanocomposite were determined by Field Emission Scanning Electron Microscopy (Carl Zeiss, FE-SEM Oxford Instrument EDAX). The Infrared (IR) spectrum of both nanoparticles and the functionalized nanocomposite were recorded using an IR spectrophotometer (PerkinElmer UTAR) in the region $4000 - 400 \text{ cm}^{-1}$. The Thermogravimetric Analysis (TGA) of the nanocomposite was obtained from Perkin-Elmer Pyris Diamond 6000 analyzer under a nitrogen atmosphere using a heating range of $20-800^\circ\text{C}$ at a rate of $10^\circ\text{C min}^{-1}$. The magnetic properties of the nanocomposites were examined using vibrating sample magnetometer (VSM) for an applied magnetic field between $\pm 20 \text{ kOe}$. The absorbance of

the analyte was studied using the UV Spectrophotometer by Thermo Scientific Evolution 300, GENESYS 10S at 264 nm, 244, and 195 nm for IBF, ACE, and STR, respectively.

3.3. Methodology

3.3.1. Synthesis of Nickel Ferrite nanoparticles:

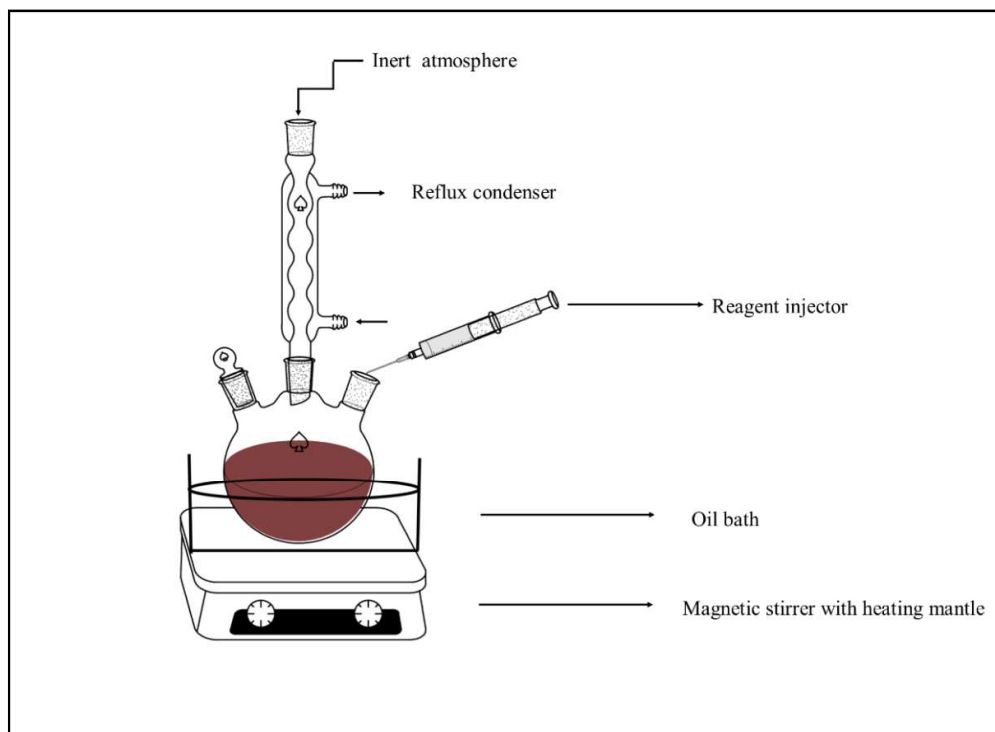


Figure 1: Schematic representation of the experimental set up of the co-precipitation method

The nickel ferrite nanoparticles were synthesized using the co-precipitation method as reported by Springer et al. (2016), with certain modifications. A representation of the experimental setup is given in Figure 1. A mixture of 2 mmol of ferric chloride and 1 mmol of nickel chloride solutions was taken in a three-necked reflux flask and placed in a hot oil bath maintained at a uniform temperature of 80°C. The contents were stirred until a homogenous mixture was obtained. 4 mmol of oleic acid and 4 mmol of octylamine and were added serially, in a dropwise manner. 50 ml of 10 mmol sodium hydroxide solution was added to the above mixture dropwise and the bath temperature was increased to 100 °C. The contents were continuously stirred for 45 min to obtain the precipitate, this was separated by centrifugation at 15000 rpm, 8 °C and washed several times with ethanol and

distilled water. The precipitate was further decanted and dried at 60°C overnight and then subjected to calcination at 400°C for 1 hr.

The above procedure was repeated twice by changing the proportions between oleic acid and octylamine, as shown in Table 6. to optimize the size of the nanoparticles.

Table 6. Optimization of nickel ferrite nanoparticle synthesis

FeCl ₃ (mmol)	NiCl ₂ (mmol)	NaOH (mmol)	Oleic acid (mmol)	Octylamine (mmol)
2	1	10	4	4
2	1	10	4	8
2	1	10	4	10

3.3.2. Preparation of GPTS coated nickel ferrite nanoparticles.

The nickel ferrite nanoparticles synthesized by the above method was coated with GPTS with modification by Stober method as follows (Zhou et al. 2016b). 0.5 g of NFO nanoparticles were suspended in 400 ml of ethanol and sonicated with a mixture of ammonia hydroxide (20 ml), and water (25 ml) for 15 min. This mixture was kept for 3 hrs at 40 °C after the addition of 4 ml of Tetraethyl orthosilicate (TEOS) dropwise. These silica-coated nanoparticles were later separated from the resulting solution with a magnet and centrifuged thrice with ethanol and water consecutively. The NFO@SiO₂ were further coated with Glycidyloxypropyltriethoxysilane (GPTS) to surface with epoxy groups. In order to achieve this, the silica coated nickel ferrite nanoparticles were transferred into 150 ml of toluene. To this solution 1 ml of GPTS is added and the mixture was stirred for 24 hrs at 70°C. The silane-modified NFO@SiO₂ nanocomposite were washed with 50 % ethanol three times and dried in a vacuum for 24 hrs. The procedure was repeated for 2 ml and 3 ml of GPTS and the optimal GPTS concentration was further used for attaching L-cysteine.

3.3.3. Grafting of L-cysteine onto NFO@ SiO₂@GPTS nanoparticles:

L-cysteine was attached to GPTS coated nickel ferrite nanoparticles by using a modified method of (Zhang et al. 2014) by adding 0.5 g of NFO@SiO₂@GPTS nanoparticles dispersed in 50 ml water and sonicated for 5 min. 3, 4, 7 & 9 mmol of L-cysteine was added to four different flasks containing 50 ml of NFO@SiO₂@GPTS nanoparticles and the solutions were maintained at pH 10.0. The mixtures were stirred for 24 hrs, and the nanocomposites were collected, washed with ethanol three times to remove residual unattached compounds.

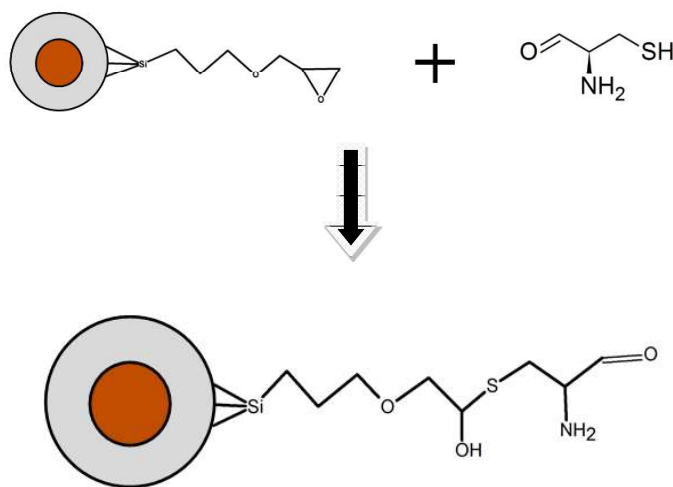


Figure 1.1: Schematic representation of L-cysteine onto NFO@SiO₂@GPTS nanoparticles

3.3.4. Synthesis of APTS coated NiFe₂O₄ composites.

The silica coated nickel ferrite nanocomposite (NFO@SiO₂) was synthesized by the Stober method (Kollarahithlu and Balakrishnan 2018). This NFO@SiO₂ was further functionalized with aminopropyltrimethoxysilane (APTS) by adding 10 mg of NFO@SiO₂ in 30 ml ethanolic solution and stirred for 30 min. To this solution, 20 μL of APTS was added and stirred for 3 hrs and centrifuged at 10000 rpm for 15 mins. The particles were washed with ethanol to remove any residual compounds or unattached APTS molecules and dried at 60°C for 12 hrs. Thus, a ninhydrin assay was performed as an initial test to confirm the presence of APTS on the surface of the nanocomposite. Further, FTIR, FESEM analysis was performed to confirm the functionalization of the APTS onto the nanoparticles.

The procedure was repeated for two more concentrations of APTS 40 μL and 60 μL respectively, as represented in table 7.

Table 7. Optimization of synthesis of NFO@SiO₂@APTS

NFO@SiO ₂ (mg)	APTS (μL)	Ethanol (ml)
10	20	30
10	40	30
10	60	30

The process of surface modification of the NFO@SiO₂@APTS nanocomposite synthesis is summarised and shown in Figure. 1.2.

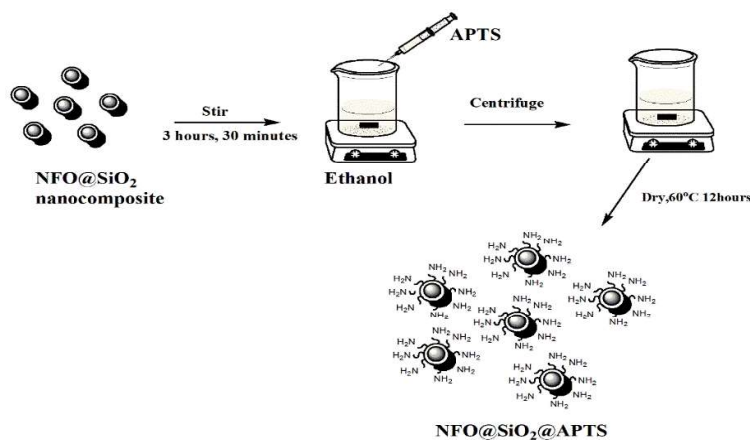


Figure 1.2: Schematic representation of the synthesis of NFO@SiO₂@APTS

3.3.5. Ninhydrin Test.

Ninhydrin Test is usually carried out for the detection of amine groups in any samples. Initially, the 0.2 % w/v of Ninhydrin solution was mixed into a solution containing 1 mg of APTS coated nanocomposite particles and 300 μl of distilled water and further mixed with 600 μl of Ninhydrin solution. 900 μl of the made-up sample was heated at 80 °C for 15 min. The appearance of the purple colour will indicate the presence of amine groups in the mixture. Post the cooling process; the nanocomposites were separated using a Neodymium magnet.

3.3.6. Grafting of 2-hydroxypropyl- β -cyclodextrin (HPCD) to NFO@SiO₂@APTS

The synthesis of cyclodextrin coated nanoparticles was achieved via esterification by using maleic anhydride. 5 mg of the NFO@SiO₂@APTS was taken and stirred in 30 ml DMSO for 30 min. To this mixture, 10 mg of HPCD was added, followed by 1 mmol maleic anhydride, and the reaction was carried out by stirring and maintaining at 60°C for 1 hr in an inert atmosphere by stirring and maintaining. Further, the nanoparticles were collected and centrifuged at 10,000 rpm for 15 min. The nanocomposites thus collected were washed with ethanol until a clear supernatant was obtained and dried at 60°C overnight. The procedure was repeated for different concentrations of maleic anhydride (2 mmol, 3 mmol).

Thus, this NFO@SiO₂@APTS-HPCD nanocomposite produced was investigated for its adsorptive properties towards the three target pharmaceutical compounds viz., IBF, ACE, and STR.

3.4. Adsorption of Acetaminophen, Ibuprofen and Streptomycin by NFO@SiO₂@GPTS

3.4.1. Batch adsorption Experiments

Adsorbent properties of the NFO nanocomposite were investigated by analyzing the influence of various parameters such as adsorption time, adsorbent mass, the effect of pH, and reaction time by batch experiments at room temperature. 10 mg of NFO nanocomposite material was stirred for 30 mins in the dark until the sorbent attains equilibrium. To study the effect of pH on the adsorption of all the three pharmaceuticals, the initial concentration of IBF (10 mg L⁻¹) and the initial adsorbent dosage of 10 mg. The solution was placed in a magnetic stirrer and agitated; aliquots of samples were taken every 5 mins up to 30 mins by decantation. The supernatant was filtered using 0.45 μ m and analyzed for the residual concentration of IBF was measured at 244 nm wavelength using UV- Spectrophotometer. Further, the adsorption efficiencies of the NFO composite were analyzed for all three pharmaceuticals at different pharmaceutical concentrations, and the adsorption kinetics was investigated in a range of (10-50 mg L⁻¹). Similarly, the experiments were performed for uptakes for STR and ACE, and the results are tabulated.

The removal efficiency of ACE, IBF, and STR were calculated using the following equation (1)

$$\text{Removal efficiency} = \frac{C_o - C_t}{C_t} \times 100 \quad (1)$$

Where, the initial and final concentrations of the adsorbate – pharmaceuticals are given by C_o (mmol L⁻¹) and C_t (mmol L⁻¹). The samples are were collected at predetermined time intervals, filtered and collected, and the residual concentrations of target compounds were determined.

The adsorption capacity 'q_t' at time 't' was calculated according to the following equation:

$$q_t = \frac{(C_o - C_t)V}{m} \quad (2)$$

Where, the quantity of target compound adsorbed by the composite is given by q_t is, m is the mass of the composites, and the initial solution volume (L) is represented by V .

3.4.2. Adsorption of Acetaminophen, Ibuprofen and Streptomycin by NFO@SiO₂@APTS. (Batch adsorption Experiments)

As the NFO@SiO₂@APTS showed higher adsorption efficiency for lower concentrations of the target pharmaceuticals. The pharmaceutical concentration range of (6-14 mg L⁻¹), the adsorbent dosage of 10-30 mg and a pH range of 3.0 – 8.0 was considered. The adsorbent properties of the NFO nanocomposite were investigated by analyzing the influence of various parameters as mentioned in section 3.4.1.

3.4.3. Adsorption of Acetaminophen, Ibuprofen and Streptomycin by NFO@SiO₂@APTS@HPCD. (Batch adsorption Experiments)

The NFO@SiO₂@APTS@HPCD were investigated for their adsorption efficiency by analyzing the various parameters as mentioned in section 3.4.2.

3.4.4. Adsorption isotherm

The adsorption isotherm for the NFO nanocomposite – pharmaceuticals' systems were determined by using 10 mg concentration of nanocomposites in 100 ml of the given pharmaceuticals at a concentration between 6- 14 mg L⁻¹. The IBF, ACE and STR solutions were mixed at pH-6.0, pH-7.0, and pH-5.0, respectively for 30 mins in 250 ml flasks. Aliquots were collected, decanted and analyzed for IBF, ACE and STR concentrations from

their respective samples using a UV spectrophotometer. The nature of the interaction between the pharmaceutical pollutants and the nanocomposite and maximum adsorption capacity was elucidated by analyzing the obtained data with Langmuir and Freundlich adsorption isotherms as given in Eq. (3) & (5).

$$\frac{C_e}{q_e} = \frac{1}{K_L} + \frac{1}{q_m C_e} \quad (3)$$

Where, q_e is the amount of contaminant retained at equilibrium (mg g^{-1}); q_m is maximum sorption capacity (mg g^{-1}). (L mg^{-1}) C_e is the equilibrium concentration of contaminant (mg L^{-1}); and K_L is the Langmuir model parameter related to adsorption energy.

Freundlich adsorption isotherm model describes a non-uniform active site energy distribution, which is represented as,

$$\log q_{eq} = \log k_F + \frac{1}{n} \log C_e \quad (4)$$

Where q_e is the amount of contaminant retained at equilibrium (mg g^{-1}); and C_e is the equilibrium concentration of contaminant (mg L^{-1}), and k_F and n denote the Freundlich constants.

3.4.5. Regeneration of the adsorbent NFO@SiO₂@GPTS

The desorption experiments were carried out by described by (Zhang et al. 2013) with some modifications IBF adsorbed nanomaterial was stirred in a 10ml mixture of water and HCl (0.01M L⁻¹) solution for 20 min. The pH of the mixture was about 3.0- 4.0, and the adsorbent was separated magnetically and decanted. Finally, it was washed with water and ethanol to remove excess HCl or NaOH.

3.4.6. Regeneration of the adsorbent NFO@SiO₂@APTS

The desorption experiments were carried out, as described by (Hozhabr Araghi and Entezari 2015). Post the adsorption process; the pharmaceutical pollutant loaded nanocomposites were stirred in 25 ml of the 0.01 M NaOH solution maintained at pH between 8.0- 9.0 for 1 hr. Finally, the solution mixture was washed with distilled water and ethanol to remove the pharmaceuticals, and the adsorbent was separated magnetically. The washing process was repeated until no pharmaceuticals were detected in the supernatant by

the UV spectrophotometer. The reusability of the regenerated adsorbents was investigated by conducting adsorption experiments for many cycles.

3.4.7. Regeneration of the adsorbent NFO@SiO₂@APTS-HPCD

The desorption of the pharmaceuticals attached to the nanocomposites was carried out by stirring a buffered solution of 30 ml maintained at pH 8.0 for 1 hr. The solution mixture was later washed with ethanol to remove the pharmaceuticals in the solution, and the adsorbent was magnetically decanted. The adsorbents were washed till no pharmaceuticals were detected in the supernatant by the UV spectrophotometer. Post this process, the adsorbents were investigated for regeneration ability by conducting adsorption experiments for many cycles.

CHAPTER 4

RESULTS AND DISCUSSION

The nickel ferrite nanoparticles which were synthesized by co-precipitation method were characterized XRD analysis to determine the crystalline nature of the nanoparticles. The morphology of the crystalline nanoparticles was further studied by HRTEM and the optimized nickel ferrite nanoparticles were determined. The nanoparticles were then coated with glycidyloxypropyltrimethoxysilane (GPTS) and aminopropyltrimethoxysilane (APTS). The coated nanoparticles attained a spherical morphology with FTIR confirming the formation of coating by the presence of functional groups on the coated nanoparticles. GPTS required attaching of cysteine to be used as an adsorbent, this resulted in reduction of yield. Thus, APTS coated nanoparticles were further coated with hydroxypropyl- β -cyclodextrin (HPCD) which was analysed for its crystallinity and morphology by XRD and FESEM. The formation of the HPCD grafted nanocomposite was confirmed by the bond formation with the NFO@APTS. The as-prepared nanocomposite with silane coatings and post coating with HPCD was analysed for its adsorption efficiency towards target pharmaceuticals IBF, ACE and STR. In comparison to the silane coatings alone, the HPCD grafting proved to be more efficient in the removal of the target pharmaceutical pollutants.

4.1. X-Ray Diffraction analysis

4.1.1 Optimization of the size distribution of nanoparticles:

The NiFe₂O₄ nanoparticles, which is represented by the code NFO 1, NFO 2 and NFO 3, were analyzed by XRD, as shown in Fig. 4.1. The XRD pattern of the nanoparticles reveals the standard pattern of NiFe₂O₄ (ICDD No: 01-086-2267) with the diffraction planes (220), (311), (400), (511), and (440) confirming the cubic spinel phase (Streckova et al. 2015). No mixed phases were observed from XRD, which indicates the purity of the sample. The average crystallite size for the most intense peak (311) was calculated using the Debye-Scherrer formula.

$$D = \frac{kl}{b\cos\theta} \quad (3)$$

Where, D is the average crystallite size, k is the Scherrer constant (0.9), λ is the wavelength (0.154 nm), β is the angular width of the half-maximum intensity and θ is the Bragg's angle in degree units. Further XRD peaks also confirm the polycrystalline nature of the nanoparticles. It can be observed that with the increase in surfactant ratio, the peaks widen, this could be attributed to the nanocrystalline nature of the particles. This is in concordance with the work by Khoso et al. (2021) wherein the wider peaks confirm the reduction in the size of the nanoparticles. The lattice constant (a) and the full width half maximum (FWHM) β was calculated for each of the samples from the values obtained from XRD data as depicted in Table 8.

Table 8. The lattice constants and crystallite size of varied ratios of surfactant concentrations.

Sample Code	Ratio (mmol)	D, Crystallite size nm	Lattice parameter (a)Å
NFO 1	1:1	12.31	8.39
NFO 2	1:2	10.55	8.34
NFO 3	1:2.5	9.97	8.28

The lattice parameter "a" was calculated using the Bragg equation:

$$a = d \times (h^2 + k^2 + L^2)^{(1/2)} \quad (4)$$

Where "d" is the lattice distance and (hkl) is the miller indices. As it is evident that NFO 3 has wider peaks in comparison to NFO 2 and NFO 1, indicating the nanocrystalline nature of the nanoparticles. Hence, NFO 3 was considered for further experiments.

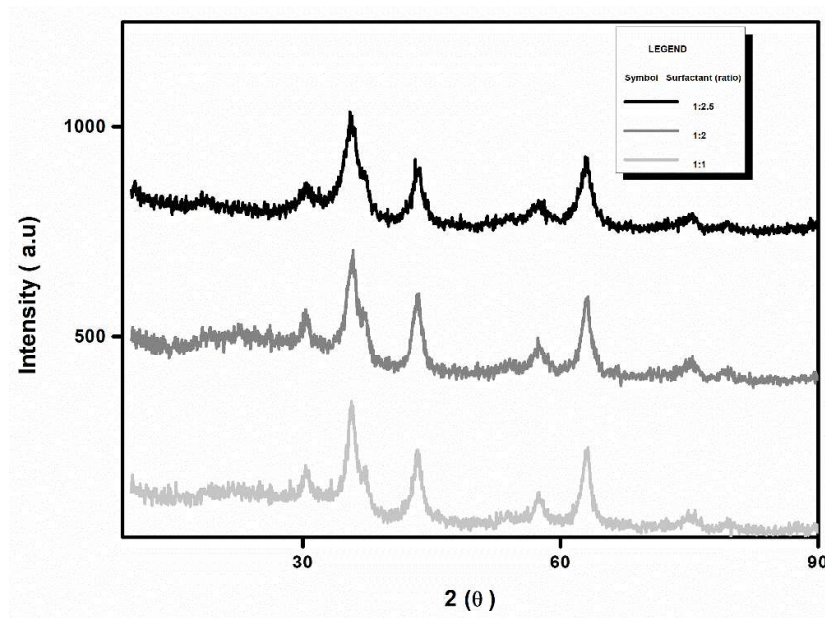


Figure 4.1: XRD graphs of nickel ferrite nanoparticles for different ratios (1:1, 1:2, 1:2.5)

The optimized NiFe_2O_4 nanoparticles were further modified with GPTS-Cys as represented in the Figure 4.2. The XRD pattern exhibited significant increase in intensity of the planes (220), (311), (400), (511) and (440). Reduction in the peak width could be attributed to the increase in the size of the nanoparticles which is further confirmed by TEM analysis as shown in Figure 4.5. The peak at the angle 23.21 could be attributed to SiO_2 which is in concordance with the work reported by (Khalafi-Nezhad et al. 2015). Thus, the results confirm the covalent grafting of $\text{SiO}_2@\text{GPTS}$ with NFO nanoparticles also the modification did not change the phase of the NFO nanoparticles. The average crystallite size of nanoparticles is calculated by considering the peak with maximum intensity i.e., (311) which was found to be 9.24 nm.

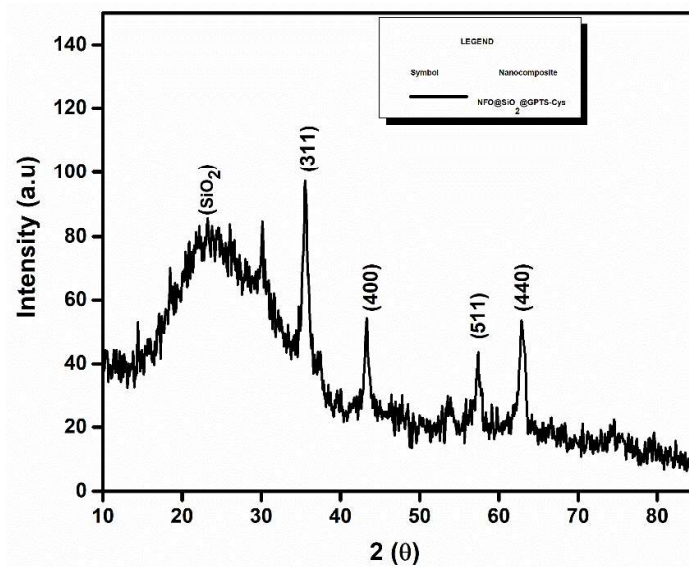


Figure 4.2: XRD patterns of NFO@SiO₂@GPTS-Cys

The NiFe₂O₄ nanoparticles which were modified with APTS were also investigated for their XRD pattern as represented in Figure 4.3. It can be observed that the APTS modified nanocomposite exhibit a higher peak intensity in comparison to the cysteine attached GPTS nickel ferrite nanocomposite. This could be due to the fact that the GPTS coating on the nickel ferrite nanoparticles provided an extra layer of cysteine molecule attached to it. However, in the former case the nickel ferrite nanoparticle contains only the APTS coating. From the XRD pattern it can also be concluded that the coating of APTS onto the nanoparticles did not affect its crystallinity. Which is in concordance with the work by (Wang et al. 2010) wherein the crystallinity of the nanoparticles was stable even after the coating of APTS. One more prominent observation in this XRD pattern is the peak broadening and the decrease in the peak intensity of the nickel ferrite nanoparticles after coating of APTS. Similar results were also reported by (Ghutepatil et al. 2019) where the APTS coated MnFe₂O₄ showed peak widening and decrease in peak intensity in comparison to the bare MnFe₂O₄.

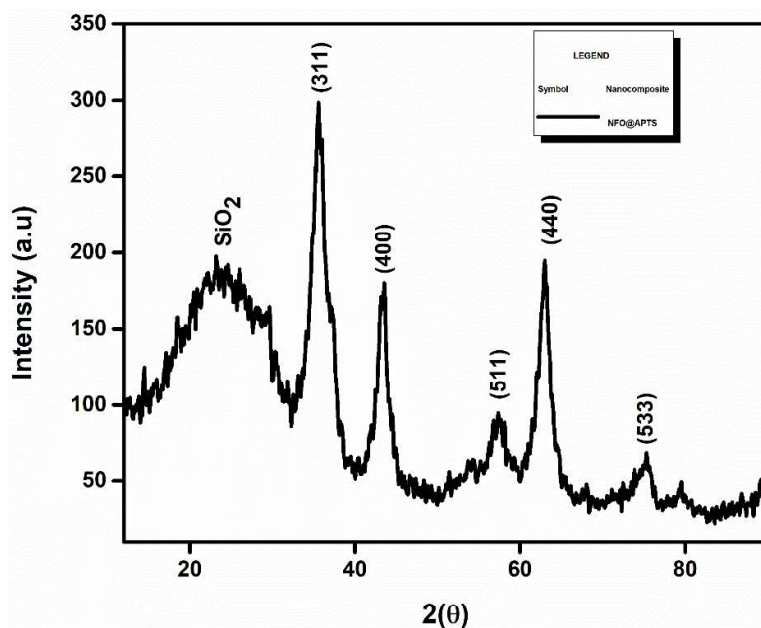


Figure 4.3: XRD patterns of NFO@SiO₂@APTS nanocomposite

The HPCD-APTS modified NiFe₂O₄ nanoparticles when analysed for their XRD pattern, it was noted that there no significant difference in the XRD patterns. However, the peak from 20 to 35 °C widened as depicted in the Figure 4.4. This could be attributed to HPCD grafting on the NFO@SiO₂@APTS, this similar observation was also seen when GPTS coating was attached with L-cysteine. However, in both the cases the crystallinity and phase of the nanoparticles was not affected. Similar results were also reported by Cao et al. (2009) wherein, the broad band from 18 - 29 °C was attributed to the amino silane and the β-cyclodextrin onto the iron oxide nanoparticles. This is in concordance with the data obtained in the current research. However, the peaks obtained in the current work at 18 - 29 °C are wider, this could be assumed to be the silica coating along with APTS. The rest of the peaks appear to be narrower thus indicating the increase in the size of the nanocomposites. An interesting observation in the XRD patterns of NFO@SiO₂@APTS-HPCD is the peak from 10- 29°C appears to be split into two peaks. This is consistent with data reported by (Nasiri and Alizadeh 2021) wherein two peaks were observed due to the amorphous nature of the HPCD. The rough peaks with comparatively lower intensities for NFO@SiO₂@GPTS-Cys, NFO@SiO₂@APTS and NFO@SiO₂@APTS-HPCD could be attributed to the silica coating onto the magnetic nanocomposites. This is consistent with the work by Singh et al. (2021) ,where coating APTS to silica magnetic nanoparticles reduced the peak width, thereby confirming the bonding of silane with the nanoparticles.

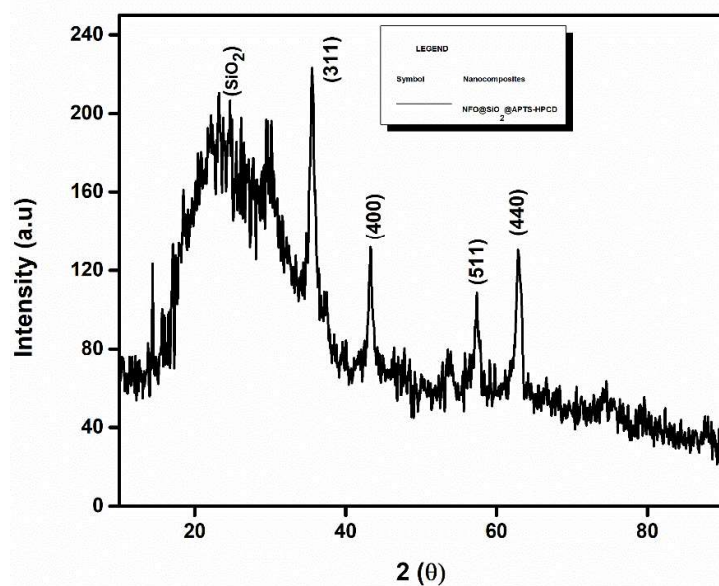
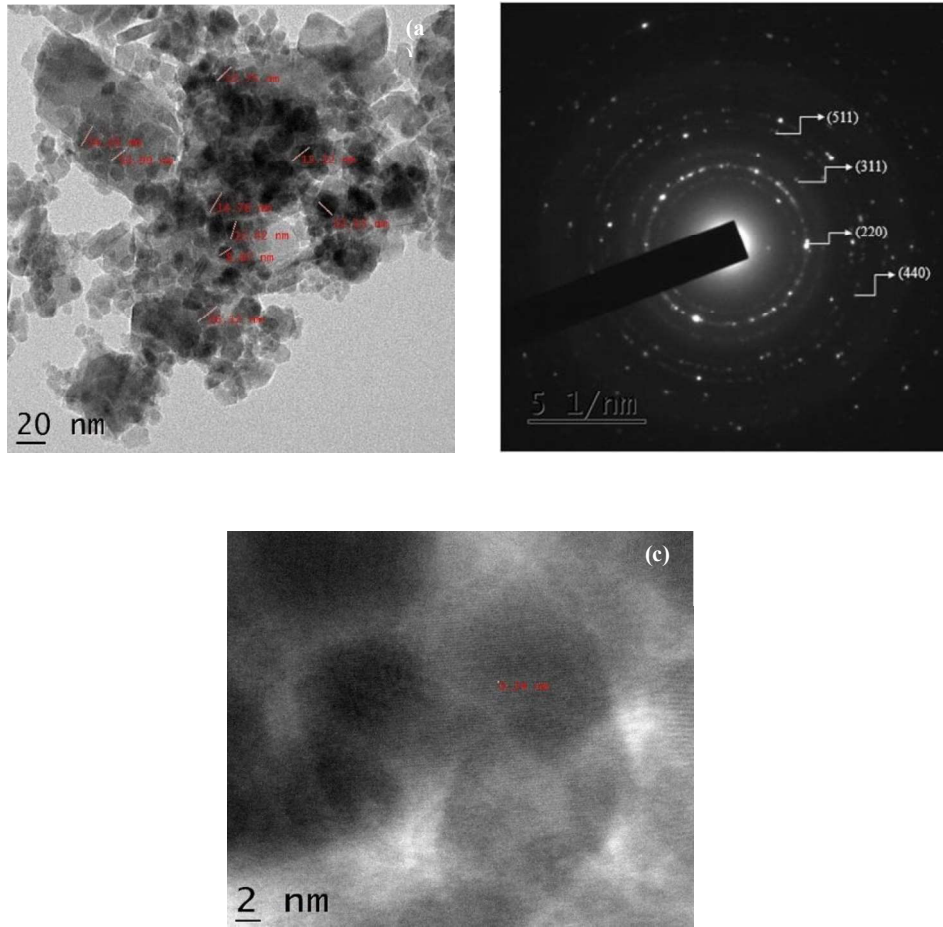


Figure 4.4: XRD patterns of NFO@SiO₂@APTS-HPCD

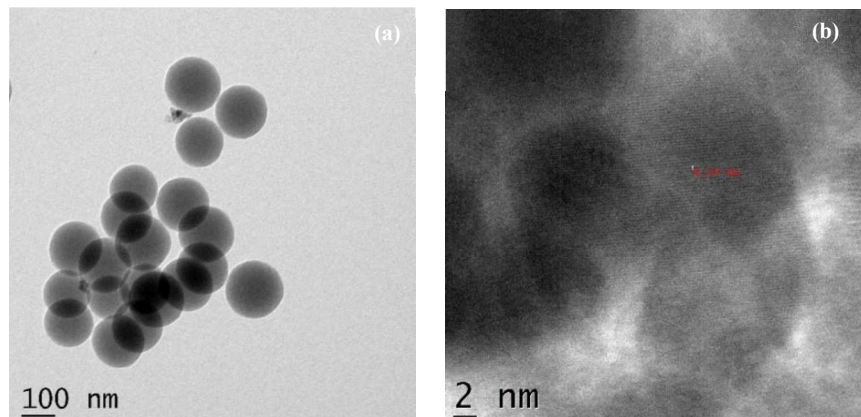
4.2. Transmission Electron Microscopy analysis:

The morphology and the size of the nickel ferrite nanoparticles were determined by TEM analysis as shown in Figure. 4.5 (a). The TEM results indicate that spherical NFO nanostructures obtained by the co-precipitation method is uniform in morphology and has a narrow range of particle size. The prepared nanoparticles revealed a narrow size distribution between 8-16 nm with cuboidal and spherical morphology. Moreover, the size range was smaller compared to the previously reported value of 28 nm for the single domain limit of NFO nanoparticles (Maaz et al. 2009). The corresponding presence of lattice fringes as depicted in the Figure 4.5 (b) obtained from the HRTEM images indicates the high crystallinity of the material and interplanar spacing, d (Å) of 0.24 nm, which is in good agreement with the $h k l$ indices of (311) plane of face-centred cubic crystal. The interplanar spacing calculated from the SAED pattern of the bare nickel ferrite nanoparticles contains four rings from the corresponded to their respective $h k l$ indices: 4.80 Å (220), 1.47 Å (440), 2.53 Å (311), 1.60 Å (511). Figure. 4.5 (c) exhibits a good arrangement of the lattice fringes confirming the good crystallinity with a lattice spacing of 0.24 nm, which attributes to the (311) plane orientation. The NFO nanoparticles when coated with GPTS-Cys were analysed for their size and morphology by TEM analysis as represented in Figure .4.6. Post coating of GPTS-Cys on to the silica nickel ferrite nanoparticles, it attained a narrow size

distribution of 130-150 nm. This confirms the covalent grafting of the coating onto the as-synthesised nanoparticles.



**Figure 4.5: a) TEM image of nickel ferrite nanoparticles at 20 nm scale (8 -16 nm);
b) SAED pattern of nickel ferrite nanoparticles; c) lattice fringes of nickel ferrite nanoparticles at 2 nm scale.**



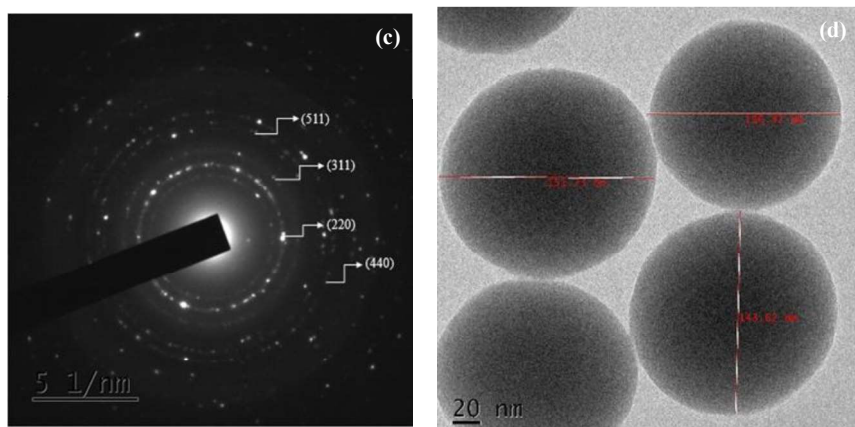
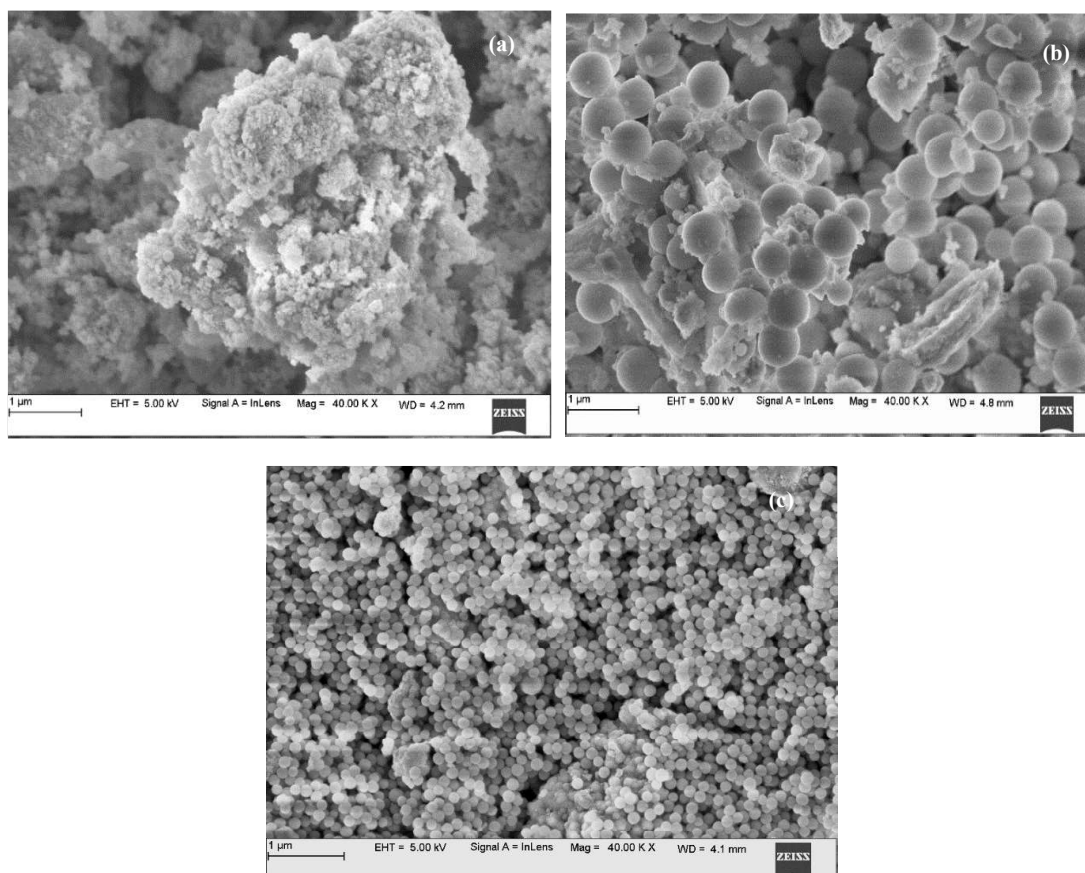


Figure 4.6: TEM- HRTEM images of NiFe₂O₄ nanoparticles (a) 100 nm scale (b) 2 nm scale (c) Corresponding SAED pattern and (d) NiFe₂O₄@SiO₂@GPTS@Cys nanomaterial at 20 nm scale

4.3. Field Emission Scanning Electron Microscopy analysis

The coating of APTS which was performed for three different concentrations i.e 20 μ L, 40 μ L and 60 μ L was analysed for its morphology as depicted in Figure 4.7. The APTS coating that provided stable disperse particles was chosen for further experiments. From Figure 4.7 (a) it can be seen that for 20 μ L APTS the particles appear agglomerated and no uniform structures are observed. This could be due to the incomplete polymerization of the APTS molecules onto the surface of the nanoparticles. Further increasing the concentration to 40 μ L the spherical nanocomposites were witnessed, however, the Figure 4.7 (b) shows incomplete polymerization as the particles appear to be aggregated. When the concentration of the APTS was increased further to 60 μ L uniform surface with excellent dispersibility was observed as depicted in Figure 4.7 (c). This completes the silanization process between the aminosilane and the silica groups. During this process the silanes undergo condensation to form polymers; these polymers form covalent siloxane bonds with the exposed silanol groups of silica (Yamaura et al. 2004). As indicated in the Figure 4.5 (a) the particle size distribution of the synthesized nickel ferrite nanoparticles was observed to be around 10 – 15 nm. Post functionalization nanocomposite with APTS an increase in particle size was observed ranging between 50-100 nm. This confirms the coating of the APTS onto NFO@SiO₂. which is in accordance with the literature Šulek et al. (2010b) wherein NFO the size of the silica coated magnetite nanoparticles was observed to increase after coating with APTS.

The elemental composition of NFO composite after coating with silica followed by APTS was determined using EDX analysis as shown in Figure 4.7 (b) and (c). Nickel, Iron, Oxygen, and Silicon were found at relevant peaks of the EDX graph. It can also be observed that the spectrum shows higher carbon levels in Figure 4.7(c) compared to Figure 4.7 (b) due to the presence of hydrocarbon chains in APTS. A study on the elemental composition of SiO₂-Co@APTS core-shell nanoparticles by (Zhang et al. 2016) reported a similar kind of increase in carbon peak due to the presence of APTS. Further, the presence of amine functional groups on the surface of the nanocomposite was confirmed by FTIR analysis. The HPCD molecules are amorphous and poorly soluble in their native form, however when functionalized onto the nanoparticles or to substrate they become highly soluble and increase the dispersibility of the nanoparticles (Yu et al. 2014). Thus, they form aggregates in water when present in their native form (Bonini et al. (2006). In the case of solvents like DMSO these CD molecules have weak interaction with each other and do not form any networks (Deng and Thompson 2010) . In the current work HPCD exhibits weak hydrogen bonding with APTS, to improve this interaction the hydroxyl groups have to converted into carboxyl groups. Thus, a catalyst like maleic anhydride will aid in the conversion of hydroxyl groups to carboxyl groups which in turn will be responsible for the interaction between the HPCD and the APTS of the nanocomposite.



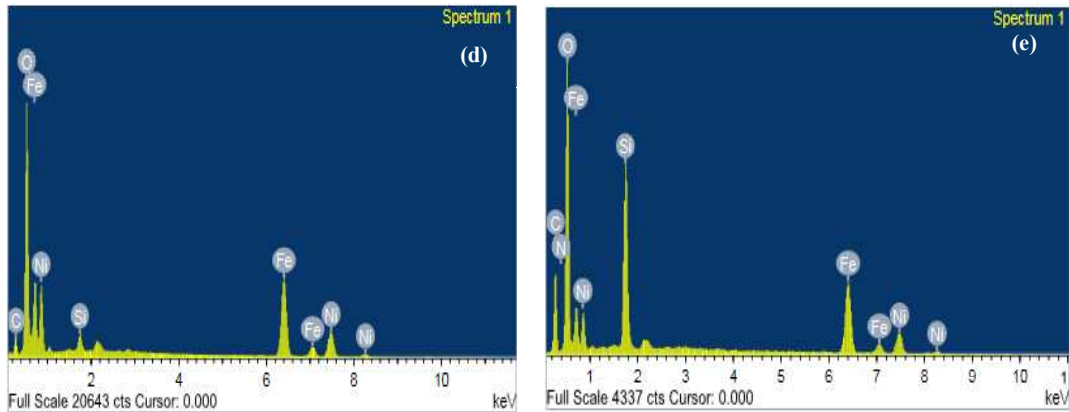
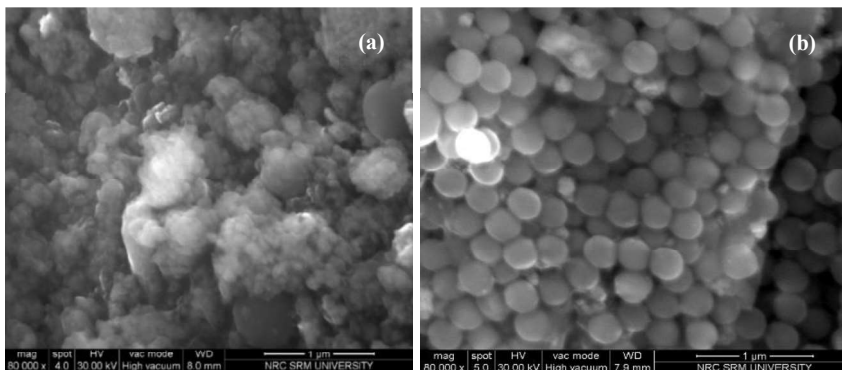


Figure 4.7: FESEM analysis performed at 40kX magnification at 1 μm scale of different APTS coating concentrations (a) 20 μL (b)40 μL and (c)60 μL (d) EDX analysis of NFO@SiO₂(e)NFO@SiO₂@APTS (60 μL)

The formation of bonds was further confirmed by the FTIR analysis. From the Figure 4.8 (a) it can be noted that 1 mmol concentration of maleic anhydride resulted in the formation aggregates with no defined morphologies. However, increasing the concentration further to 2 mmol a uniform coating on the nanocomposite was observed. The formation of the coating confirms the bonding between the amine groups of NiFe₂O₄@SiO₂@APTS with carboxyl groups of modified HPCD forming stable amide bonds which can be correlated with the work by Reza et al. (2021). When the concentration of maleic anhydride was increased further to 3 mmol high agglomeration was observed as indicated in the Figure 4.8 (c). This could be due to the increased concentration of maleic anhydride resulting in the formation crosslinking of the polymer molecules(Renard et al. 2005).



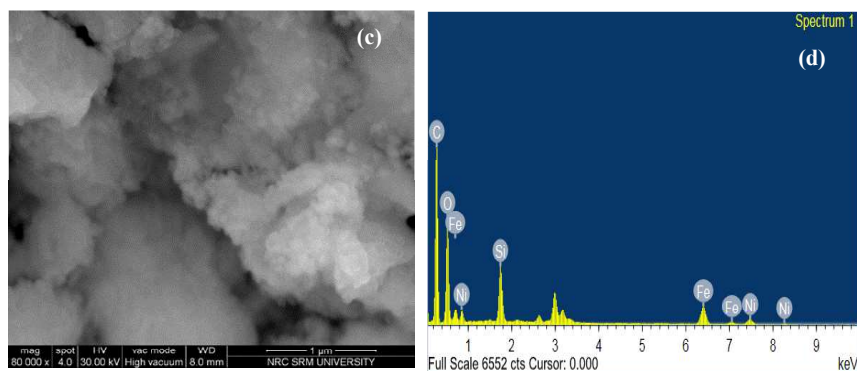


Figure 4.8: FESEM analysis performed at 30kX magnification at 1 μm scale of different concentrations of maleic anhydride (a) 1 mmol (b) 2 mmol and (c) 3 mmol (d) EDX analysis of NiFe₂O₄@SiO₂(e)NiFe₂O₄@SiO₂@APTS (60 μL)

Thus, 2 mmol concentration of maleic anhydride was chosen as the optimum concentration required for the coating HPCD onto the NiFe₂O₄@SiO₂@APTS.

4.4. FTIR analysis

The FTIR spectral analysis of the nickel ferrite nanoparticles was carried out between the wave numbers 400 and 4000 cm⁻¹ from Figure 4.9. The characteristic vibration bands of NFO confirms the spinel structure of the nanoparticles wherein, the absorption bands at 401cm⁻¹ and 543.07cm⁻¹ corresponds to the vibration of the octahedral groups and tetrahedral groups respectively (Liu et.al 2013), which are indicative of the formation of nickel ferrite nanoparticles. The absorption peak at 579 cm⁻¹ represents the intrinsic stretching vibration of the metal at the tetrahedral site (Kasapoglu et al. 2007). The less intensive peak at ~1600 cm⁻¹ and ~2300 cm⁻¹ represents O-H stretching vibration interaction H bonds and the traces of CO₂ adsorbed (Maensiri et al. 2007). It can also be observed that the normal mode of vibration of tetrahedral cluster is higher than the vibration of the octahedral cluster. This is due to the tetrahedral cluster having shorter bond lengths and the octahedral cluster having longer bond lengths (Lassoued et al. 2018).

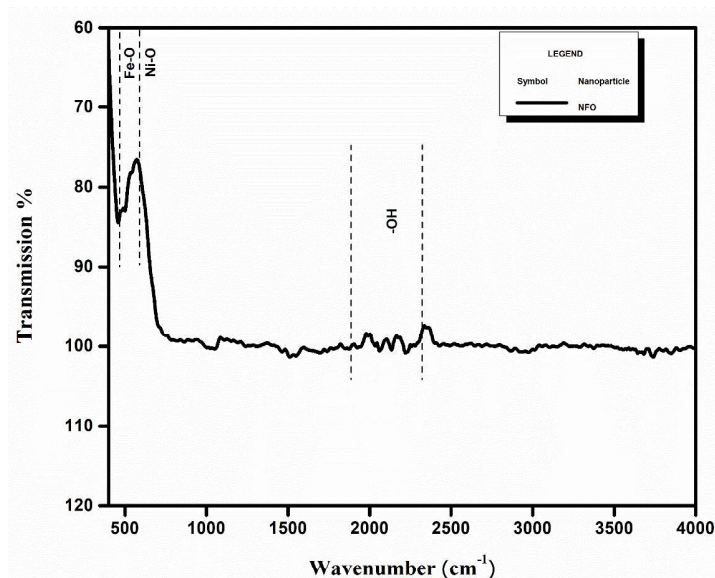


Figure 4.9: FTIR spectrum of nickel ferrite nanoparticles

The FTIR Spectrum of the bare and the coated NFO nanoparticles were performed at frequencies ranging between 400 - 4000 cm^{-1} as represented in Figure 4.10. The figure reveals the vibration bands of Ni-O and Fe-O indicate the presence of nickel ferrite nanoparticles. Further, the presence of GPTS on the surface of nickel ferrite nanoparticles was confirmed by the characteristic absorption bands at 943.11 cm^{-1} and 1077 cm^{-1} band which corresponds to the presence of epoxy group and Si-O-C stretching respectively (Tiringer et al. 2018a). In the NFO@SiO₂@GPTS@Cys nanomaterial spectrum, new bands at 1621 cm^{-1} and 1583 cm^{-1} emerge as a result of nucleophilic addition between the thiol and the epoxy groups (Nair et al. 2014) NFO@SiO₂@GPTS@Cys. This bonding takes place due to the basic condition created by sodium hydroxide in which the hydroxide group deprotonates the thiol group to form thiolates (Stuparu and Khan 2016). The thiolate acts as a nucleophile and attacks the less hindered site of the epoxide unit which is known as the ring opening reaction, thus leading to a thio-ether linkage and a secondary hydroxyl group (Konuray et al. 2017). This bond formation delineates the ambiguity of the adsorption of ibuprofen taking place which is discussed below.

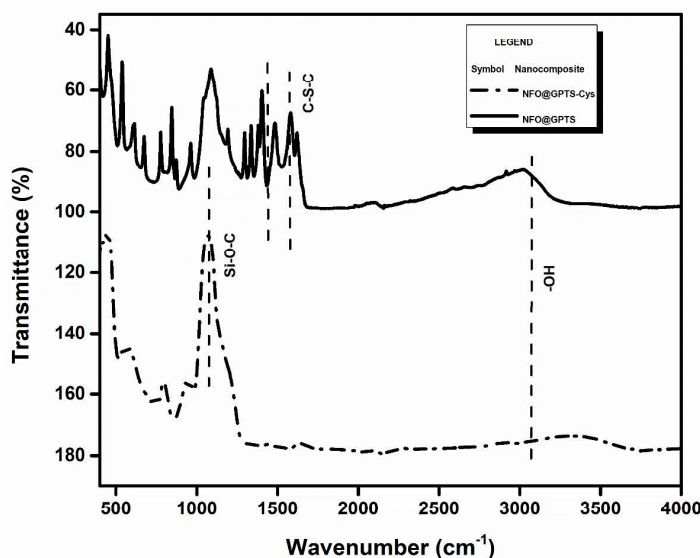


Figure 4.10: FTIR spectrum of (a)NFO@SiO₂@GPTS@Cys (b) NFO@SiO₂@GPTS (c) NFO

The FTIR spectrum of the APTS modified NFO@SiO₂ nanocomposites Figure 4.11 exhibits the vibration modes at 1073 cm⁻¹ in the graph may be attributed to the presence of the silanol group (Chapa Gonzalez et al. 2014). Also, the vibration modes at 1645 cm⁻¹, 3440 cm⁻¹ correspond to the NH stretching and bending of the propyl groups on the surfaces of NFO@SiO₂@APTS nanocomposites. These absorbance bands indicate successful bonding of the APTS on the surfaces of NFO@SiO₂, which is in concordance with the results reported in the literature (Karim et al. 2012; Shahbazi et al. 2019). Confirmation of the presence of aminosilane on the composite surface is discussed further in TGA.

The NFO@SiO₂@APTS nanocomposites post grafting with HPCD revealed vibration bands at that are responsible for the grafting. Since the bonding of HPCD with APTS is a new approach, no literature was available for the comparison of the data. Thus, in order to determine the bond formation of carboxyl group and amine groups of APTS, this work can be correlated with the similar work by (Badruddoza et al. (2012) wherein, the carboxymethyl-β-cyclodextrin was successfully grafted onto the APTS coated iron oxide nanoparticles. The vibration modes that correspond to the hydroxyl groups of the cyclodextrins appear with a sharp peak at 3400 cm⁻¹ as indicated in the Figure 4.12. However, the HPCD molecules are reported to show vibration modes between 1600- 3400

cm^{-1} as reported by Yuan et al. (2015) where they studied the the different substitution sites of HPCD. The absence of this vibration band confirms the formation of carboxyl groups. As HPCD molecules do not form bonds readily with the amine groups, maleic anhydride was used to catalyse the reaction. The maleic anhydride converts an OH group to a carboxylic acid forming $-\text{O}-\text{CO}-\text{CH}=\text{CH}-\text{COOH}$. The presence of the new vibration modes from $1500 - 800 \text{ cm}^{-1}$ corresponds to the amide bond formation which is agreement with the work by Ji et al. (2020) wherein the amide bond formation in protein were studied. Thus, the HPCD was successfully grafted onto the $\text{NFO@SiO}_2\text{@APTS}$ nanocomposite as depicted in Figure 4.12.

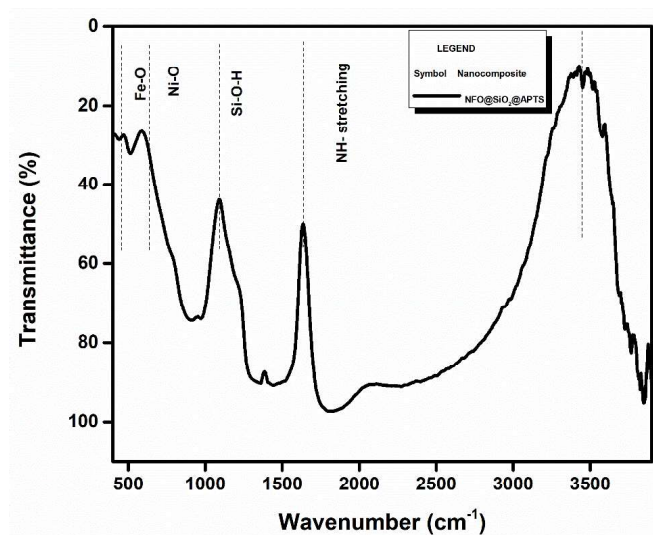


Figure 4.11: FTIR analysis of the $\text{NFO@SiO}_2\text{@APTS}$ nanocomposite

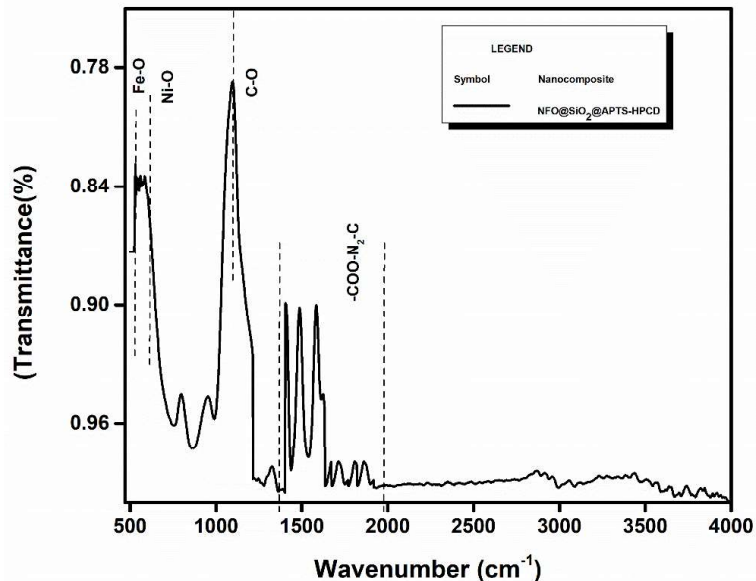


Figure 4.12: FTIR analysis of the NFO@SiO₂@APTS-HPCD nanocomposite

4.5. TGA analysis

The TGA curve represents the thermal behaviour of the prepared NiFe₂O₄ sample consists of the following three stages. The first stage occurs at the temperature range of 30 -116°C with a mass loss of 11 wt.% owing to the loss of absorbed water molecules. The second weight-loss region is around 10.91 wt% between 116 °C and 300 °C, which could be attributed to the evaporation of surfactants present in the sample. The third stage takes place at a temperature from 300 °C to 676 °C corresponds to the solid-solid interaction between the produced nickel and ferric oxides with a weight loss of 18.78 wt.%. Further, the crystallisation occurs at temperatures above 668 °C as shown in Figure 4.13. At a temperature above 668 °C there is no weight loss which indicates the formation of pure nickel ferrite nanoparticles.

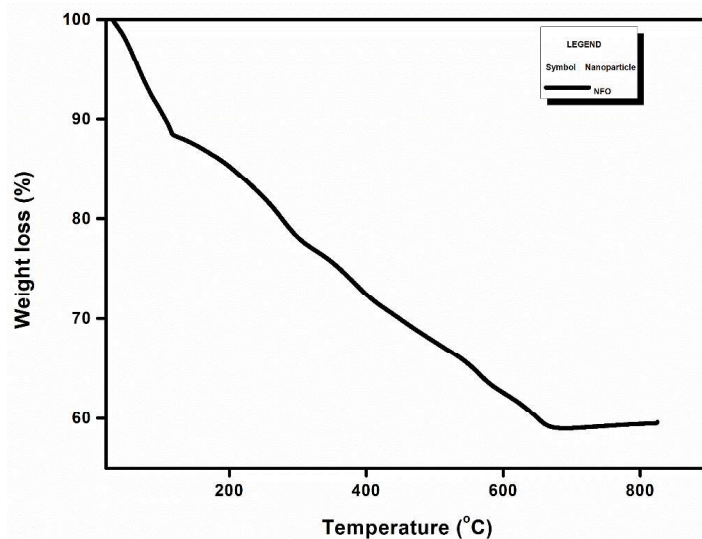


Figure 4.13:

Thermogravimetric analysis curve of nickel ferrite nanoparticles

The thermogravimetric analysis of L-cysteine modified GPTS coated nickel ferrite nanoparticles was examined under a nitrogen atmosphere at 100-800 °C at 10°C min⁻¹ as shown in Figure 4.14. At a temperature range of 10-223°C, a slight mass loss is observed which could be due to the evaporation of the adsorbed solvent molecules. The first decomposition could be attributed to the breakdown of organic compounds present like GPTS-cysteine at a temperature range of 231°C. Further, the thermal decomposition of the rest of the nanomaterial takes place at a temperature range of 231-557 °C. The thermal decomposition of the silane-modified nickel ferrite nanoparticles occurs in three stages. The first two stages correspond to the thermal decomposition resulting in vaporization of the solvent molecules, followed by the GPTS-cysteine coating of the nanomaterial respectively. Whereas the last decomposition occurs due to the decomposition of the residual compounds of the nanomaterial. Similar results have also been reported by Enache et.al (2016) wherein the decomposition of ICPTES - cysteine takes place below 230 °C.

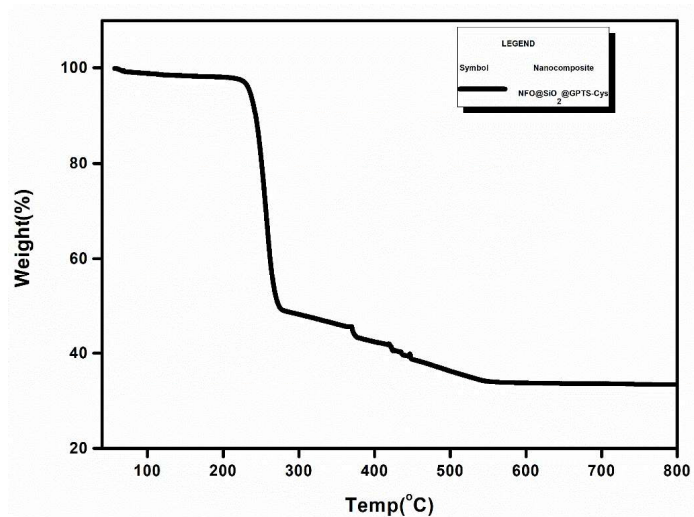


Figure 4.14: TGA analysis of NiFe₂O₄@SiO₂@GPTS-Cys from 40 °C to 860 °C.

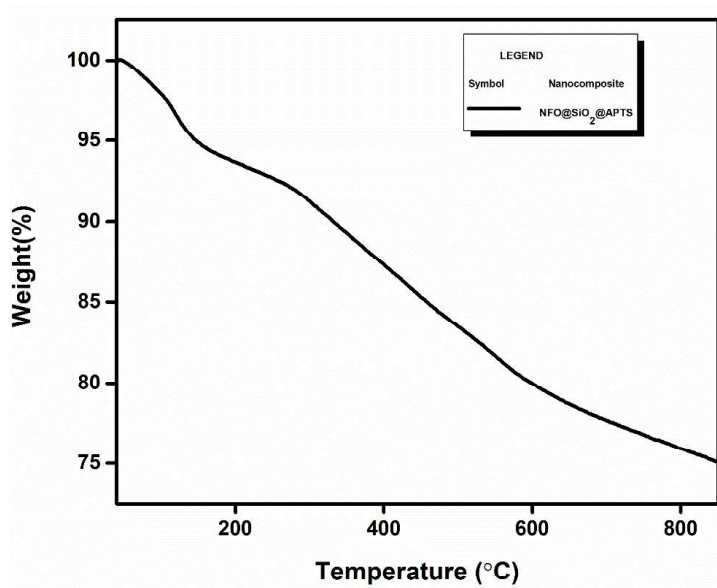


Figure 4.15: TGA analysis of the composite from 40 °C to 860 °C of the APTS coated NFO@SiO₂ nanocomposite.

The TGA analysis of sample NiFe₂O₄@SiO₂@APTS, as depicted in Figure. 4.15 shows two different weight losses. The first weight loss is observed at 108 °C this could be due to the release of the solvent absorbed on the surface of the NiFe₂O₄ nanoparticle. The thermal decomposition of the sample progresses up to 267 °C, with a weight loss of up to 5%. A similar phenomenon takes place in the case of smaller molecules like water and ethanol

that are entrapped in porous matrices (Hozhabr Araghi and Entezari 2015). The second weight loss of 13%, was observed with further increase in temperature from 267 °C to 692 °C, which could be due to the decomposition of organic ligands (Varganici et al. 2012), that are present in APTS coated on the surface of silica-coated nanoparticles (Čampelj et al. 2009; Shen et al. 2011). Thus, the total weight loss has been estimated to be 19% of the nanocomposite.

The thermogravimetric analysis of the nanocomposite post grafting of HPCD was analysed as represented in Figure 4.16. The weight loss occurs at two stages, wherein the first decomposition could be attributed to the release of water and solvent molecules present on the nanocomposite observed at 80 – 185 °C. The second stage of the weight loss takes place from 185 – 410 °C, here the decomposition of the APTS molecules that are attached the cyclodextrin cavities could be taking place. The mass loss of 1.01 % was observed for the HPCD grafted nanocomposite. This is in concordance with the report by (Cao et al. 2009b) wherein the aminosilane iron oxide nanoparticles were grafted with cyclodextrins. Thus, the total weight loss observed from the two stages 1.5 % which confirms the functionalization of the HPCD on to the nanocomposite. The current work is also agreement with the Swain et al. (2020) where a very small weight loss was observed post functionalization with the cyclodextrin.

4.6.VSM analysis:

The specific magnetisation of the sample is investigated using VSM measurement with applied magnetic field of $20\text{k}\pm\text{Oe}$ at room temperature 300K. The magnetic property of the nanoparticles was measured using a hysteresis curve. The graph depicts a clear 'S' shaped curve portraying the superparamagnetic behaviour at room temperature as shown in the Figure 4.17 The magnetisation versus the magnetic field hysteresis curve of NiFe_2O_4 sample is a completely a narrow hysteresis loop with $M_s = 30.01 \text{ emu g}^{-1}$ and $M_r = 2.01 \text{ emug}^{-1}$ and has almost negligible coercivity. Thus, the saturation magnetisation is found to be lower than that of the bulk material, which is about 55 emu g^{-1} (Jang et. al., 2007). The decrease in saturation magnetisation of the nanoparticles compared to the bulk can be attributed to the presence of canted and disordered spins which prevents the aligning of the spins along the direction of the field (Berkowitz et al. 1980). Along with this effect being pronounced in the smaller particles; the higher number of atoms present on the surface of nanoparticles decreases the saturation magnetisation.

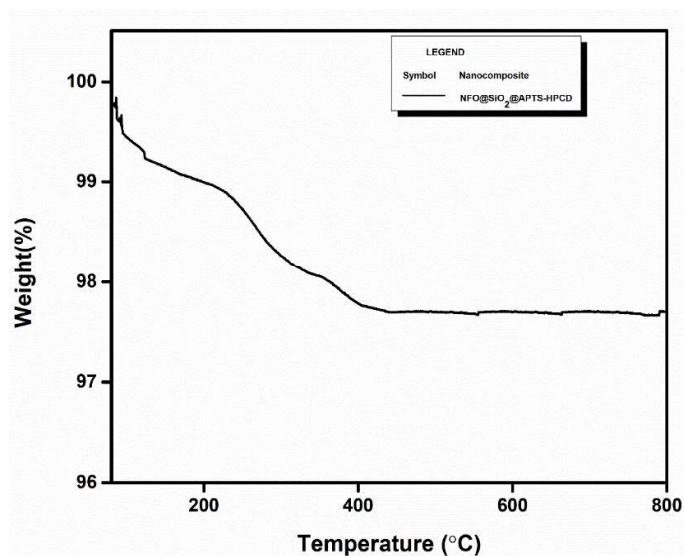


Figure 4.16: TGA analysis of the composite from 40 °C to 860 °C of the HPCD coated NiFe₂O₄@SiO₂@APTS nanocomposite.

To investigate the magnetic properties of the NiFe₂O₄ spheres VSM was performed at 300K. The hysteresis loops show a characteristic superparamagnetic behavior for both of NFO@SiO₂@GPTS and of NFO@SiO₂@GPTS-Cys as shown in Figure 4.18. The saturation magnetisation of NFO@SiO₂@GPTS-Cys is found to be 8.86 emu g⁻¹ which is relatively lower than that of NFO@SiO₂@GPTS (16.02 emu g⁻¹) due to the coating of cysteine. Even at this lower external magnetic field the adsorption of pollutants was found to be effective and becomes the key factor at the time of regeneration of nanoparticles. Similar results have also been reported by Quanguo et.al (2010), where the iron oxide nanoparticles coated with aminosilanes and mercaptosilanes showed lower saturation magnetisation. Further attachment of cysteine had slightly lowered the level of saturation magnetisation.

The magnetic hysteresis curves of the APTS coated and uncoated composites were studied to illustrate the magnetic properties of NFO nanocomposites, as shown in Figure 4.19. It can be observed that the saturation magnetisation (Ms) is 29 emu g⁻¹ and 22 emu g⁻¹ at 20 kOe for NFO and NFO@SiO₂@APTS, respectively. It is evident from the VSM graph that the organic APTS coated nanocomposite has a reduction in Ms, which indicates the formation of the aminosilane coating on the surface of the nanoparticles (Dhavale et al.

2018b; Liu et al. 2004; Sahoo et al. 2016). Further, NFO@SiO₂@APTS exhibited superparamagnetic behavior with nearly zero coercivity and remanence and also responded quickly to an external magnetic field. This phenomenon is favorable for the separation of nanocomposite (solid-liquid separation) post adsorption process and reuse it as a potential adsorbent for many cycles.

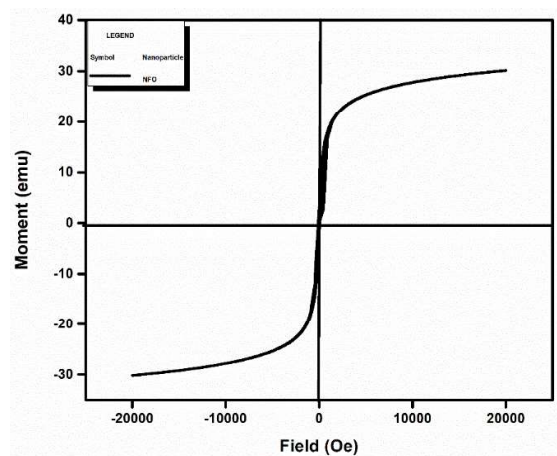


Figure 4.17: Hysteresis loop of the as-prepared nickel ferrite nanoparticles

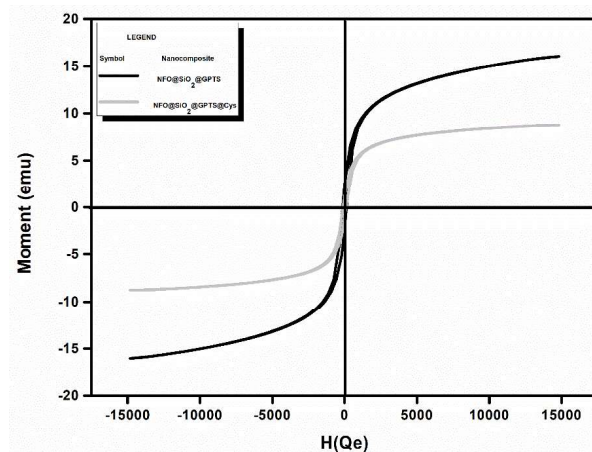


Figure 4.18: VSM analysis of NFO@SiO₂@GPTS and of NFO@SiO₂@GPTS@Cys

The VSM analysis of the HPCD grafted NFO@SiO₂@APTS nanocomposite was also performed to analyze the effect of the grafting on the magnetic properties. As depicted in Figure 4.20 the nanocomposite exhibits a saturation magnetisation (M_s) of 13.24 emu g⁻¹, with zero coercivity and remanence. The M_s value is low compared to the reported value of NFO@SiO₂@APTS as mentioned in the Figure 4.19. This further confirms the

successful functionalization of the HPCD onto the surface of the NFO@SiO₂@APTS. This result is in good agreement with a recent report by Jahanbakhsh et al. (2021) where, the successful functionalization of the carboxymethyl-β-CD led to a significant decrease in the saturation magnetization.

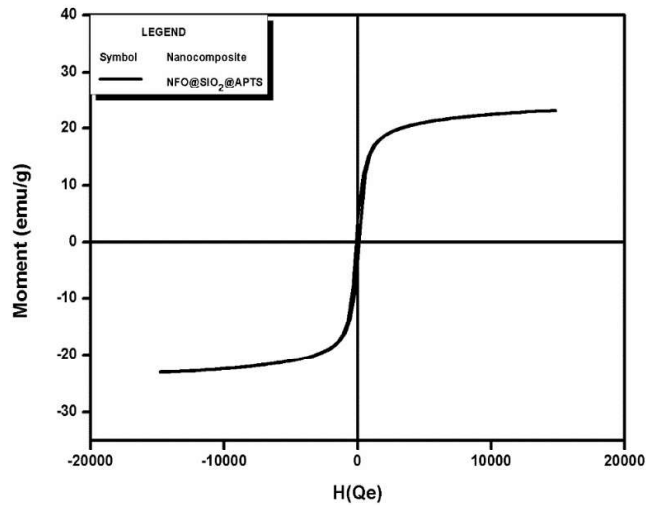


Figure 4.19: VSM magnetisation curve of NFO nanoparticles and NFO@SiO₂@APTS composite.

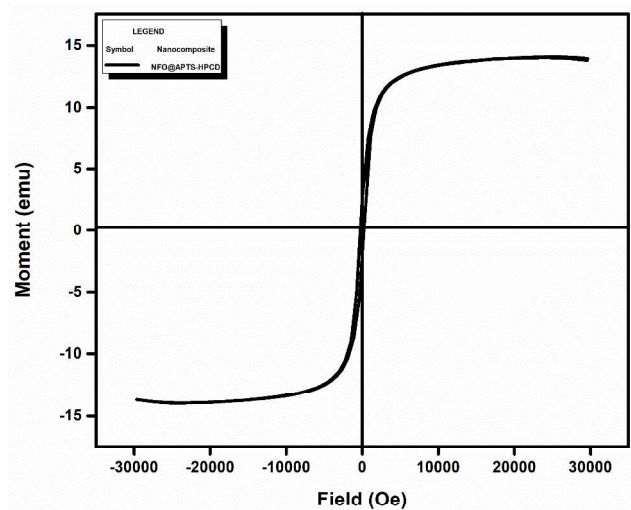
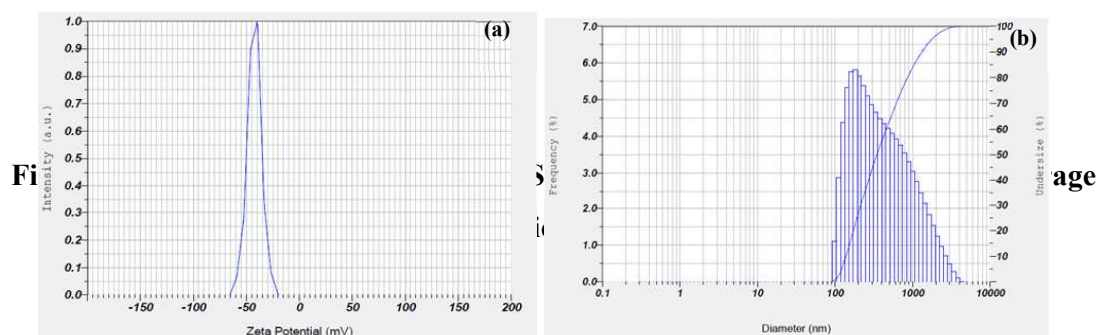


Figure 4.20: VSM magnetisation curve of NFO@SiO₂@APTS-HPCD nanocomposite.

4.7. Dynamic Light Scattering

The information attaining to the hydrodynamic diameter of the core and the functionalised material can be obtained by the DLS analysis. The hydrodynamic diameter of the functionalised nanoparticles was noted to be 313.7nm (Figure 4.21(b)). Amino acid L-cysteine behaves like a zwitterionic molecule with respect to pH (Caldeira et al. 2013). As reported by (Sangeetha and Philip 2013) at pH greater than 5.07 L-cysteine is negatively charged due to the presence of carboxyl group and positively charged due to the presence of ammonium group. Thus, the zeta potential analysis of the NFO@SiO₂@GPTS-Cys was observed to be -42.3mV as depicted in Fig. 4.21(a)). This is concordance with the report by (Bagbi et al. 2017).



4.8. Ninhydrin Test

The successful functionalisation of silica nanocomposites with amino groups was evaluated using the Ninhydrin Test. Figure 4.22 (a) shows the absorbance peak of the supernatant solution at 570 nm under UV-Spectrophotometer, which confirms the Ruhemann's purple chromophore due to the presence of amine groups present in the supernatant that has its origin from aminosilane functionalised NFO@SiO₂. The intensity of the purple color chromophore formation indicated in Figure 4.22 (b) is proportional to the amine concentration, which is in concordance with the literature (Arévalo-Cid et al. 2018; Chertok et al. 2010). Thus, establishing the functionalisation of APTS on NFO@SiO₂ is evident from Ninhydrin Test.

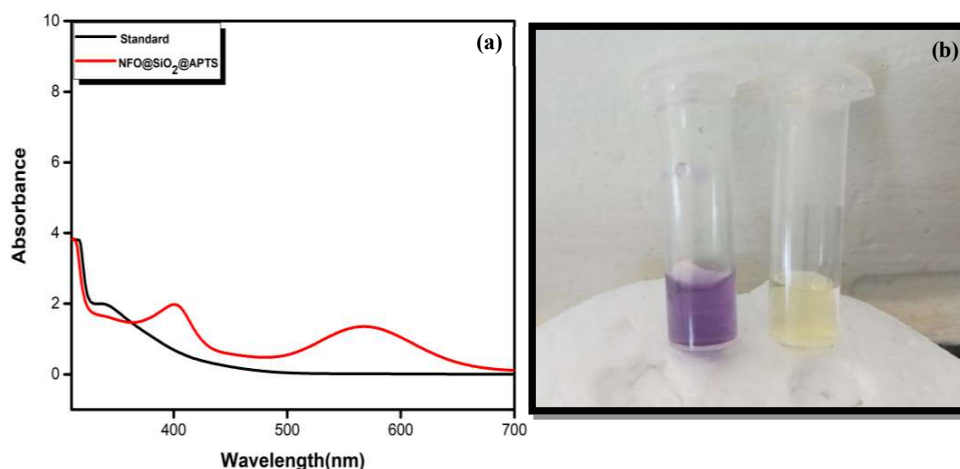


Figure 4.22 a) Absorbance peak observed at 570 nm (b) Ninhydrin colorimetric assay conformation

4.9. Adsorption studies of NFO@SiO₂@GPTS-Cys for removal of IBF.

4.9.1. Effect of pH on sorption capacity

One of the trivial factors influencing the adsorption of pollutants is the surface charge of nanoparticles which is attained by the variation in the pH of the solution. In this study, adsorption of ibuprofen has been carried out for pH ranging between 4.0 - 9.0. The adsorption capacity of 10 mg of the nano-adsorbent for 50 mg L⁻¹ concentration of Ibuprofen, represented in Figure 4.23 revealed that the adsorption of Ibuprofen increases with increase in pH and attains a maximum value at pH 6.0. From the literature it is known that the L-cysteine attains isoelectric point (PI) at pH 5.2 and at this pH, the carboxylic acid undergoes deprotonation and the amine groups attain -NH³⁺ due to protonation thus forming a zwitterionic configuration (Ashjari et al. 2015). When the pH of the solution was maintained at pH 6.0 the carboxyl group gets deprotonated which helps in the optimum adsorption of ibuprofen. The pH of the solution >pH 6.0 resulted in no adsorption of Ibuprofen molecules as the carboxyl group of the cysteine gets deprotonated completely. This increased negative charge could result in the repulsion of IBF molecules. Thus, pH 6.0 was considered for further optimization of the batch studies.

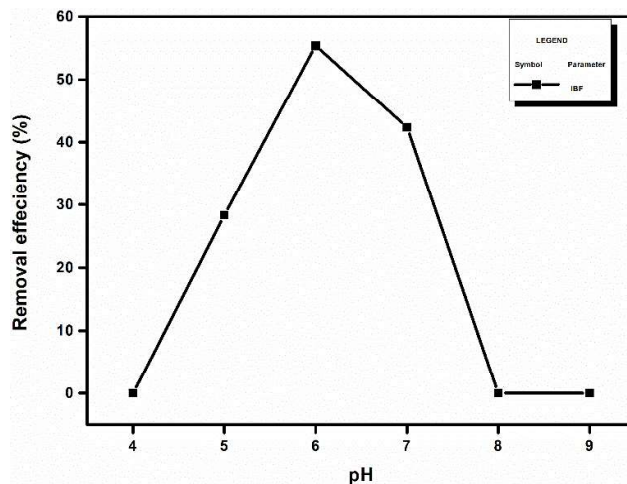


Figure 4.23: Effect of pH on the initial concentration of ibuprofen (50 mg L^{-1}) and dosage 10 mg of the catalyst loading

4.9.2. Effect of Cysteine concentration on adsorption:

The effect of different cysteine coating concentrations (3-9 mmol) required for the adsorption of ibuprofen was studied at fixed pH 6.0 and initial concentration of 50 mg L^{-1} . As represented in Figure 4.24, it was observed that for a concentration of 3, 5, and 9 mmol of L-cysteine coating with 1:1, 1:0.5, 1:0.3 showed adsorption capacity of 14.54%, 38.72%, and 27.67% respectively as shown in Figure 4.24. However, the highest adsorption capacity of NFO@SiO₂@GPTS@Cys for IBF, 55.38% was observed at a concentration ratio of 1:0.7. This could be associated with maximum active sites from the cysteine molecule available for the attachment of IBF. At pH 6.0 the carboxyl group of L-cysteine gets deprotonated which is confirmed by the negative charge obtained by the zeta potential analysis as mentioned in Figure 4.21 (a). These active functional sites interact with the sodium salt of IBF in the solution generating a maximum adsorption of IBF at pH 6.0.

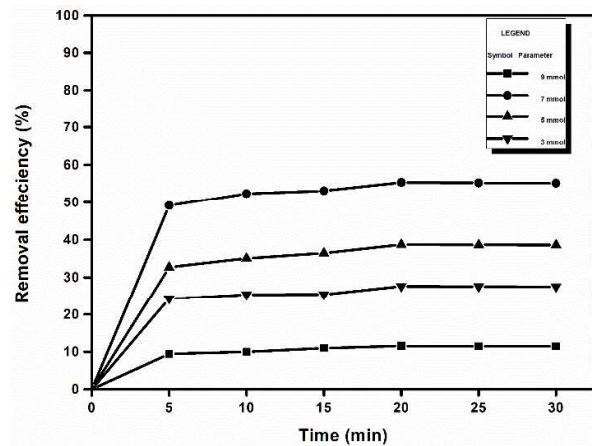


Figure 4.24: Effect of Cysteine concentration (3,5,7 and 9 mmol) on the initial concentration of ibuprofen (50mg L⁻¹) and dosage 10 mg of the catalyst loading

4.9.3. Effect of nanomaterial dosage:

The amount of nanomaterial required for adsorption Ibuprofen for different dosage was further studied as shown in Figure 4.25. The initial concentration of ibuprofen i.e., 50 mg L⁻¹ was considered for varied nanomaterial dosage of 10, 30 and 50 mg. It can be observed that with the increase in the nanomaterial dosage the adsorption of ibuprofen increases. This could be due to the availability of more functional sites with an increase in the quantity of the nanomaterial. However, when the adsorption dosage was increased beyond 30 mg the adsorption capacity decreased. This could be due to the aggregation of molecules at the adsorption site (Rajamanickam and Shanthi 2016). Thus, from the results, it can be inferred that 30 mg of the nanomaterial is the optimum dosage for maximum adsorption of 50 mg L⁻¹ of IBF.

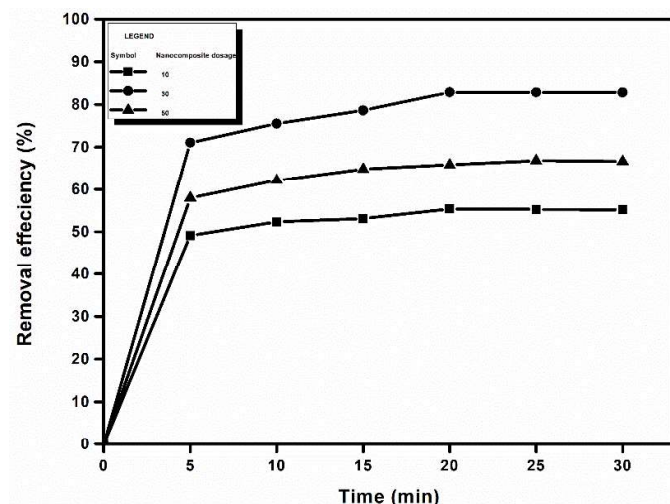


Figure 4.25: Effect of nanomaterial dosage (10, 30, 50 mg) for an initial concentration of 50 mgL⁻¹

4.9.4. Effect of Ibuprofen concentration

Samples of 50 mg of cysteine grafted nickel ferrite nanoparticles were added to different concentrations (50-300 mg L⁻¹) of 100 mL IBF solution and the pH was maintained at 6.0. The nanoparticles and IBF solutions were mixed thoroughly and stirred continuously at room temperature. Aliquot samples were taken from each solution every 5 min by decantation for 30 min. Finally, absorbance was measured for each individual sample. From Figure 4.26 it is evident that the adsorption equilibrium is attained within 20 min. Further, it can be observed that highest adsorption of 82.90% was obtained from 50 mg L⁻¹ of IBF solution. However, the increase in the concentration of IBF from 100 to 300 mg L⁻¹, the sorption capacity was found to decrease which may be due to the increase in competition of the IBF compounds towards the active sorption sites of the nanoparticles. Recently, Ding et al. (2017) analysed the effect of IBF on the *Navicula sp.*, where the biochemical characteristics of these species were significantly retarded at IBF concentrations up to 50 mgL⁻¹. Hence, the NFO@SiO₂@GPTS@Cys could be used as potential candidate for IBF at a concentration of 50 mgL⁻¹.

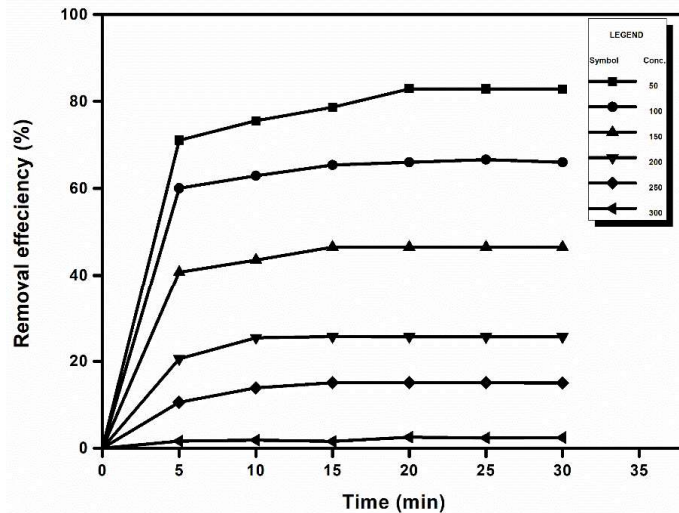


Figure 4.26: Effect of IBF concentration (50-300 mg L⁻¹) for the nanomaterial dosage of 30 mg and pH 6.0

4.9.5. Adsorption Isotherms

The correlation coefficients (R) = 0.98 from the Figure 4.27 (a), are closer to 1 for the Langmuir isotherm. Hence, from the data evaluation of the two models, it was observed that Langmuir model is the best fit describing the sorption process for the adsorbents compared to Freundlich model (Figure 4.27(b)). Therefore, based on the equilibrium model, IBF sorption process occurs through a monolayer sorption process on a homogeneous surface. This is in concordance with reports by Enache et.al (2013) in which similar adsorption pattern was observed for the cysteine attached to ICPTES. The table 9 shows data calculated from experimental fitting data of the Langmuir and Freundlich isotherms.

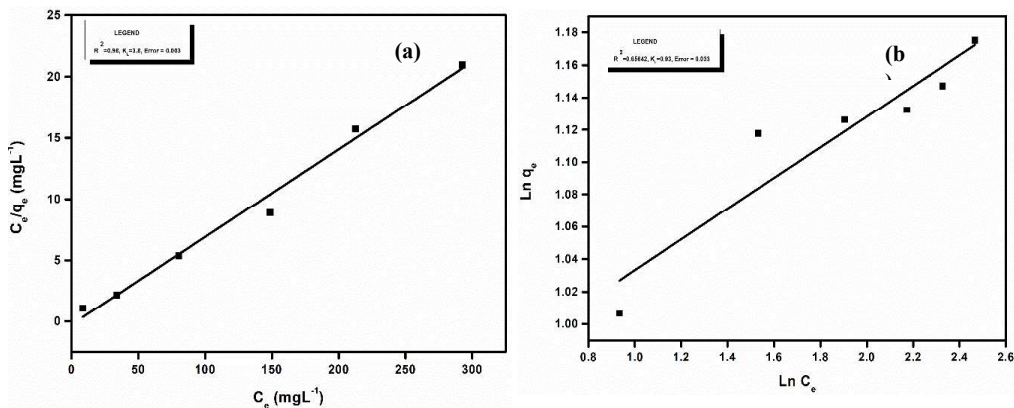


Figure 4.27: (a) Langmuir adsorption model (b) Freundlich adsorption model for IBF sorption onto NFO@SiO₂@GPTS@Cys

4.9.6. Adsorption kinetics

The adsorption kinetics has been studied to determine the kinetic model that fits the Ibuprofen sorption onto the cysteine functionalised magnetic nanoparticles. According to the results presented in this study, it can be concluded that the cysteine functionalisation was effective in binding to Ibuprofen present in the aqueous systems up to 80.92%. The pseudo-second-order kinetic model can be represented by the equation:

$$\frac{1}{q_t} = \frac{1}{kq_e^2} + \frac{t}{q_e} \quad (5)$$

wherein, K is the rate constant of second order adsorption (g mg⁻¹min⁻¹) (Robati 2013). The Fig. 4.28 (a) depicts the straight-line plot of t/q against t to determine the pseudo-second-order kinetic model from which it can be observed that the adsorption kinetics of the experimental data best fits the pseudo-second-order kinetics as shown in Table I. The Figure 4.28 (a) depicts the straight-line plot of t/q against t to determine the pseudo-second-order kinetic model from which it can be observed that the adsorption kinetics of the experimental data best fits the pseudo-second-order kinetics as shown in Table 9.

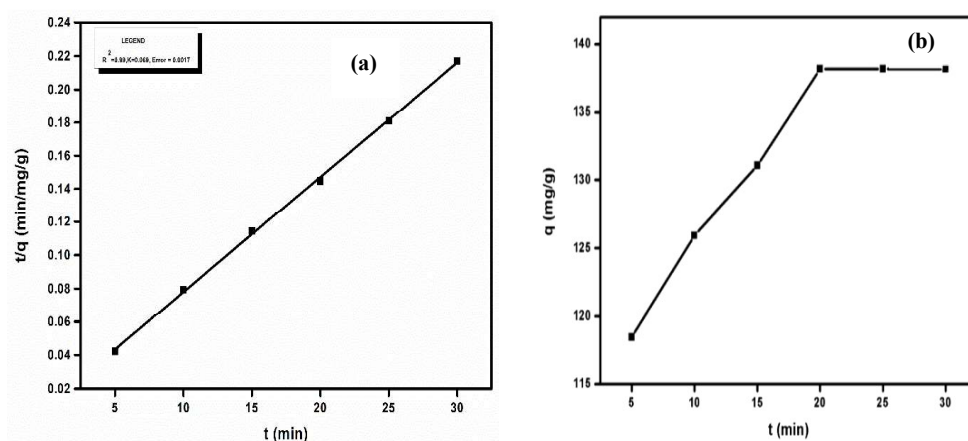


Figure 4.28: Pseudo-Second order kinetics (a) maximum adsorption capacity (b) of IBF sorption onto NFO@SiO₂@GPTS@Cys

Table 9: Adsorption kinetics and adsorption isotherm parameters

Adsorption kinetics			Adsorption isotherm				
Pseudo second order Parameters			Langmuir Isotherm parameters			Freundlich Isotherm parameters	
q_e (mg g ⁻¹)	K_1	R^2	Q_{max} (mg g ⁻¹)	K_L (L mg ⁻¹)	R^2	K_F [(mg g ⁻¹) (L mg ⁻¹) ^{1/n}]	R^2
0.217	0.069	0.98	138.1	3.8	0.98	0.93	0.85

4.20. Reusability of the NFO@SiO₂@GPTS@Cys nanomaterial

The adsorbent does not show any significant adsorption after pH 6.0 this is due to the affinity of the amine and carboxyl groups of cysteine towards ibuprofen. To study the desorption efficiency, the nanomaterial was dispersed in a mixture of water and acetone as the ibuprofen is soluble in organic solvents. As shown in Figure 4.29, the adsorption efficiency was found to be 80% even after three cycles. Therefore, this nanomaterial could be used as an efficient adsorbent for the removal of ibuprofen from aqueous solutions.

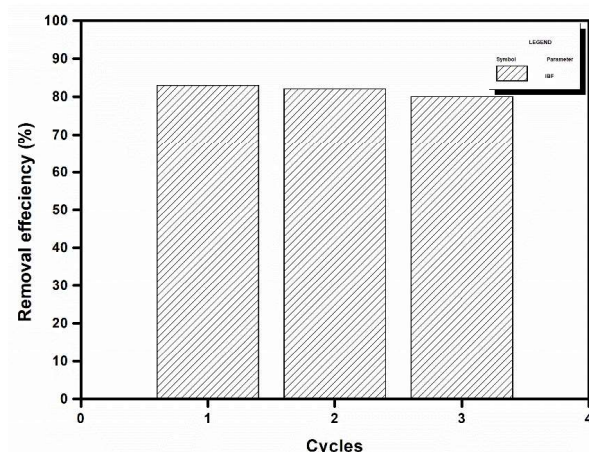


Figure 4.29: Reusability of the NFO@SiO₂@GPTS@Cys nanomaterial for 3 cycles at pH 6.0; nanomaterial dosage 30 mg; time 30 min.

4.11. Mechanism of IBF removal

When the thiol group of the L-cysteine is bound to the silane the other two functional groups are free to attach to the IBF molecules in the aqueous system. The mechanism of IBF uptake takes place due to the interactions between the intermolecular hydrogen bonding of hydroxyl and carbonyl of the IBF with the amino and carboxylate groups of the L-cysteine respectively. It exhibits highly negative charge on the surface due to the deprotonation of the carboxyl groups to carboxylate groups. Thus, the carbonyl groups can react with the hydroxyl group of IBF. However, the presence of negligible charge of amino groups may also aid in the bonding process. Further increase to pH 7.0 the L-cysteine behaves like a zwitterion which could be the reason of reduction in efficiency beyond pH 6.0. The adsorption of IBF by the L-cysteine A hypothetical diagram of the mechanism is shown below in Figure 4.30.

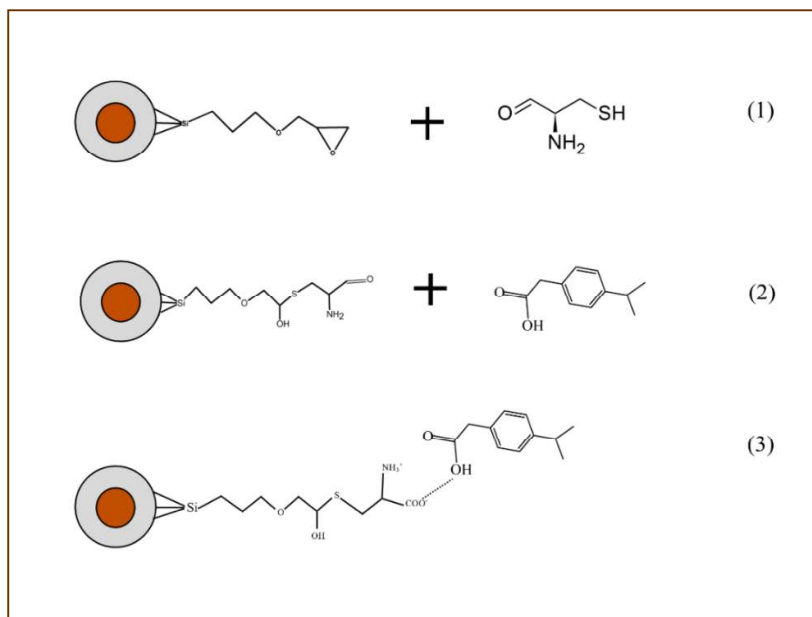


Figure 4.30: Plausible mechanism for the removal of IBF

4.12. Adsorption studies of NFO@SiO₂@APTS for removal of IBF, ACE and STR

4.12.1. Influence of pH on pharmaceutical uptake:

The pH of the adsorption experiment plays a trivial role in the uptake of pharmaceuticals. The removal of the pharmaceuticals of interest in the current study was studied in the pH

range of 4.0 – 8.0 for an initial adsorbent dosage of 10 mg and a pollutant concentration of 6 mg. In the case of IBF, it was observed that there was no significant removal at acidic pH. However, as the pH reached neutral condition, 33 % removal of IBF was observed (Figure 4.31 a). The removal observed could be due to the medium acid, carboxylic group in IBF. The removal efficiency of ACE was seen at pH 6.0 to be 26%, which could be due to a weak acid phenol that binds to the amine of aminosilane under the formation of a salt, which is reversible. Acetaminophen is a weak acid; therefore, it partially dissociates in water to form anions (Wong et al. 2018a). Both the pharmaceuticals are stable close to neutral pH, which makes the chemisorption possible. Less removal at acidic pH could be due to the cleaving of the adduct by the acid because they form a salt with the amino groups of the aminosilane which is in concordance with the literature. For instance, Vakili et al., (2019), observed that APTS modified chitosan/ nano activated carbon composite beads exhibited maximum adsorption of acetaminophen at 24 hrs. However, the removal of streptomycin took place at pH 5.0 and was found to be slightly lower (14%) as it is a strong base that often-released sulfates to the environment (Figure 4.31c). The strong guanidine moiety of streptomycin can bind to hydrogen and does not bind to the amino groups, which may attribute the lower removal efficiencies. In the adsorption process of all the three pharmaceuticals, it can be observed that the removal efficiency reduces at pH >7 which may be due to the dissolution of the silica surfaces at basic pHs, as reported in the literature (Barczak 2019; Pham et al. 2012). Also, the adsorption of drugs was found to be effective between pH 5.0 to 7.0, which may be due to the presence of the anionic forms of particular drugs at acidic pH (Kamarudin et al. 2013; Manzano et al. 2008) .

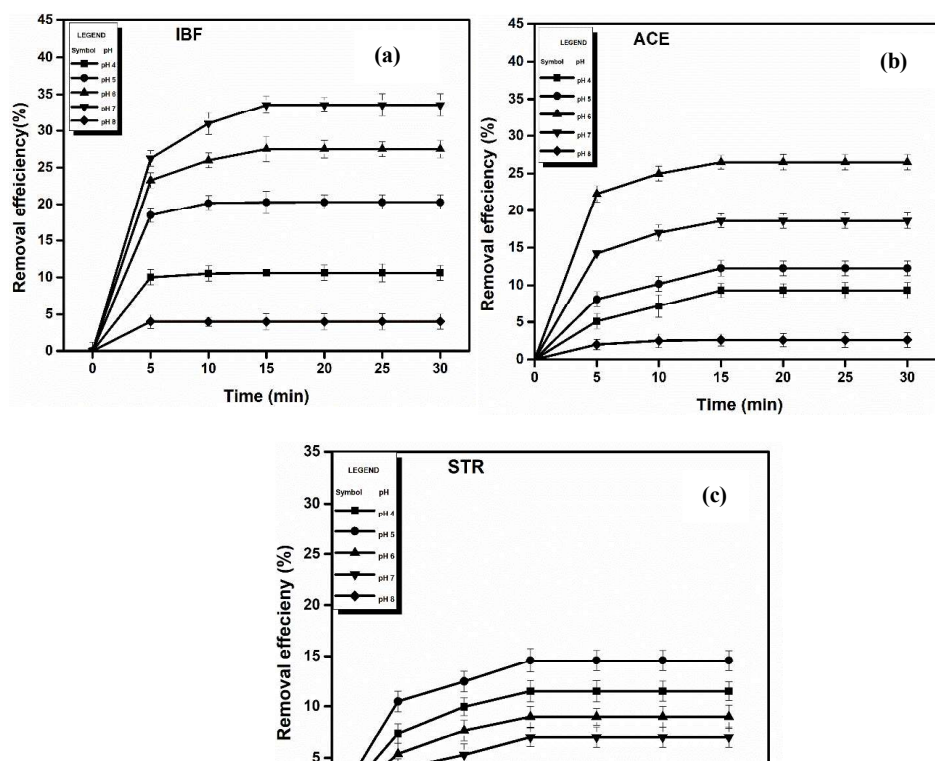


Figure 4.31. Effect of pH on the adsorptive removal of (a) Ibuprofen, (b) acetaminophen (c) streptomycin

4.12.2. Effect of nanocomposite dosage:

The adsorbent concentration plays a critical role in enhancing the removal efficiency of the pharmaceuticals. The adsorption experiment conducted for initial pharmaceutical concentration of 6 mg L⁻¹ and an initial nanocomposite dosage of 10 mg exhibited 33%, 26%, and 14% within 15 mins for IBF, ACE, and STR, as shown in Figure 4.32. As the dosage of the adsorbent was increased from 10 to 20 mg, there was no noteworthy increase in adsorption. Further, increasing the adsorbent dosage from 20-30 mg also showed no significant uptake of pharmaceuticals and seemed to be saturated at 10 mg. This implies that 10 mg of the nanocomposite would suffice for the removal of the pharmaceuticals. Thus, further experiments were carried out on the optimised pH and adsorbent dosage of 10 mg.

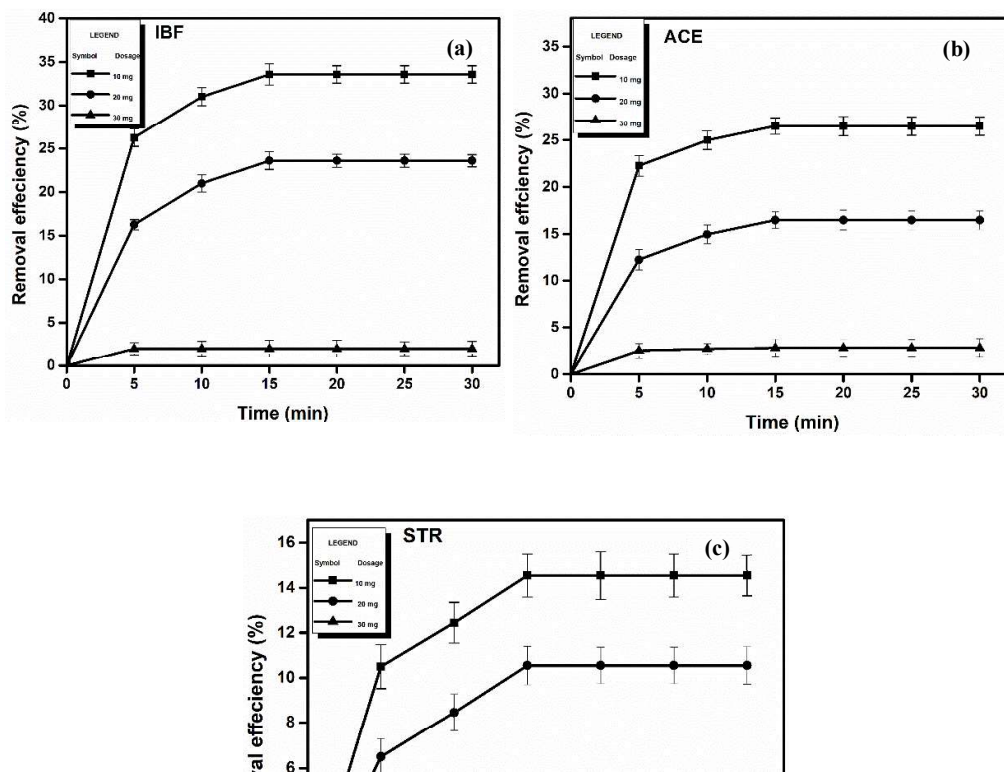


Figure 4.32: Effect of nanocomposite dosage on the adsorption of (a) IBF, (b) ACE, and (c) STR

4.12.3. Effect of pharmaceutical concentration

The removal efficiency of the nanocomposite was further optimised by analysing the influence of pharmaceutical concentrations as represented in Figure 4.33. The adsorption of the pharmaceutical pollutants for different concentrations of 6, 8, 10, 12, and 14 mg L⁻¹ was conducted at the optimum nanocomposite dosage of 10 mg and pH 5.0, 6.0, and 7.0 for STR, ACE, and IBF respectively. It can be observed that the adsorption increased up to 12 mg L⁻¹ and gets saturated with no further uptake. This, could be due to the saturation of the adsorption sites due to the increase in pharmaceutical concentration. However, in the case of streptomycin, the percentage of adsorption was seemingly lower up to 70% when compared to IBF and ACE, which is 97% and 94%, respectively, for the concentration of 12 mg L⁻¹ of the respective pollutants. Further, the adsorption kinetics and isotherm of the adsorption process were determined.

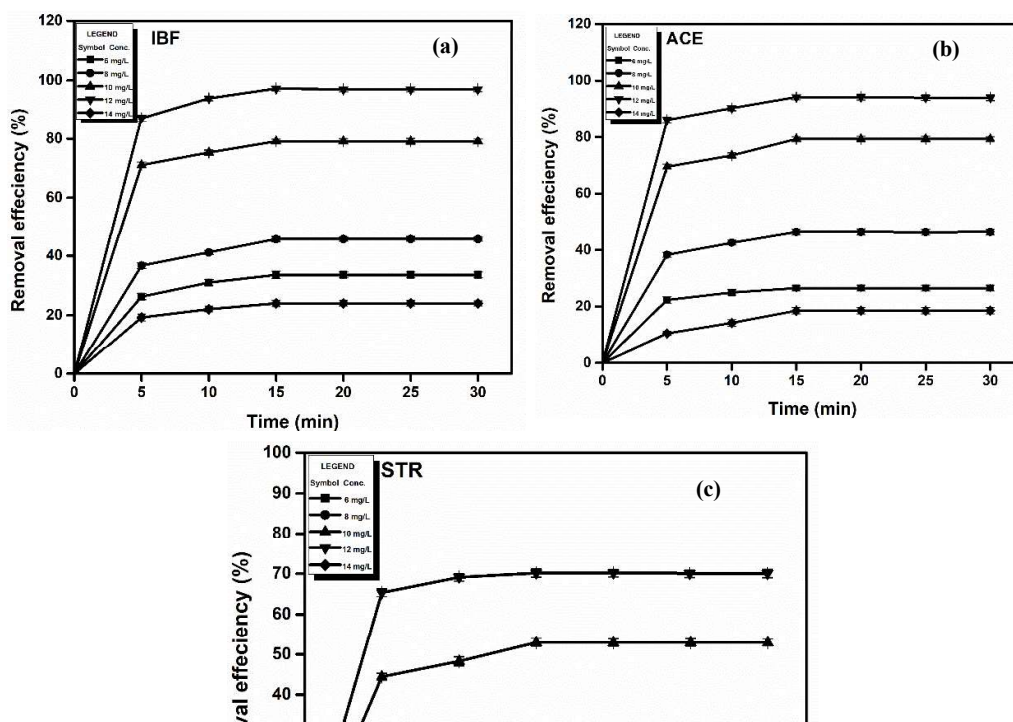


Figure 4.33. Effect of pharmaceutical concentration (12 mg L⁻¹) on the nanocomposite (a) IBF, (b) ACE, and (c) STR

4.12.4. Adsorption kinetics and isotherm:

The kinetic models for the sorption of the pharmaceuticals IBF, ACE, and STR onto the NFO@SiO₂@APTS, is analysed. As observed in Figure 4.34, the sorption kinetics of the following study seemed to follow the pseudo-second-order kinetic model, with a plot of t/q against t of the experimental data with higher R^2 values and a perfect linear fit, which is represented by the equation (5). Where the rate constant of the second-order equation, is represented by K ($\text{g mg}^{-1}\text{min}^{-1}$).

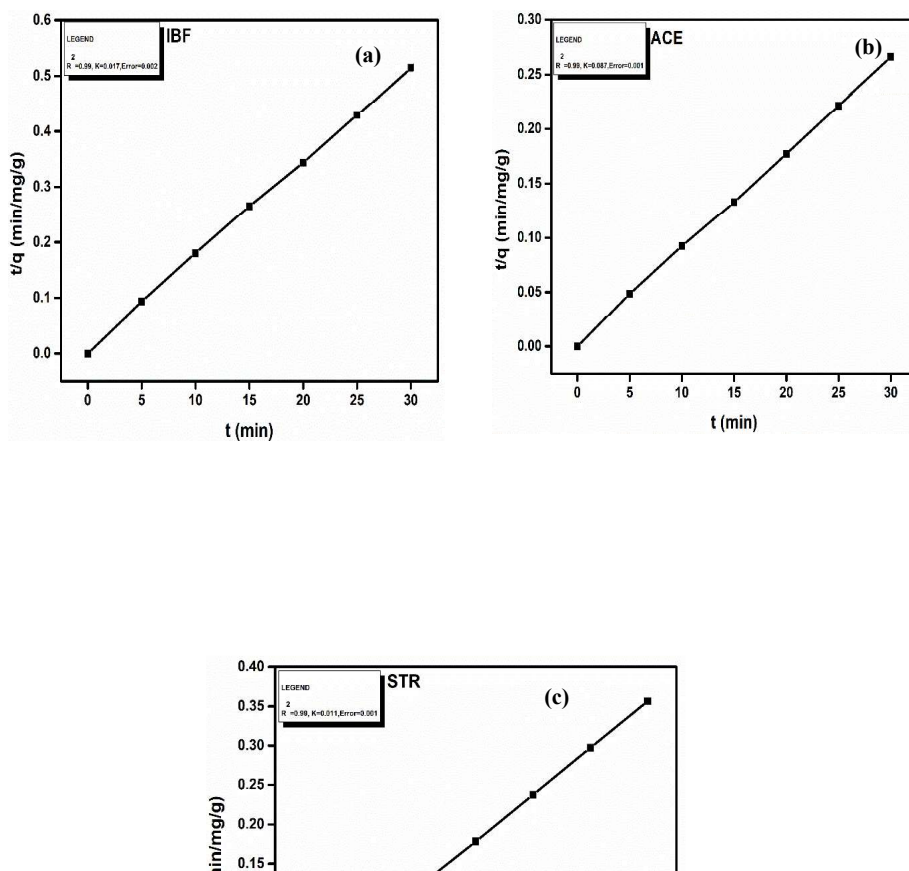


Figure 4.34: Pseudo second order kinetics of the experimental data for a) IBF b) ACE and c) STR

Further, the adsorption isotherm models, Langmuir and Freundlich's isotherms are shown as Figure 4.35 and Figure 4.37. It can be observed that the Langmuir isotherm model shows a better fit for the adsorption data compared to Freundlich isotherm, as represented in Table 10. Thus, the adsorption process follows a monolayer molecular adsorption onto the nanocomposite surface with a maximum adsorption capacity of 59, 58 and 49 mg g⁻¹ for IBF, ACE, and STR respectively.

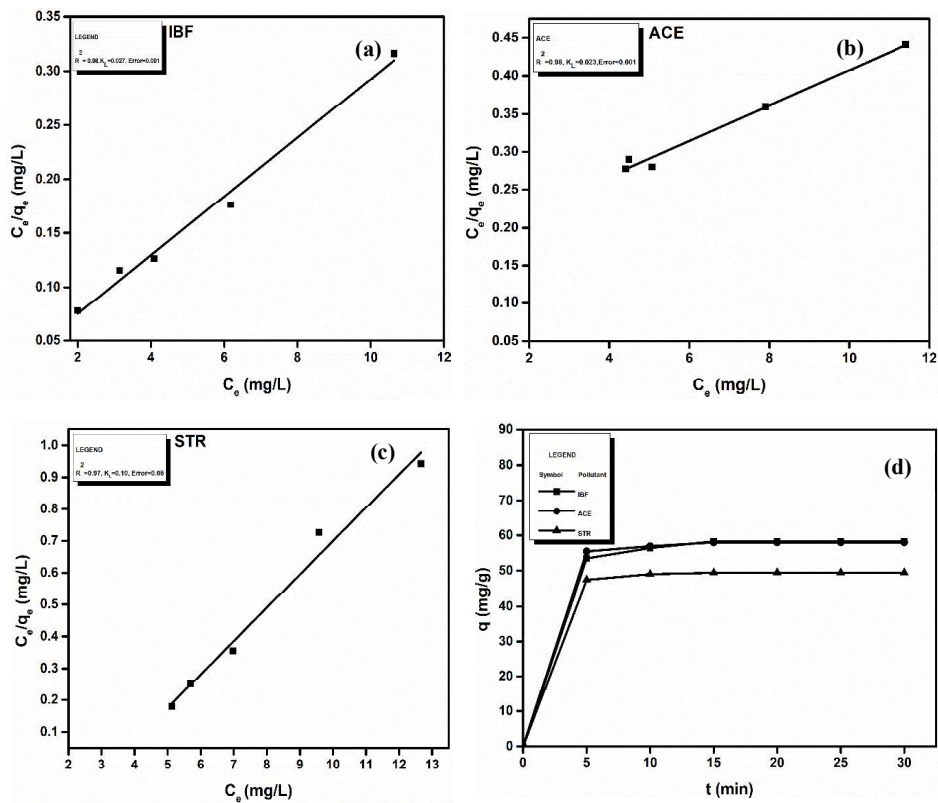


Figure 4.35: Langmuir adsorption isotherm of the experimental data for a) IBF b) ACE and (c) STR and (d) maximum adsorption capacity.

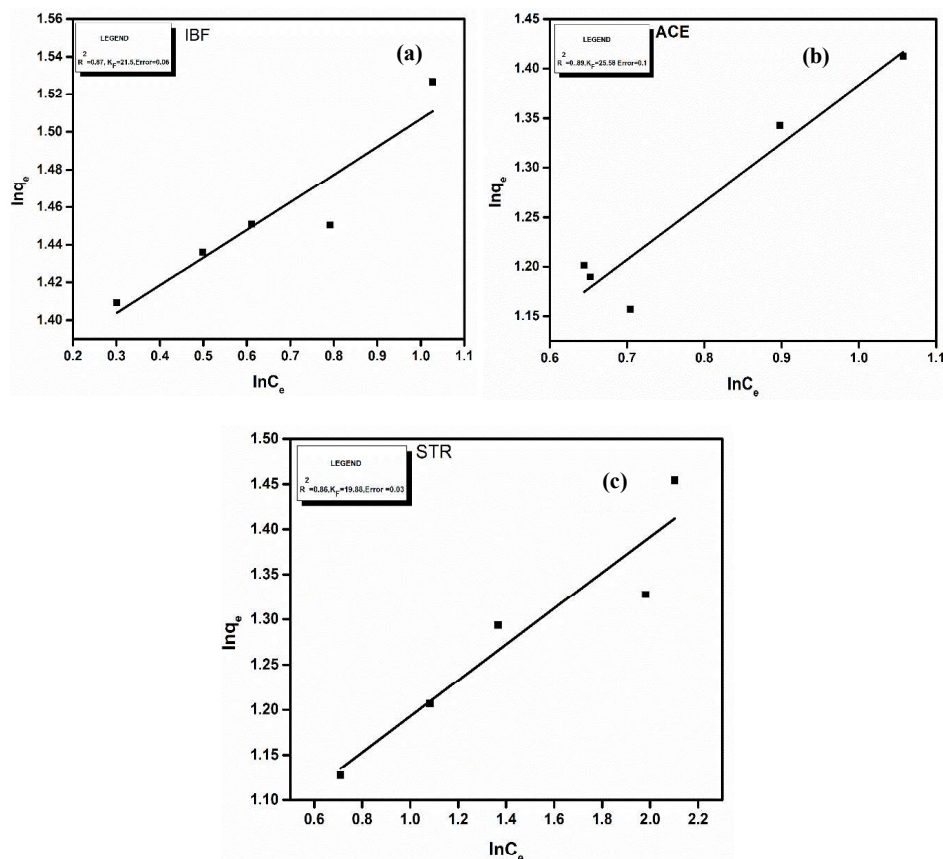


Figure 4.36: Freundlich adsorption isotherm of the experimental data for a) IBF b) ACE and c) STR

The adsorption mechanism of the respective pharmaceuticals with the NFO@SiO₂@APTS can be illustrated, as shown in Figure 4.37. Amine groups present in the NFO@SiO₂@APTS gets easily protonated and favour the adsorption of anionic compounds in acidic medium by electrostatic interaction (Tiringer et al. 2018b). In an acidic medium of pH ranging from 4.0 to 6.0, the NH₂ groups get protonated, producing NH³⁺, which attributes to the formation of hydrogen bonds between the OH group STR and NH³⁺. A similar reaction is expected to take place between ACE, which will be present in its anionic form, thus facilitating the binding of the hydroxyl group with the protonated form of amine (NH³⁺). In the case of IBF, carboxyl (-COOH) groups could attract the protonated aminopropyl groups, thus forming strong bonds with silanol groups. This could

be the reason for the higher removal of IBF (97%) when compared to ACE (94%) and STR (70%).

Table 10: Adsorption kinetics and adsorption isotherm parameters

Adsorption kinetics of pseudo-second-order parameters					Adsorption isotherms				
					Langmuir isotherm			Freundlich isotherm	
S. No.	Pharmaceutical	q_e	K_1	R^2	Q_{max} (mg g ⁻¹)	K_L (L mg ⁻¹)	R^2	K_F [(mg g ⁻¹) (L mg ⁻¹) ^{1/n}]	R
1.	IBF	0.5	0.01	0.99	59	0.02	0.98	21	0.87
2.	ACE	0.5	0.08	0.99	58	0.02	0.98	25	0.89
3.	STR	0.6	0.50	0.99	49	0.10	0.97	19	0.86

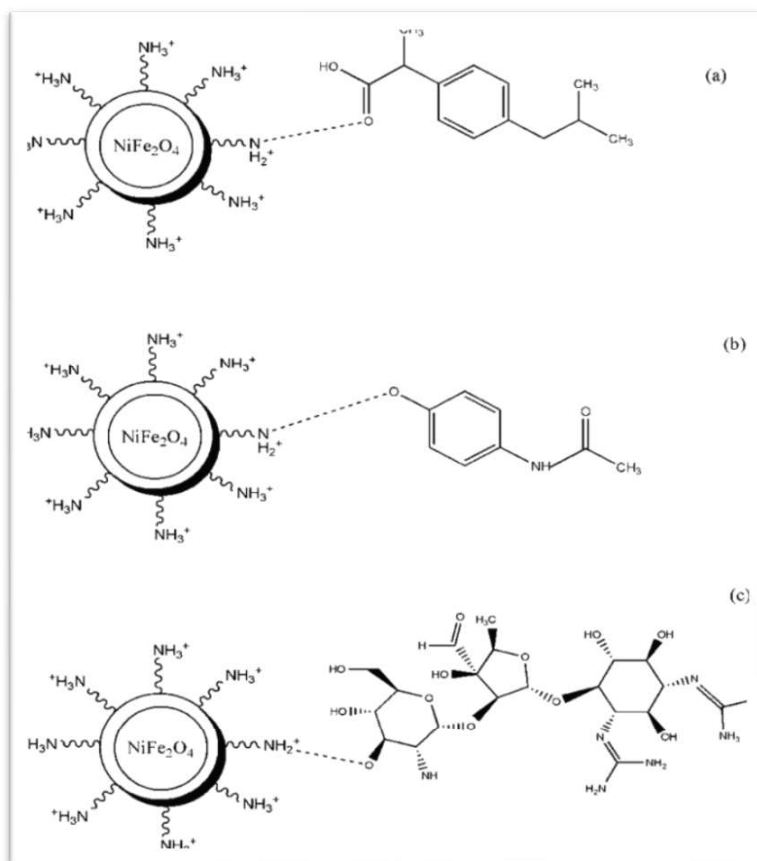


Figure 4.37: Schematic representation of the adsorption mechanism of NFO@SiO₂@APTS nanocomposite to (a) IBF, (b) ACE, and (c) STR

4.12.5. Reusability

The ability of nanocomposites to get regenerated enhances the pollutant removal efficiency many folds. The nanocomposites that were subjected to regeneration (desorption process) and reused for adsorption of the pharmaceuticals once again expressed high removal efficiencies of 97, 93, and 70% for IBF, ACE, and STR, respectively (first cycle). The first cycle removal efficiencies of the pharmaceuticals are found to be similar to the efficiencies obtained with fresh nanocomposites. Subsequently, three more cycles also showed removal in the declining order from 97% to 92% for IBF, which is still fair acceptance in the process of pharmaceutical pollutants from the aqueous phase. Similar results are obtained for ACE and STR with hardly a few percentage decreases, 4 – 5% in their removal efficiencies. After four cycles of regeneration, pharmaceutical removal efficiencies of the nanocomposites were found to be decreasing to 45%, 44%, and 20% as indicated in Figure 4.38. The loss of the surface properties of the nanocomposite during the consecutive adsorption and desorption cycles could be the reason for the decrease in efficiency. The functional groups that are available on the APTS nanocomposites would have exhausted due to washing with acids and mechanical forces applied during multiple desorption process.

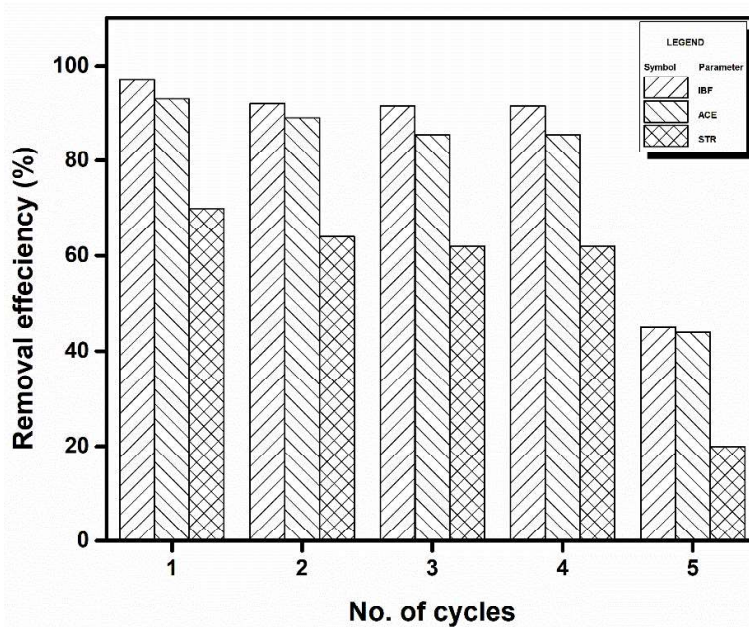


Figure 4.38. Regeneration capacity up to four cycles.

4.13. Adsorption studies of NFO@SiO₂@APTS-HPCD for the removal of IBF, ACE and STR

4.13.1. Effect of pH on the pharmaceutical adsorption.

The influence of pH was on the adsorption of the target pharmaceutical compounds was analysed to determine the efficiency of the nanocomposite (10 mg) post grafting of HPCD. When the solution pH was maintained at 4.0 for IBF, ACE and STR, the nanocomposite exhibited a removal efficiency of 10 %, 4.97 %, 5.47 % within 5 min of interaction. As the reaction time was increased to 10th min the removal efficiency was observed to be 10.43% (IBF), 7.43 % (ACE) and 7.86 % (STR). Increasing the reaction time further it was observed that maximum removal efficiency was exhibited by the nanocomposite at the 15th min viz., 10.59 % (IBF), 9.40 % (ACE) and 10.5 % (STR). During the 15th min the nanocomposite exhibited a removal efficiency of 30.27 %. Thus, it was observed that pH 4.0 was not very effective in the removal of the target pollutants. This could be due to the weaker forces of attraction between the nanocomposite and the target pollutants (Haro et al. 2021).

When the solution pH was increased to pH 5.0 the nanocomposite exhibited a slightly higher adsorption potential around 25.6 %, 8.1 % and 9.5 % for IBF, ACE and STR during the 5th min of adsorbent-adsorbate interaction. It was observed that nanocomposite displayed higher adsorption efficiency towards IBF at pH 5.0. This could be due to the interaction between the isobutyl group of the IBF with the core of the HPCD molecule. The IBF structure attains different charges based on the pH of the solution, the dissociation constant (pKa) of IBF is at 5.2, at pH < pKa Ibuprofen is cationic, while at pH > pKa it is anionic (Miranda et al. 2021). As the surface of the nanocomposite is highly negative the plausible adsorption that could take place is at pH 5.0 in this study, thus favouring the adsorption behaviour of the nanocomposite. At pH 6.0, during 5th min of the reaction time the nanocomposite revealed the adsorption efficiency of 22 %, 13.91 % and 18.4 % for IBF, ACE and STR respectively. During the 10th min the adsorption potential was observed to be 24.58 %, 16.90 %, 20.65 % and the 15th min the adsorption efficiency was noted to be 25.60 %, 18.54 % and 22.99 % for IBF, ACE and STR respectively. No significant adsorption was observed at this particular pH, thus proving that the solution at pH 6.0 was not effective for adsorption. As neutral condition was achieved the adsorption efficiency of the nanocomposite significantly increased to 12 %, 24.40 %, 26.79% for 5th min; 16.14 %,

26.87 %, 28.45 % for 10th min and 17.58 %, 30.35 %, 31.55 % for 15th min. From the 4.39 (b) and (c) it can be observed that adsorption ACE and STR was effective at pH 5.0 and 7.0 respectively. In the case of ACE, the dissociation constant (pKa) is 9.4 (Quesada et al. 2019), and at pH < pKa it exists in protonated state. On the other hand, the HPCD exists in protonated state in acidic medium, this confirms the lower adsorption potential the nanocomposite at pH 4.0 and 5.0. However, the adsorption increased significantly at pH 7.0. This could be attributed to the reduction in the protonation of hydroxyl groups of HPCD (Paul et al. 2016). This can be corroborated with report by (Rahman and Nasir 2020) wherein they reported β -CD to attain positive charge in acidic medium. Beyond pH 7.0 ACE starts attaining a negative charge which results in electrostatic repulsion between ACE and nanocomposite.

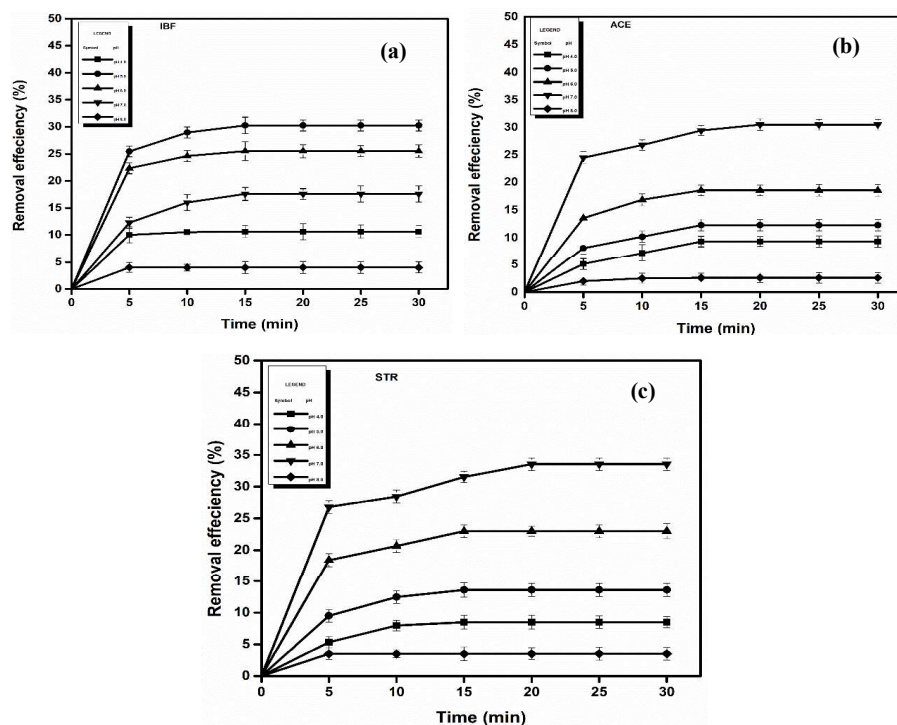


Figure 4.39. Effect of pH on the adsorptive removal of (a) Ibuprofen (pH 5.0), (b) acetaminophen (pH 7.0) (c) streptomycin (pH 7.0)

Similar observation was also reported by (Wong et al. 2018b) where the ACE molecules attained a neutral state after pH 6.0. In the case of streptomycin, it is present in triprotonated state at pH 7.0 (Orgován and Noszál 2012) which makes it highly positive. Since STR is highly basic, the adsorption could take place only in the acidic condition and it was found to be optimum at pH 7.0 as represented in Figure 4.39 (c). The plausible reason for

adsorption could be the reduced protonation of the hydroxyl groups of the nanocomposite at pH 6.0, positive charge of the streptomycin at this particular pH. Thus, pH 5.0, 7.0 and 6.0 were maintained as the optimum pH conditions for IBF, ACE and STR for further experiments.

4.13.2. Effect of adsorbent dosage against the pharmaceutical adsorption.

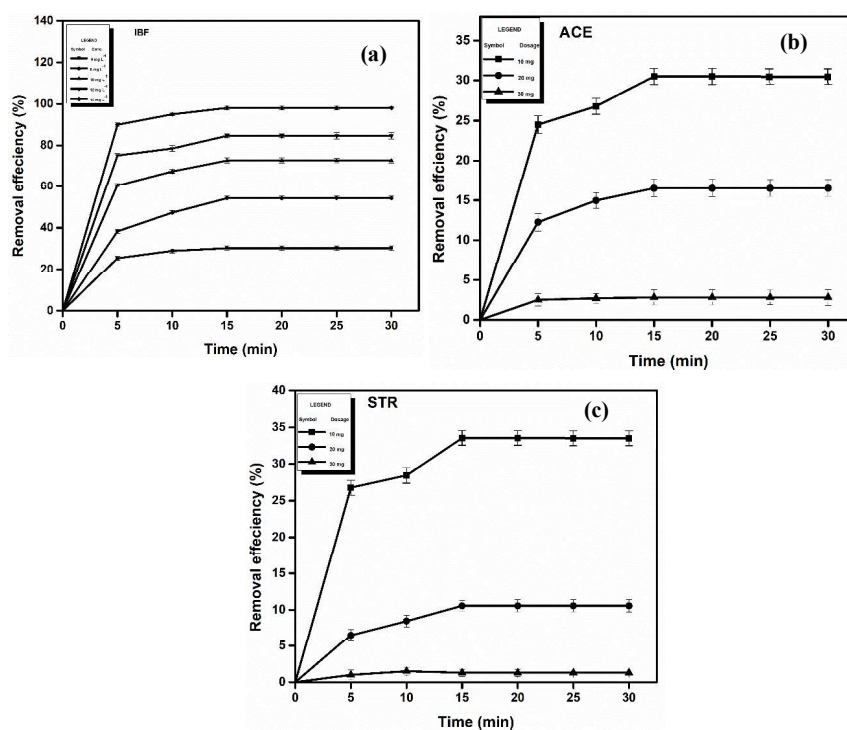


Figure 4.40: Effect of nanocomposite dosage on the adsorption of (a) IBF, (b) ACE, and (c) STR

The adsorbent dosage is another significant parameter which determines the efficiency of the nanocomposite. The dosage was varied at 10 mg, 20 mg and 30 mg at pH 5.0, 7.0 and 6.0 against IBF, ACE and STR respectively. As depicted for the initial pharmaceutical concentrations of 6 mg L⁻¹ in the Figure 4.40, for an initial dosage for 10 mg the removal of the nanocomposite was observed to be 30.27 %, 30.5 % and 33.5 % for IBF, ACE and STR respectively. As the dosage quantity was increased to 20 mg, the adsorption efficiency was observed to decrease to 23.58%, 16.5% and 10.55%. This could be due to the saturation of the available active sites on the nanocomposite. Further, the quantity of the nanocomposite was increased to 30 mg and it was observed that there was significant reduction in the removal efficiency up to 2 %, 2.8%, 1.29 % for IBF, ACE and STR

respectively. This could be due to the saturation of the active sites of the HPCD grafted nanocomposite and the competition of the pharmaceutical pollutants to occupy the active sites resulting in decrease of the adsorption efficiency of the nanocomposite.

4.13.3. Effect of pharmaceutical concentration on adsorption efficiency.

The final trivial factor in determining the efficiency of the nanocomposite is the quantity of the pharmaceutical concentration that could adsorb on to the nanocomposite dosage of 10 mg. At an initial concentration of 6 mg L⁻¹ the adsorption efficiency of the nanocomposite was reported to be 30.27 %, 30.5 %, 33.55 % for IBF, ACE and STR respectively. The removal efficiency was observed to increase up to 54.12 %, 52.56 %, 33.5 % (IBF, ACE, STR) at a pharmaceutical concentration of 8 mg L⁻¹. In order to determine the maximum removal efficiency of the nanocomposite the pharmaceutical concentration was increased further to 10 mg L⁻¹.

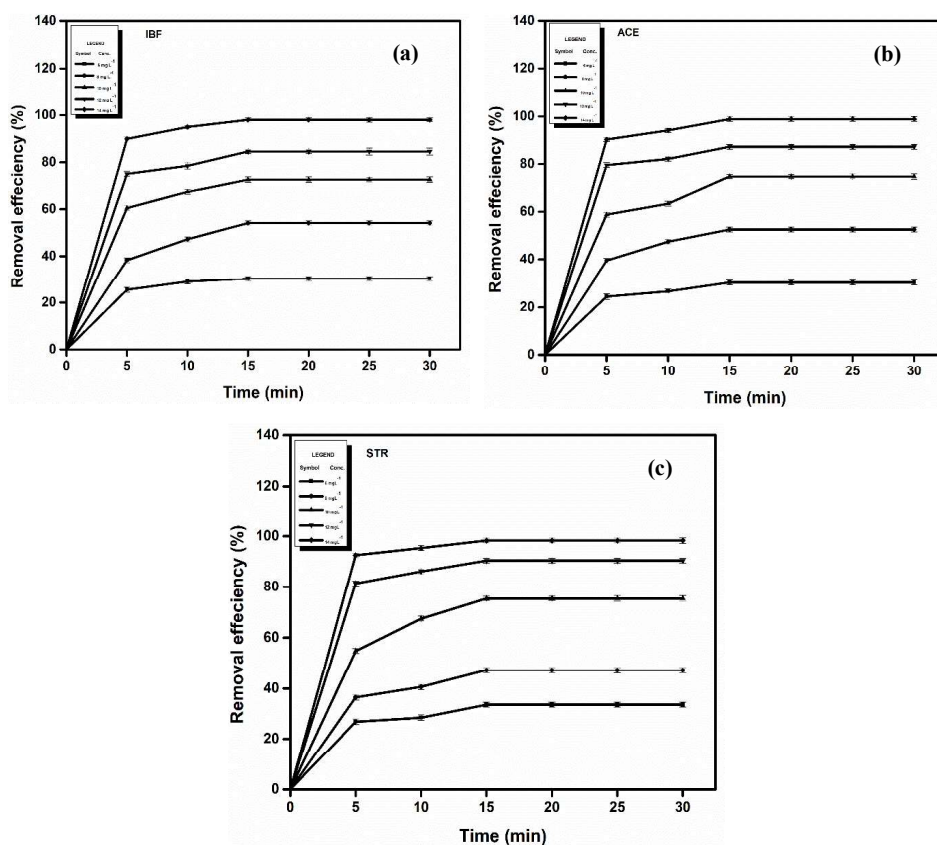


Figure 4.41. Effect of pharmaceutical concentration (10 mg L⁻¹) on the nanocomposite (a)IBF, (b) ACE, and (c) STR

As noted from the Figure 4.41 it was observed that the nanocomposite still exhibits adsorption efficiency of 72.63 %, 74.76 %, 75.34 % (IBF, ACE, STR). Since the nanocomposite continued to represent higher potential of adsorption the pharmaceutical concentration was increased to 12 and 14 mg L⁻¹. The removal efficiency was observed to be highest for 14 mg L⁻¹ which was up to 98.01 %, 98.89 %, 98.3 % whereas 12 mg L⁻¹ was observed to have 84.58 %, 90.41 %, 98.3 % for IBF, ACE and STR respectively. Thus, it was observed that maximum adsorption was obtained for 14 mg L⁻¹. Thus, the HPCD functionalization onto the NFO@SiO₂@APTS was proven to be highly beneficial towards adsorption of the target pharmaceutical pollutants.

4.13.4. Adsorption kinetics and isotherm

The sorption kinetics of nanocomposite (NFO@SiO₂@APTS-HPCD) against the pharmaceuticals IBF, ACE, and STR was analysed. The adsorption kinetics was noted to follow the pseudo-second-order kinetic model, wherein a plot of t/q against t of the experimental data with higher R² values and a perfect linear fit was determined and calculated. This is represented by the equation (5). The rate constant of the second-order equation, is represented by K (g mg⁻¹min⁻¹).

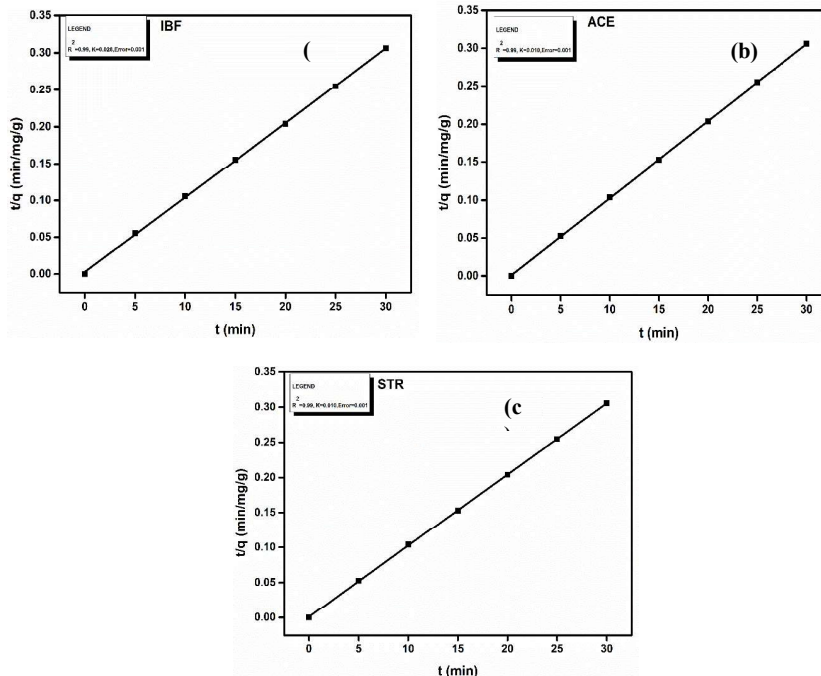


Figure 4.42: Pseudo second order kinetics of the experimental data for a) IBF b) ACE and c) STR

Further, the adsorption isotherm models, Langmuir and Freundlich's isotherms are shown as Figure 4.43 and Figure 4.44. It can be observed that the Langmuir isotherm model shows a better fit for the adsorption data compared to Freundlich isotherm, as represented in Table 11. Thus, the adsorption process follows a monolayer molecular adsorption onto the nanocomposite surface with a maximum adsorption capacity of 137.21, 137.86 and 137.86 mg g⁻¹ for IBF, ACE, and STR respectively.

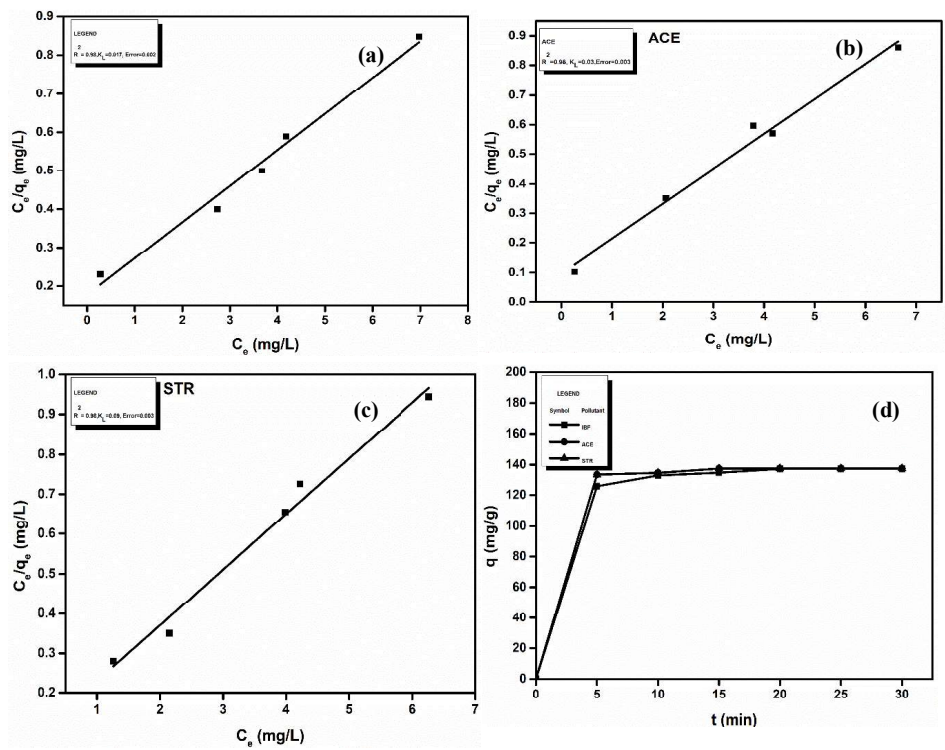
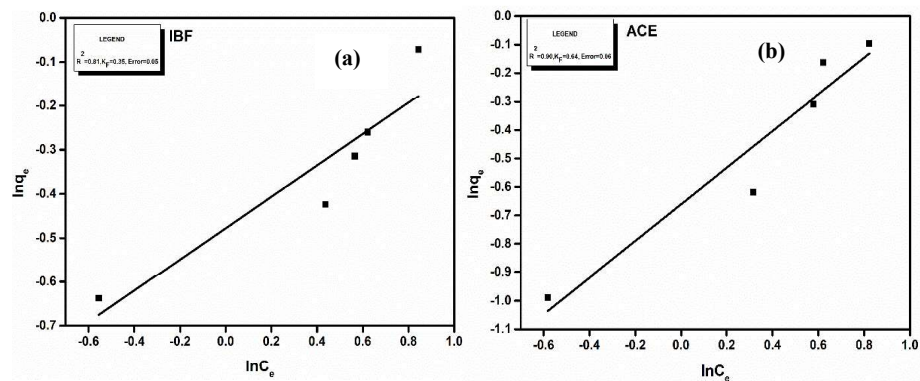


Figure 4.43: Langmuir adsorption isotherm of the experimental data for a) IBF b) ACE and c) STR and (d) maximum adsorption capacity.



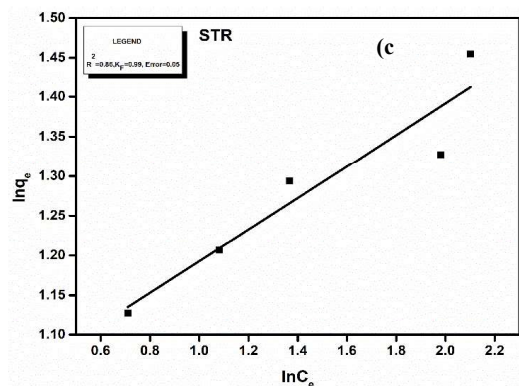


Figure 4.44: Freundlich adsorption isotherm of the experimental data for a) IBF b) ACE and c) STR

The plausible adsorption mechanism of the NFO@SiO₂@APTS-HPCD against the respective pharmaceuticals can be illustrated, as shown in Figure 4.45. As mentioned above the hydroxyl groups of HPCD gets protonated at acidic pH which can facilitate the hydrogen bond formation with the carbonyl groups of IBF. This can be corroborated with result by Celebioglu & Uyar, (2019) where the possible interaction responsible for the interaction between IBF and hydroxyl groups of HPCD is hydrogen bonding. ACE exists as a cation at pH < pK_a and at pH 3.0- 6.0 the hydroxyl groups of HPCD will be highly protonated which could be the reason for lower adsorption of ACE. However, at pH 7.0 there is reduction of the protonated groups of HPCD which could be the reason for higher adsorption of ACE at this particular pH. In the case of streptomycin which is a highly strong base, becomes highly protonated at pH 7.0 due to the presence of amino groups. As the hydroxyl groups of HPCD witness a reduction in protonation the protonation of the STR molecules favors the adsorption with nanocomposite. Beyond this pH the target pharmaceuticals molecules do not favor the interaction with nanocomposite resulting in reduction of the removal efficiency of the nanocomposite beyond pH 7.0. Thus, as-synthesized nanocomposite NFO@SiO₂@APTS@HPCD was observed to have higher adsorption potential in comparison to the silane coated nanocomposites.

Table 11: Adsorption kinetics and adsorption isotherm parameters

Adsorption kinetics of pseudo-second-order		Adsorption isotherms	
S. No.	Pharmaceuticals	K_F (mg g^{-1} [L mg^{-1}] $^{1/n}$)	R
1.	IBUPROFEN	0.34	0.81
2.	ACETAMINOPHEN	0.64	0.90
3.	STREPTOMYCIN	0.99	0.86

Figure 4.45: Schematic representation of the adsorption mechanism of NFO@SiO₂@APTS nanocomposite to (a) IBF, (b) ACE, and (c) STR

4.13.5. Reusability

The regeneration capacity of the nanocomposite determines augments its potential to remove the pharmaceutical pollutant. When the nanocomposites were subjected to batch experiments and then desorption process. The adsorption potential of the reused nanocomposite against the target pharmaceuticals revealed removal efficiencies ~98% for

all the three pharmaceuticals in the first cycle. The result was observed to be similar to the removal efficiencies of the fresh nanocomposite. In the second cycle the removal efficiency reduced by only 1-2 %, and a similar trend was observed for the subsequent third and fourth cycles. By the fifth cycle however, the removal efficiency reduced to 92 %, 91 % and 93 % for IBF, ACE and STR respectively. This reduction in efficiency of the nanocomposite could be due to the consecutive usage and washing cycles. However, the HPCD grafted nanocomposites still exhibited significant potential up to ~92 % till the fifth cycle. When the NFO@SiO₂@APTS nanocomposite exhibited reusability up to 4 cycles with a good removal efficiency of ~90 %, a reduction in the removal efficiency was observed at the 5th cycle. However, the NFO@SiO₂@APTS@HPCD nanocomposites exhibited good reusability even up to 5th cycle with a removal efficiency of ~92%. Thus, the NFO@SiO₂@APTS@HPCD can be used as a potential candidate towards the removal of the pharmaceutical pollutants.

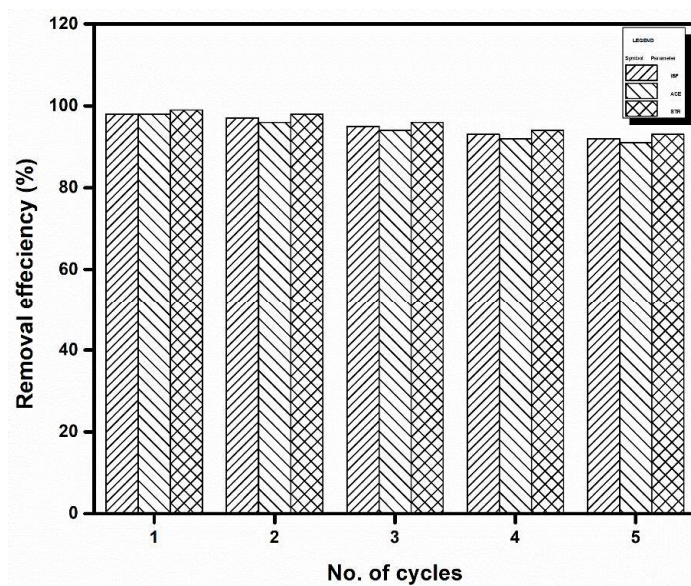


Figure 4.46. Regeneration capacity up to four cycles.

CHAPTER 5

CONCLUSION

5.1. Summary and significant findings

The nickel ferrite nanoparticles were synthesized by the coprecipitation method as it produces higher yield and requires lower temperature for the synthesis. Nickel ferrite nanoparticles were chosen for their superparamagnetic nature at the size below 20 nm. As the synthesis of the nickel ferrite nanoparticles is well established the present study has focused on the effect of the surfactant's oleic acid and octylamine. These surfactants help in maintaining the morphology and stability of the nanoparticles. The physiochemical properties of the nanoparticles were determined by the characterization studies such as XRD, FESEM, EDS, TEM, TGA, FTIR and zeta potential analysis. The optimized ratio of the surfactant responsible for narrow size distribution of the nickel ferrite nanoparticles was determined and used further experiments. These nickel ferrite nanoparticles were coated with 2 different types of silanes separately viz., 3-aminopropyltriethoxysilane and 2-glycidyloxypropyltriethoxysilane. Both the silane coatings were optimized and the stable coating of silane concentration was determined by characterization studies such as XRD, FESEM, EDS, TEM, TGA, FTIR and zeta potential analysis. The adsorption potential of these nanocomposites was analyzed against the three target pharmaceutical compounds ibuprofen, acetaminophen and streptomycin using a UV spectrophotometer at 264 nm, 244, and 195 nm for IBF, ACE, and STR, respectively. The nanocomposite was observed to follow pseudo second kinetics and showed best fit towards Langmuir isotherms. This confirmed the uniform layer adsorption of all three pharmaceuticals compounds. It was observed that the GPTS coating was only able to take IBF and was showed zero uptake towards ACE and STR which could be due to the electrostatic repulsion between the nanocomposite surface and functional groups of ACE and STR. Hence, aminosilane coating was considered for further attachment of HPCD for 2 main reasons; 1) APTS@NFO was found to be more stable in comparison to the GPTS. 2) The GPTS coating alone will not aid in the adsorption of the pharmaceuticals. Hence the surface had to be

treated further to open the ring structure of GPTS molecule. Although the process required for the opening of the glycidyl group was simple the yield obtained was lower. Further, the NFO@SiO₂@APTS-HPCD was evaluated for its stability and removal efficiency towards the target pharmaceutical compounds. The nanocomposite thus developed excellent adsorption potential towards all the three pharmaceutical compounds and good regeneration capacity up to 4 cycles.

In summary the nickel ferrite nanoparticles synthesized by co-precipitation method and further coated with aminosilane had a stable morphology and was utilized for grafting HPCD. The nanocomposites were evaluated for their removal efficiency before and after coating with HPCD. The following important conclusions were drawn from the adsorption studies of the target pharmaceutical compounds by NFO@SiO₂@APTS-HPCD:

- The NFO nanoparticles synthesized by co-precipitation was observed to have cubic spinel phase with the diffraction planes (220), (311), (400), (511), and (440) with a average crystalline size of 9.97 nm.
- The TEM analysis of the NFO nanoparticles revealed a narrow size distribution of 8-16 nm. HRTEM image of the nanoparticles reveal high crystallinity of the material and interplanar spacing, d (Å) of 0.24 nm, which is in good agreement with the $h k l$ indice of (311) plane of face-centred cubic crystal.
- The interplanar spacing calculated from the SAED pattern of the bare nickel ferrite nanoparticles contains four rings from the corresponded to their respective $h k l$ indices: 4.80 Å (220), 1.47 Å (440), 2.53 Å (311), 1.60 Å (511).
- The FTIR analysis of the NFO nanoparticles confirmed the formation nickel ferrite which was represented by the absorption bands from 400 – 600 cm⁻¹.
- The VSM analysis of NFO nanoparticles exhibited a completely a narrow hysteresis loop with $M_s = 30.01$ emu g⁻¹ and $M_r = 2.01$ emug⁻¹ and has almost negligible coercivity.

- The thermal properties of the NFO nanoparticles exhibited total weight loss 40.69 % and beyond 668 °C no weight loss was observed which indicates the formation of pure nickel ferrite.
- The NFO@GPTS-Cys nanocomposite formation showed significant increase in the peak of the planes (220), (311), (400), (511) and (440). The peak at 23.21 could be attributed to SiO₂ which further confirmed the nanocomposite formation.
- The size of the nanocomposite obtained from TEM analysis was noted contain a narrow size distribution of 130-150 nm.
- The bonding of the cysteine with NFO@SiO₂@GPTS was confirmed by the presence of bands at 1621 cm⁻¹ and 1583 cm⁻¹ emerge as a result of nucleophilic addition between the thiol and the epoxy groups.
- The TGA analysis of the NFO@SiO₂@GPTS-Cys revealed the thermal decomposition of the sample taking place at three stages. Wherein, the first two stages correspond to the thermal decomposition of solvent molecules, whereas the last decomposition occurs due to the decomposition of the residual compounds of the nanomaterial.
- The DLS analysis of the functionalized nanocomposite exhibited a hydrodynamic diameter of 313.7 nm. Zeta potential analysis exhibited to be -42.3mV at pH 6.0 which could be attributed to the presence of carboxyl group.
- The VSM analysis of the NFO@SiO₂@GPTS-Cys nanocomposite exhibits a saturation magnetisation of 8.86 emu g⁻¹, which was lower compared to the NFO@SiO₂@GPTS which was 16.02 emu g⁻¹.
- The XRD pattern of NFO@SiO₂@APTS nanocomposite had higher intensity in comparison to the NFO@SiO₂@GPTS-Cys which could be the presence of cysteine in this nanocomposite. The APTS coating did not affect the crystallinity of the nanocomposites.

- The FESEM analysis of the NFO@SiO₂@APTS was observed to have a narrow size distribution of 50-100 nm which was smaller compared to NFO@SiO₂@GPTS-Cys which was 130 to 150 nm.
- The elemental composition of NFO@SiO₂@APTS exhibit relevant peaks of Nickel, Iron, Oxygen, and Silicon in EDX spectrum; thereby confirming the formation of the nanocomposite.
- The presence of aminosilane on the nanocomposite was confirmed by FTIR analysis wherein, the presence of vibration modes at 1645 cm⁻¹, 3440 cm⁻¹ that correspond to the NH stretching and bending of the propyl groups on the surfaces of NFO@SiO₂-NH₂ nanocomposites.
- Addition of Ninhydrin solution onto NFO@SiO₂@APTS exhibits a peak at 540 nm which can be ascribed for the presence of amine groups in the nanocomposite.
- The TGA analysis of the NFO@SiO₂@APTS nanocomposite exhibited a total weight loss of 19 %.
- The VSM analysis of the NFO@SiO₂@APTS nanocomposite shows a lower saturation magnetization of 22 emu g⁻¹ which is again lower than the NFO nanoparticles.
- The adsorption efficiency for 30 mg NFO@SiO₂@GPTS-Cys was noted to be 80% for 50 mg L⁻¹ of IBF within 20 minutes. However, no adsorption of ACE and STR took place due to the electrostatic repulsion of the molecules.
- The regeneration capacity was noted to be 80 % even after three cycles of adsorption.
- The adsorption process was evaluated by the Langmuir and Freundlich isotherms and was observed to be a good fit with correlation coefficient of R²=0.98 which is closer to 1 for the Langmuir isotherm. The adsorption kinetics was observed to follow the pseudo second order model.

- The NFO@SiO₂@APTS nanocomposite (10 mg) within 15 min presented an adsorption efficiency for for 12 mg L⁻¹ of the pollutant concentration to be 97.01%, 94.12% and 70.13% for IBF, ACE and STR respectively.
- The regeneration capacity of the nanocomposite was observed to be to decrease after the third cycle.
- The sorption kinetics showed an excellent fit towards the pseudo-second-order kinetic model. Also, the sorption process was observed to be a better fit for Langmuir adsorption isotherm with a R² = 0.99 for all the three pollutants in comparison to the Freundlich isotherm which was R² =0.98. Hence the nanocomposites adsorption on the nanocomposites seemed to follow a monolayer sorption process.
- Finally, the adsorption efficiency of the NFO@SiO₂@APTS-HPCD nanocomposite reveal 10 mg of nanocomposite was sufficient for the removal of 14 mg L⁻¹ to be 98.01 %, 98.89 %, 98.3 % for IBF, ACE and STR respectively.
- The regeneration capacity of the NFO@SiO₂@APTS-HPCD nanocomposite was observed to be ~92% up to 5 cycles.
- The experimental data evaluation of the sorption process revealed a best fit for Langmuir adsorption isotherm with a R² =0.99 for all the three pollutants; thus implying to follow a monolayer sorption process. Further, the sorption kinetics was observed to follow Pseudo-second order kinetics.

In conclusion, the surfactants oleic acid and octylamine where successful in providing stable nickel ferrite nanoparticles with a narrow size distribution. The formation of nickel ferrite nanoparticles is confirmed the presence of vibration bands in FTIR analysis. The coating of the nanoparticles with two silanes viz., GPTS and APTS proved beneficial for the nanoparticles as it exhibited good removal efficiency towards pharmaceutical pollutants. However, the NFO@SiO₂@GPTS-Cys nanocomposite seemed to be very selective and was able to remove only IBF and showed sign of removal towards ACE and STR. The NFO@SiO₂@APTS on the other hand showed promising adsorption capacity towards the removal of the target pharmaceutical compounds. As NFO@SiO₂@APTS

showed better adsorption efficiency this particular nanocomposite was chosen for grafting HPCD. The HPCD grafting onto the NFO@SiO₂@APTS nanocomposite was performed to determine the influence of HPCD on the removal efficiency. It was observed that grafting HPCD onto the nanocomposite proved to be beneficial by enhancing the removal efficiency ~98 % against all the three target pollutants. The adsorption mechanism in all the three types of nanocomposites occurs mainly due to the electrostatic attraction between the nanocomposites and the target pollutants. Thus, these nanocomposites provide a new approach and present as promising candidates for water purification.

5.2.FUTURE SCOPE OF WORK

The area of nanotechnology that has evolved with highly impulse improved materials is the growing research in water remediation. In this regard, combination of the magnetic and cyclodextrin nanosystems has been explored for their applications from drug delivery to water remediation. These β -cyclodextrin based systems have shown good binding capacity towards pharmaceutical compounds; hence their employability towards removal of pharmaceutical pollutants will be highly favored. The recent insights have explored the multifunctional properties of nanoparticles by tailoring the functional groups on the surface of the nanoparticles with suitable moieties for the removal of a wide range of pollutants. This work need not be limited for the removal of a few selective pharmaceutical pollutants. The functional groups present on the surface of the nanocomposite can be selectively tuned by varying the pH of the solution thereby can be used to adsorb a wide range of pollutants.

The nanomaterial produced can be used as nanofilters by integrating the nanocomposite formed into the polymer matrix. This matrix can be used to selectively remove the pharmaceutically active pollutants by tailoring the surface functionalities. The matrix can also be used as a molecularly imprinted polymer for the removal of a wide range of pollutants serving as a multifunctional tool. The pollutants can be removed and the added advantage of the recyclability of the nanocomposite obliterates the need for a new nanomaterial for each process. This reduces the cost of the water remediation on a large scale which would serve as an added advantage for the developing countries.

REFERENCES

- Abdolmaleki, A., Mallakpour, S., and Borandeh, S. (2015). "Efficient heavy metal ion removal by triazinyl- β -cyclodextrin functionalized iron nanoparticles." *RSC Adv*, 5(110), 90602–90608.
- Adegoke, O., Takemura, K., and Park, E. Y. (2018). "Plasmonic Oleylamine-Capped Gold and Silver Nanoparticle-Assisted Synthesis of Luminescent Alloyed CdZnSeS Quantum Dots." *ACS Omega*, 3(2), 1357–1366.
- Akbar Hoseini, S., and Khademolhoseini, S. (2016). "Investigation of the structural, optical and magnetic properties of nickel ferrite nanoparticles synthesized through modified sol-gel method." *Journal of Materials Science: Materials in Electronics*, 27(6), 5943–5947.
- Allegaert, K., Mian, P., Lapillonne, A., and Anker, J. N. van den. (2019). "Maternal paracetamol intake and fetal ductus arteriosus constriction or closure: a case series analysis." *Br J Clin Pharmacol*, 85(1), 245–251.
- Alsbaiee, A., Smith, B. J., Xiao, L., Ling, Y., Helbling, D. E., and Dichtel, W. R. (2015). "Rapid removal of organic micropollutants from water by a porous β -cyclodextrin polymer." *Nature*, 529(7585), 190–194.
- Alsbaiee, A., Smith, B. J., Xiao, L., Ling, Y., Helbling, D. E., and Dichtel, W. R. (2016). "Rapid removal of organic micropollutants from water by a porous β -cyclodextrin polymer." *Nature*, 529(7585), 190–194.
- Amanulla, B., Subbu, H. K. R., and Ramaraj, S. K. (2018). "A sonochemical synthesis of cyclodextrin functionalized Au-FeNPs for colorimetric detection of Cr⁶⁺ in different industrial waste water." *Ultrason Sonochem*, 42, 747–753.
- Andal, V., and Buvanewari, G. (2014). "Removal of Lead Ions By NiFe₂O₄ Nanoparticles."
- Andreozzi, R., Caprio, V., Marotta, R., and Radovnikovic, A. (2003). "Ozonation and H₂O₂/UV treatment of clofibric acid in water: A kinetic investigation." *J Hazard Mater*, 103(3), 233–246.
- Annie Vinosha, P., Xavier, B., Ashwini, A., Ansel Mely, L., and Jerome Das, S. (2017). "Tailoring the photo-Fenton activity of nickel ferrite nanoparticles synthesized by low-temperature coprecipitation technique." *Optik (Stuttg)*, 137, 244–253.
- Arévalo-Cid, P., Isasi, J., and Martín-Hernández, F. (2018). "Comparative study of core-shell nanostructures based on amino-functionalized Fe₃O₄@SiO₂ and CoFe₂O₄@SiO₂ nanocomposites." *J Alloys Compd*, 766, 609–618.
- Argish, V., Chithra, M., Anumol, C. N., Sahu, B. N., Sahoo, S. C., Argish, V., Chithra, M., Anumol, C. N., Sahu, B. N., and Sahoo, S. C. (2015). "Magnetic studies of magnesium ferrite nanoparticles prepared by sol-gel technique." *AIP Conf Proc*, 1728(May), 020623.
- Ashjari, M., Dehfuly, S., Fatehi, D., Shabani, R., and Koruji, M. (2015). "Efficient functionalization of gold nanoparticles using cysteine conjugated protoporphyrin IX for singlet oxygen production in vitro." *RSC Adv*, 5(127), 104621–104628.
- Asokarajan, R., Benial, A. M. F., and Neyvasagam, K. (2013). "Structural , Optical And Surface Morphological Properties of Nanosized Nickel Ferrite Particles By Co-Precipitation Method." *International Journal of NanoScience and Nanotechnology*, 4(1), 113–120.

- Aswathy, B., Avadhani, G. S., Suji, S., and Sony, G. (2012). "Synthesis of β -cyclodextrin functionalized gold nanoparticles for the selective detection of Pb²⁺ ions from aqueous solution." *Front Mater Sci*, 6(2), 168–175.
- Ba, S., Jones, J. P., and Cabana, H. (2014). "Hybrid bioreactor (HBR) of hollow fiber microfilter membrane and cross-linked laccase aggregates eliminate aromatic pharmaceuticals in wastewaters." *J Hazard Mater*, 280, 662–670.
- Badrudodoza, A. Z. M., Hidajat, K., and Uddin, M. S. (2010). "Synthesis and characterization of β -cyclodextrin-conjugated magnetic nanoparticles and their uses as solid-phase artificial chaperones in refolding of carbonic anhydrase bovine." *J Colloid Interface Sci*, 346(2), 337–346.
- Badrudodoza, A. Z. M., Junwen, L., Hidajat, K., and Uddin, M. S. (2012). "Selective recognition and separation of nucleosides using carboxymethyl- β -cyclodextrin functionalized hybrid magnetic nanoparticles." *Colloids Surf B Biointerfaces*, 92, 223–231.
- Badrudodoza, A. Z. M., Shawon, Z. B. Z., Tay, W. J. D., Hidajat, K., and Uddin, M. S. (2013a). "Fe₃O₄/cyclodextrin polymer nanocomposites for selective heavy metals removal from industrial wastewater." *Carbohydr Polym*, 91(1), 322–332.
- Badrudodoza, A. Z. M., Shawon, Z. B. Z., Tay, W. J. D., Hidajat, K., and Uddin, M. S. (2013b). "Fe₃O₄/cyclodextrin polymer nanocomposites for selective heavy metals removal from industrial wastewater." *Carbohydr Polym*, 91(1), 322–332.
- Badrudodoza, A. Z. M., Tay, A. S. H., Tan, P. Y., Hidajat, K., and Uddin, M. S. (2011). "Carboxymethyl- β -cyclodextrin conjugated magnetic nanoparticles as nano-adsorbents for removal of copper ions: Synthesis and adsorption studies." *J Hazard Mater*, 185(2–3), 1177–1186.
- Bagbi, Y., Sarswat, A., Mohan, D., Pandey, A., and Solanki, P. R. (2017). "Lead and Chromium Adsorption from Water using L-Cysteine Functionalized Magnetite (Fe₃O₄) Nanoparticles." *Sci Rep*, 7(1), 1–15.
- Barczak, M. (2019). "Amine-modified mesoporous silicas: Morphology-controlled synthesis toward efficient removal of pharmaceuticals." *Microporous and Mesoporous Materials*, 278(January), 354–365.
- Behera, S. K., Oh, S. Y., and Park, H. S. (2012). "Sorption removal of ibuprofen from water using selected soil minerals and activated carbon." *International Journal of Environmental Science and Technology*, 9(1), 85–94.
- Berkowitz, A., Lahut, J., and VanBuren, C. (1980). "Properties of magnetic fluid particles." *IEEE Trans Magn*, 16(2), 184–190.
- Bhatarai, B., Muruganandham, M., and Suri, R. P. S. (2014). "Development of high efficiency silica coated β -cyclodextrin polymeric adsorbent for the removal of emerging contaminants of concern from water." *J Hazard Mater*, 273, 146–154.
- Bhosale, S. V., Ekambe, P. S., Bhoraskar, S. V., and Mathe, V. L. (2018). "Effect of surface properties of NiFe₂O₄ nanoparticles synthesized by dc thermal plasma route on antimicrobial activity." *Appl Surf Sci*, 441, 724–733.

- Blanco-Esqueda, I. G., Ortega-Zarzosa, G., Martínez, J. R., and Guerrero, A. L. (2015). "Preparation and characterization of nickel ferrite-sio₂/ag core/shell nanocomposites." *Advances in Materials Science and Engineering*, 2015.
- Bomila, R., Venkatesan, A., and Srinivasan, S. (2018). "Structural, luminescence and photocatalytic properties of pure and octylamine capped ZnO nanoparticles." *Optik (Stuttg)*, 158, 565–573.
- Bonini, M., Rossi, S., Karlsson, G., Almgren, M., Nostro, P. lo, and Baglioni, P. (2006). "Self-assembly of β -cyclodextrin in water. Part 1: Cryo-TEM and dynamic and static light scattering." *Langmuir*, 22(4), 1478–1484.
- Buschow K.H.J. (2008). *Handbook of Magnetic Materials*.
- Caldeira, E., Piskin, E., Granadeiro, L., Silva, F., and Gouveia, I. C. (2013). "Biofunctionalization of cellulosic fibres with l-cysteine: Assessment of antibacterial properties and mechanism of action against *Staphylococcus aureus* and *Klebsiella pneumoniae*." *J Biotechnol*, 168(4), 426–435.
- Čampelj, S., Makovec, D., and Drogenik, M. (2009). "Functionalization of magnetic nanoparticles with 3-aminopropyl silane." *J Magn Magn Mater*, 321(10), 1346–1350.
- Cao, H., He, J., Deng, L., and Gao, X. (2009a). "Fabrication of cyclodextrin-functionalized superparamagnetic Fe₃O₄/amino-silane core-shell nanoparticles via layer-by-layer method." *Appl Surf Sci*, 255(18), 7974–7980.
- Cao, H., He, J., Deng, L., and Gao, X. (2009b). "Fabrication of cyclodextrin-functionalized superparamagnetic Fe₃O₄/amino-silane core-shell nanoparticles via layer-by-layer method." *Appl Surf Sci*, 255(18), 7974–7980.
- Carballa, M., Omil, F., Lema, J. M., Llompart, M., García-Jares, C., Rodríguez, I., Gómez, M., and Ternes, T. (2004). "Behavior of pharmaceuticals, cosmetics and hormones in a sewage treatment plant." *Water Res*, 38(12), 2918–2926.
- Carpenter, G., Sen, R., Malviya, N., and Gupta, N. (2015). "Microwave-assisted synthesis and characterization of nickel ferrite nanoparticles." 020029, 020029.
- Celebioglu, A., and Uyar, T. (2019). "Fast Dissolving Oral Drug Delivery System Based on Electrospun Nanofibrous Webs of Cyclodextrin/Ibuprofen Inclusion Complex Nanofibers." *Mol Pharm*, 16(10), 4387–4398.
- Chang, Y., Dou, N., Liu, M., Jiang, M., Men, J., Cui, Y., Li, R., and Zhu, Y. (2020). "Efficient removal of anionic dyes from aqueous solution using CTAB and β -cyclodextrin-induced dye aggregation." *J Mol Liq*, 309.
- Chapa Gonzalez, C., Martínez Pérez, C. A., Martínez Martínez, A., Olivas Armendáriz, I., Zavala Tapia, O., Martel-Estrada, A., and García-Casillas, P. E. (2014). "Development of antibody-coated magnetite nanoparticles for biomarker immobilization." *J Nanomater*, 2014.
- Chen, B., Chen, S., Zhao, H., Liu, Y., Long, F., and Pan, X. (2019). "A versatile B-cyclodextrin and polyethyleneimine bi-functionalized magnetic nanoadsorbent for simultaneous capture of methyl orange and Pb(II) from complex wastewater." *Chemosphere*, 216, 605–616.
- Chen, D. H., and He, X. R. (2001). "Synthesis of nickel ferrite nanoparticles by sol-gel method." *Mater Res Bull*, 36(7–8), 1369–1377.

- Chen, X., Parker, S. G., Zou, G., Su, W., and Zhang, Q. (2010). "β-cyclodextrin-functionalized silver nanoparticles for the naked eye detection of aromatic isomers." *ACS Nano*, 4(11), 6387–6394.
- Cheng, J., Chang, P. R., Zheng, P., and Ma, X. (2014). "Characterization of magnetic carbon nanotube-cyclodextrin composite and its adsorption of dye." *Ind Eng Chem Res*, 53(4), 1415–1421.
- Chertok, B., David, A. E., and Yang, V. C. (2010). "Polyethyleneimine-modified iron oxide nanoparticles for brain tumor drug delivery using magnetic targeting and intra-carotid administration." *Biomaterials*, 31(24), 6317–6324.
- Chi, Y., Yuan, Q., Li, Y., Zhao, L., Li, N., Li, X., and Yan, W. (2013). "Magnetically separable Fe₃O₄@SiO₂@TiO₂-Ag microspheres with well-designed nanostructure and enhanced photocatalytic activity." *J Hazard Mater*, 262, 404–411.
- Chinnaiyan, P., Thampi, S. G., Kumar, M., and Mini, K. M. (2018). "Pharmaceutical products as emerging contaminant in water: relevance for developing nations and identification of critical compounds for Indian environment." *Environ Monit Assess*, 190(5), 288.
- Chopra, S., and Kumar, D. (2020). "Ibuprofen as an emerging organic contaminant in environment, distribution and remediation." *Heliyon*, 6(6), e04087.
- Chun, J., Seo, S. W., Jung, G. Y., and Lee, J. (2011). "Easy access to efficient magnetically recyclable separation of histidine-tagged proteins using superparamagnetic nickel ferrite nanoparticle clusters." *J Mater Chem*, 21(18), 6713–6717.
- Cooper, E. R., Siewicki, T. C., and Phillips, K. (2008). "Preliminary risk assessment database and risk ranking of pharmaceuticals in the environment." *Science of the Total Environment*, 398(1–3), 26–33.
- Cova, T. F., Murtinho, D., Aguado, R., Pais, A. A. C. C., and Valente, A. J. M. (2021). "Cyclodextrin Polymers and Cyclodextrin-Containing Polysaccharides for Water Remediation." *Polysaccharides*, 2(1), 16–38.
- Crini, G. (2008). "Kinetic and equilibrium studies on the removal of cationic dyes from aqueous solution by adsorption onto a cyclodextrin polymer." *Dyes and Pigments*, 77(2), 415–426.
- Cui, Y., Li, Y., Yang, Y., Liu, X., Lei, L., Zhou, L., and Pan, F. (2010). "Facile synthesis of amino-silane modified superparamagnetic Fe₃O₄ nanoparticles and application for lipase immobilization." *J Biotechnol*, 150(1), 171–174.
- Dabagh, S., and Dini, G. (2019). "Synthesis of Silica-Coated Silver-Cobalt Ferrite Nanoparticles for Biomedical Applications." *J Supercond Nov Magn*, 32(12), 3865–3872.
- Daniel, D., Dionísio, R., Alkimi, G. D. de, and Nunes, B. (2019). "Acute and chronic effects of paracetamol exposure on *Daphnia magna*: how oxidative effects may modulate responses at distinct levels of organization in a model species." *Environmental Science and Pollution Research*, 26(4), 3320–3329.
- David, A., and Pancharatna, K. (2009). "Effects of acetaminophen (paracetamol) in the embryonic development of zebrafish, *Danio rerio*." *Journal of Applied Toxicology*, 29(7), 597–602.

- Deblonde, T., Cossu-Leguille, C., and Hartemann, P. (2011). "Emerging pollutants in wastewater: A review of the literature." *Int J Hyg Environ Health*, 214(6), 442–448.
- Deng, W., and Thompson, D. H. (2010). "PH and cation-responsive supramolecular gels formed by cyclodextrin amines in DMSO." *Soft Matter*, 6(9), 1884–1887.
- Dhavale, R. P., Waifalkar, P. P., Sharma, A., Dhavale, R. P., Sahoo, S. C., Kollu, P., Chougale, A. D., Zahn, D. R. T., Salvan, G., Patil, P. S., and Patil, P. B. (2018a). "Monolayer grafting of aminosilane on magnetic nanoparticles: An efficient approach for targeted drug delivery system." *J Colloid Interface Sci*, 529, 415–425.
- Dhavale, R. P., Waifalkar, P. P., Sharma, A., Dhavale, R. P., Sahoo, S. C., Kollu, P., Chougale, A. D., Zahn, D. R. T., Salvan, G., Patil, P. S., and Patil, P. B. (2018b). "Monolayer grafting of aminosilane on magnetic nanoparticles: An efficient approach for targeted drug delivery system." *J Colloid Interface Sci*, 529(July), 415–425.
- Ding, T., Yang, M., Zhang, J., Yang, B., Lin, K., Li, J., and Gan, J. (2017). "Toxicity, degradation and metabolic fate of ibuprofen on freshwater diatom *Navicula* sp." *J Hazard Mater*, 330, 127–134.
- Dobrowolski, R., Oszust-Cieniuch, M., Dobrzyńska, J., and Barczak, M. (2013). "Amino-functionalized SBA-15 mesoporous silicas as sorbents of platinum (IV) ions." *Colloids Surf A Physicochem Eng Asp*, 435, 63–70.
- Domínguez-Arvizu, J. L., Jiménez-Miramontes, J. A., Salinas-Gutiérrez, J. M., Meléndez-Zaragoza, M. J., López-Ortiz, A., and Collins-Martínez, V. (2017). "Optical properties determination of NiFe₂O₄ nanoparticles and their photocatalytic evaluation towards hydrogen production." *Int J Hydrogen Energy*, 42(51), 30242–30248.
- Ebele, A. J., Abou-Elwafa Abdallah, M., and Harrad, S. (2017). "Pharmaceuticals and personal care products (PPCPs) in the freshwater aquatic environment." *Emerg Contam*, Elsevier Ltd.
- El-Kemary, M., Sobhy, S., El-Daly, S., and Abdel-Shafi, A. (2011). "Inclusion of Paracetamol into β -cyclodextrin nanocavities in solution and in the solid state." *Spectrochim Acta A Mol Biomol Spectrosc*, 79(5), 1904–1908.
- El-Maraghy, C. M., El-Borady, O. M., and El-Naem, O. A. (2020). "Effective Removal of Levofloxacin from Pharmaceutical Wastewater Using Synthesized Zinc Oxid, Graphen Oxid Nanoparticles Compared with their Combination." *Sci Rep*, 10(1), 1–13.
- Fenyvesi, É., Barkács, K., Gruiz, K., Varga, E., Kenyeres, I., Zárny, G., and Sente, L. (2020). "Removal of hazardous micropollutants from treated wastewater using cyclodextrin bead polymer – A pilot demonstration case." *J Hazard Mater*, 383.
- Figueira, P., Lopes, C. B., Daniel-da-Silva, A. L., Pereira, E., Duarte, A. C., and Trindade, T. (2011). "Removal of mercury (II) by dithiocarbamate surface functionalized magnetite particles: Application to synthetic and natural spiked waters." *Water Res*, 45(17), 5773–5784.
- Flaherty, C. M., and Dodson, S. I. (2005). "Effects of pharmaceuticals on *Daphnia* survival, growth, and reproduction." *Chemosphere*, 61(2), 200–207.
- Freitas, R., Coelho, D., Pires, A., Soares, A. M. V. M., Figueira, E., and Nunes, B. (2015). "Preliminary evaluation of *Diopatra neapolitana* regenerative capacity as a biomarker for paracetamol exposure." *Environmental Science and Pollution Research*, 22(17), 13382–13392.

- Freitas, V. A. A., Maia, L. A., Belardinelli, R. E., Ardisson, J. D., Pereira, M. C., and Oliveira, L. C. A. (2017). "Magnetic iron species highly dispersed over silica: use as catalysts for removal of pollutants in water." *Environmental Science and Pollution Research*, 24(7), 6114–6125.
- Gaber Ahmed, G. H., Badía Laíño, R., García Calzón, J. A., and Díaz García, M. E. (2014). "Magnetic nanoparticles grafted with β -cyclodextrin for solid-phase extraction of 5-hydroxy-3-indole acetic acid." *Microchimica Acta*, 181(9–10), 941–948.
- Galindo, R., Mazario, E., Gutiérrez, S., Morales, M. P., and Herrasti, P. (2012). "Electrochemical synthesis of NiFe₂O₄ nanoparticles: Characterization and their catalytic applications." *J Alloys Compd*, 536, S241–S244.
- Galus, M., Jeyaranjan, J., Smith, E., Li, H., Metcalfe, C., and Wilson, J. Y. (2013). "Chronic effects of exposure to a pharmaceutical mixture and municipal wastewater in zebrafish." *Aquatic Toxicology*, 132–133, 212–222.
- Gao, J., Chen, J., Li, X., Wang, M., Zhang, X., Tan, F., Xu, S., and Liu, J. (2015). "Azide-functionalized hollow silica nanospheres for removal of antibiotics." *J Colloid Interface Sci*, 444, 38–41.
- Ge, J., Huynh, T., Hu, Y., and Yin, Y. (2008). "Hierarchical magnetite/silica nanoassemblies as magnetically recoverable catalyst-supports." *Nano Lett*, 8(3), 931–934.
- Geissen, V., Mol, H., Klumpp, E., Umlauf, G., Nadal, M., Ploeg, M. van der, Zee, S. E. A. T. M. van de, and Ritsema, C. J. (2015). "Emerging pollutants in the environment: A challenge for water resource management." *International Soil and Water Conservation Research*, 3(1), 57–65.
- Gemeay, A. H., Keshta, B. E., El-Sharkawy, R. G., and Zaki, A. B. (2020). "Chemical insight into the adsorption of reactive wool dyes onto amine-functionalized magnetite/silica core-shell from industrial wastewaters." *Environmental Science and Pollution Research*, 27(26), 32341–32358.
- George, M., Mary John, A., Nair, S. S., Joy, P. A., and Anantharaman, M. R. (2006). "Finite size effects on the structural and magnetic properties of sol-gel synthesized NiFe₂O₄ powders." *J Magn Magn Mater*, 302(1), 190–195.
- Ghosh, S., Badruddoza, A. Z. M., Hidajat, K., and Uddin, M. S. (2013). "Adsorptive removal of emerging contaminants from water using superparamagnetic Fe₃O₄ nanoparticles bearing aminated β -cyclodextrin." *J Environ Chem Eng*, 1(3), 122–130.
- Ghosh, S., Badruddoza, A. Z. M., Uddin, M. S., and Hidajat, K. (2011). "Adsorption of chiral aromatic amino acids onto carboxymethyl- β -cyclodextrin bonded Fe₃O₄/SiO₂ core-shell nanoparticles." *J Colloid Interface Sci*, 354(2), 483–492.
- Ghutepatil, P. R., Salunkhe, A. B., Khot, V. M., and Pawar, S. H. (2019). "APTES (3-aminopropyltriethoxy silane) functionalized MnFe₂O₄ nanoparticles: a potential material for magnetic fluid hyperthermia." *Chemical Papers*, 73(9), 2189–2197.
- Giannakopoulou, T., Kompotiatis, L., Kontogeorgakos, A., and Kordas, G. (2002). *Microwave behavior of ferrites prepared via sol-gel method*. *J Magn Magn Mater*.
- Goldman, Alex. (2005). *Modern ferrite technology*. Springer.
- Gómez-Morte, T., Gómez-López, V. M., Lucas-Abellán, C., Martínez-Alcalá, I., Ayuso, M., Martínez-López, S., Montemurro, N., Pérez, S., Barceló, D., Fini, P., Cosma, P., Cerón-Carrasco, J.

- P., Fortea, M. I., Núñez-Delicado, E., and Gabaldón, J. A. (2021). "Removal and toxicity evaluation of a diverse group of drugs from water by a cyclodextrin polymer/pulsed light system." *J Hazard Mater*, 402.
- Gonzalez-Rey, M., and Bebianno, M. J. (2012). "Does non-steroidal anti-inflammatory (NSAID) ibuprofen induce antioxidant stress and endocrine disruption in mussel *Mytilus galloprovincialis*?" *Environ Toxicol Pharmacol*, 33(2), 361–371.
- Guiloski, I. C., Ribas, J. L. C., Piancini, L. D. S., Dagostim, A. C., Cirio, S. M., Fávaro, L. F., Boschen, S. L., Cestari, M. M., Cunha, C. da, and Silva de Assis, H. C. (2017). "Paracetamol causes endocrine disruption and hepatotoxicity in male fish *Rhamdia quelen* after subchronic exposure." *Environ Toxicol Pharmacol*, 53, 111–120.
- Gunjakar, J. L., More, A. M., Gurav, K. v., and Lokhande, C. D. (2008). "Chemical synthesis of spinel nickel ferrite (NiFe₂O₄) nano-sheets." *Appl Surf Sci*, 254(18), 5844–5848.
- Haro, N. K., Dávila, I. V. J., Nunes, K. G. P., Franco, M. A. E. de, Marcilio, N. R., and Féris, L. A. (2021). "Kinetic, equilibrium and thermodynamic studies of the adsorption of paracetamol in activated carbon in batch model and fixed-bed column." *Appl Water Sci*, 11(2).
- Harris, R. A., Shumbula, P. M., and Walt, H. van der. (2015). "Analysis of the interaction of surfactants oleic acid and oleylamine with iron oxide nanoparticles through molecular mechanics modeling." *Langmuir*, 31(13), 3934–3943.
- He, X., Duan, J., Wang, K., Tan, W., Lin, X., and He, C. (2004). "A novel fluorescent label based on organic dye-doped silica nanoparticles for HepG liver cancer cell recognition." *J Nanosci Nanotechnol*, 585–589.
- Heberer, T. (2002). "Tracking persistent pharmaceutical residues from municipal sewage to drinking water." *J Hydrol (Amst)*, 266(3–4), 175–189.
- Helal, A. S., Mazario, E., Mayoral, A., Decorse, P., Losno, R., Lion, C., Ammar, S., and Hémadi, M. (2018). "Highly efficient and selective extraction of uranium from aqueous solution using a magnetic device: Succinyl- β -cyclodextrin-APTES@maghemite nanoparticles." *Environ Sci Nano*, 5(1), 158–168.
- Hong, F., Yan, C., Si, Y., He, J., Yu, J., and Ding, B. (2015). "Nickel ferrite nanoparticles anchored onto silica nanofibers for designing magnetic and flexible nanofibrous membranes." *ACS Appl Mater Interfaces*, 7(36), 20200–20207.
- Hou, X., Feng, J., Liu, X., Ren, Y., Fan, Z., Wei, T., Meng, J., and Zhang, M. (2011). "Synthesis of 3D porous ferromagnetic NiFe₂O₄ and using as novel adsorbent to treat wastewater." *J Colloid Interface Sci*, 362(2), 477–485.
- Hozhabr Araghi, S., and Entezari, M. H. (2015). "Amino-functionalized silica magnetite nanoparticles for the simultaneous removal of pollutants from aqueous solution." *Appl Surf Sci*, 333, 68–77.
- Huang, P., Shi, H. Q., Xiao, H. M., Li, Y. Q., Hu, N., and Fu, S. Y. (2017). "High performance surface-modified TiO₂/silicone nanocomposite." *Nature*, 7(1), 1–7.
- Iqbal, M. A., Islam, S. S., Ghosh, K., Molla, R. A., Kamaluddin, and Islam, S. M. (2017). "Silica Functionalized Magnetic Nickel Ferrite Nanoparticles as an Efficient Recyclable Catalyst for S-Arylation in Aqueous Medium." *J Inorg Organomet Polym Mater*, 27(6), 1730–1739.

Jadhav, M. R., Utture, S. C., Banerjee, K., Oulkar, D. P., Sabale, R., and Shabeer T.p., A. (2013). "Validation of a residue analysis method for streptomycin and tetracycline and their food safety evaluation in pomegranate (punica granatum l.)." *J Agric Food Chem*, 61(36), 8491–8498.

Jahanbakhsh, Z., Hosseinzadeh, H., and Masoumi, B. (2021). "Synthesis of carboxymethyl β -cyclodextrin bonded Fe₃O₄@SiO₂-NH₂ core-shell magnetic nanocomposite adsorbent for effective removal of Pb(II) from wastewater." *J Solgel Sci Technol*, 99(1), 230–242.

Jankovský, O., Rach, V., Sedmidubský, D., Huber, Š., Ulbrich, P., Švecová, M., and Bartůněk, V. (2017). "Simple synthesis of free surface nanostructured spinel NiFe₂O₄ with a tunable particle size." *J Alloys Compd*, 723, 58–63.

Ji, K., Liu, X., Lee, S., Kang, S., Kho, Y., Giesy, J. P., and Choi, K. (2013). "Effects of non-steroidal anti-inflammatory drugs on hormones and genes of the hypothalamic-pituitary-gonad axis, and reproduction of zebrafish." *J Hazard Mater*, 254–255, 242–251.

Ji, Y., Yang, X., Ji, Z., Zhu, L., Ma, N., Chen, D., Jia, X., Tang, J., and Cao, Y. (2020). "DFT-Calculated IR Spectrum Amide I, II, and III Band Contributions of N-Methylacetamide Fine Components." *ACS Omega*, 5(15), 8572–8578.

Jiang, J., and Yang, Y. M. (2007). "Facile synthesis of nanocrystalline spinel NiFe₂O₄ via a novel soft chemistry route." *Mater Lett*, 61(21), 4276–4279.

Jiang, Y., Liu, B., Xu, J., Pan, K., Hou, H., Hu, J., and Yang, J. (2018). "Cross-linked chitosan/ β -cyclodextrin composite for selective removal of methyl orange: Adsorption performance and mechanism." *Carbohydr Polym*, 182, 106–114.

Jiao, Q., Wang, Y., Hao, L., Li, H., and Zhao, Y. (2016). "Synthesis of magnetic nickel ferrite microspheres and their microwave absorbing properties." *Chem Res Chin Univ*, 32(4), 678–681.

John Xavier, S. S., Karthikeyan, C., Gnana Kumar, G., Kim, A. R., and Yoo, D. J. (2014). "Colorimetric detection of melamine using β -cyclodextrin-functionalized silver nanoparticles." *Analytical Methods*, 6(20), 8165–8172.

Jones, L., Ronan, J., McHugh, B., McGovern, E., and Regan, F. (2015). "Emerging priority substances in the aquatic environment: A role for passive sampling in supporting WFD monitoring and compliance." *Analytical Methods*.

Joshi, S., Kumar, M., Chhoker, S., Srivastava, G., Jewariya, M., and Singh, V. N. (2014). "Structural, magnetic, dielectric and optical properties of nickel ferrite nanoparticles synthesized by co-precipitation method." *J Mol Struct*, 1076, 55–62.

Jurecska, L., Dobosy, P., Barkács, K., Fenyvesi, É., and Zárny, G. (2014). "Characterization of cyclodextrin containing nanofilters for removal of pharmaceutical residues." *J Pharm Biomed Anal*, 98, 90–93.

Kale, A., Gubbala, S., and Misra, R. D. K. (2004). "Magnetic behavior of nanocrystalline nickel ferrite synthesized by the reverse micelle technique." *J Magn Magn Mater*, 277(3), 350–358.

Kamarudin, N. H. N., Jalil, A. A., Triwahyono, S., Salleh, N. F. M., Karim, A. H., Mukti, R. R., Hameed, B. H., and Ahmad, A. (2013). "Role of 3-aminopropyltriethoxysilane in the preparation of mesoporous silica nanoparticles for ibuprofen delivery: Effect on physicochemical properties." *Microporous and Mesoporous Materials*, 180, 235–241.

- Kang, E. J., Baek, Y. M., Hahm, E., Lee, S. H., Pham, X. H., Noh, M. S., Kim, D. E., and Jun, B. H. (2019). "Functionalized β -cyclodextrin immobilized on ag-embedded silica nanoparticles as a drug carrier." *Int J Mol Sci*, 20(2).
- Karaagac, O., Atmaca, S., and Kockar, H. (2016). "A Facile Method to Synthesize Nickel Ferrite Nanoparticles: Parameter Effect." *J Supercond Nov Magn*.
- Karakaş, Z. K., Boncukcuoğlu, R., and Karakaş, İ. H. (2016). "Adsorptive properties of As(III) from aqueous solution using magnetic nickel ferrite (NiFe_2O_4) nanoparticles: Isotherm and kinetic studies." *Sep Sci Technol*, 6395(October), 1–14.
- Karim, A. H., Jalil, A. A., Triwahyono, S., Sidik, S. M., Kamarudin, N. H. N., Jusoh, R., Jusoh, N. W. C., and Hameed, B. H. (2012). "Amino modified mesostructured silica nanoparticles for efficient adsorption of methylene blue." *J Colloid Interface Sci*, 386(1), 307–314.
- Khalafi-Nezhad, A., Nourisefat, M., and Panahi, F. (2015). "l-Cysteine functionalized magnetic nanoparticles (LCMNP): a novel magnetically separable organocatalyst for one-pot synthesis of 2-amino-4H-chromene-3-carbonitriles in water." *Org Biomol Chem*, 13(28), 7772–7779.
- Khan, A. H., Aziz, H. A., Khan, N. A., Hasan, M. A., Ahmed, S., Farooqi, I. H., Dhingra, A., Vambol, V., Changani, F., Yousefi, M., Islam, S., Mozaffari, N., and Mahtab, M. S. (2018). "Impact, disease outbreak and the eco-hazards associated with pharmaceutical residues: a Critical review." *International Journal of Environmental Science and Technology*, 25(22), 21498-21524.
- Khan, A., Wang, J., Li, J., Wang, X., Chen, Z., Alsaedi, A., Hayat, T., Chen, Y., and Wang, X. (2017). "The role of graphene oxide and graphene oxide-based nanomaterials in the removal of pharmaceuticals from aqueous media: a review." *Environmental Science and Pollution Research*, 24(9), 7938–7958.
- Kharisov Boris I., Kharissova Oxana V., and Rasika Dias H. V. (2009). *Nanomaterials for environmental protection*.
- Khoso, W. A., Haleem, N., Baig, M. A., and Jamal, Y. (2021). "Synthesis, characterization and heavy metal removal efficiency of nickel ferrite nanoparticles (NFN's)." *Sci Rep*, 11(1).
- Khushboo, Sharma, P., Malik, P., and Raina, K. K. (2016). "Electro-optic, dielectric and optical studies of NiFe_2O_4 -ferroelectric liquid crystal: a soft magnetoelectric material." *Liq Cryst*, 43(11), 1671–1681.
- Kitaoka, M., and Hayashi, K. (2002). *Adsorption of Bisphenol A by Cross-Linked β -Cyclodextrin Polymer*. *J Incl Phenom Macrocycl Chem*.
- Klein, E. Y., Boeckel, T. P. Van, Martinez, E. M., Pant, S., Gandra, S., Levin, S. A., Goossens, H., and Laxminarayan, R. (2018). "Global increase and geographic convergence in antibiotic consumption between 2000 and 2015." *Proc Natl Acad Sci U S A*, 115(15), E3463–E3470.
- Klokkenburg, M., Vonk, C., Claesson, E. M., Meeldijk, J. D., Ern , B. H., and Philipse, A. P. (2004). "Direct imaging of zero-field dipolar structures in colloidal dispersions of synthetic magnetite." *J Am Chem Soc*, 126(51), 16706–16707.
- Koffeman, A. R., Valkhoff, V. E.,  elik, S., 'T Jong, G. W., Sturkenboom, M. C., Bindels, P. J. E., Lei, J. Van Der, Luijsterburg, P. A. J., and Bierma-Zeinstra, S. M. A. (2014). "High-risk use of over-the-counter non-steroidal anti-inflammatory drugs: A population-based cross-sectional study." *British Journal of General Practice*, 64(621), 191–198.

Kollarahithlu, S. C., and Balakrishnan, R. M. (2018). "Adsorption of ibuprofen using cysteine-modified silane-coated magnetic nanomaterial." *Environmental Science & Pollution Research*, 1–10.

Konuray, A. O., Fernández-Francos, X., and Ramis, X. (2017). "Analysis of the reaction mechanism of the thiol-epoxy addition initiated by nucleophilic tertiary amines." *Polym Chem*, 8(38), 5934–5947.

Kooti, M., Gharineh, S., Mehrkhan, M., Shaker, A., and Motamedi, H. (2015). "Preparation and antibacterial activity of CoFe₂O₄/SiO₂/Ag composite impregnated with streptomycin." *Chemical Engineering Journal*, 259, 34–42.

Krubicová, I., Appleton, S. L., Tannous, M., Hoti, G., Caldera, F., Pedrazzo, A. R., Cecone, C., Cavalli, R., and Trotta, F. (2020). "History of cyclodextrin nanosponges." *Polymers (Basel)*, MDPI AG.

Kruglova, A., Kråkström, M., Riska, M., Mikola, A., Rantanen, P., Vahala, R., and Kronberg, L. (2016). "Comparative study of emerging micropollutants removal by aerobic activated sludge of large laboratory-scale membrane bioreactors and sequencing batch reactors under low-temperature conditions." *Bioresour Technol*, 214, 81–88.

Kuhn, J., Aylaz, G., Sari, E., Marco, M., Yiu, H. H. P., and Duman, M. (2020). "Selective binding of antibiotics using magnetic molecular imprint polymer (MMIP) networks prepared from vinyl-functionalized magnetic nanoparticles." *J Hazard Mater*, 387.

Kumar, A., Kumar, A., Sharma, G., Al-Muhtaseb, A. H., Naushad, M., Ghfar, A. A., and Stadler, F. J. (2018). "Quaternary magnetic BiOCl/g-C₃N₄/Cu₂O/Fe₃O₄ nano-junction for visible light and solar powered degradation of sulfamethoxazole from aqueous environment." *Chemical Engineering Journal*, 334, 462–478.

Kumar, K., Gupta, S. C., Baidoo, S. K., Chander, Y., and Rosen, C. J. (2005). "Antibiotic Uptake by Plants from Soil Fertilized with Animal Manure." *J Environ Qual*, 34(6), 2082–2085.

Kumari, V., Dey, K., Giri, S., and Bhaumik, A. (2016). "Magnetic memory effect in self-assembled nickel ferrite nanoparticles having mesoscopic void spaces." *RSC Adv*, 6(51), 45701–45707.

Kunkel, U., Radke, M., Kunkel, U. W. E., and Radke, M. (2008). "Biodegradation of Acidic Pharmaceuticals in Bed Sediments : Insight from a Laboratory Experiment Biodegradation of Acidic Pharmaceuticals in Bed Sediments : Insight from a Laboratory Experiment." *Environ Sci Technol*, 42(19), 7273–7279.

Kurtan, U., Gungunes, H., Sozeri, H., and Baykal, A. (2015). "Synthesis and characterization of monodisperse NiFe₂O₄ nanoparticles." *Ceram Int*.

Lapworth, D. J., Baran, N., Stuart, M. E., and Ward, R. S. (2012). "Emerging organic contaminants in groundwater: A review of sources, fate and occurrence." *Environmental Pollution*, 163, 287–303.

Lasheras, X., Insausti, M., Gil de Muro, I., Garaio, E., Plazaola, F., Moros, M., Matteis, L. De, M. de la Fuente, J., and Lezama, L. (2016). *Chemical Synthesis and Magnetic Properties of Monodisperse Nickel Ferrite Nanoparticles for Biomedical Applications. The Journal of Physical Chemistry C*.

- Lassoued, A., Lassoued, M. S., García, S., Brahim, G., and Salah, D. (2018). "Synthesis and characterization of Ni-doped α -Fe₂O₃ nanoparticles through co-precipitation method with enhanced photocatalytic activities." *Journal of Materials Science: Materials in Electronics*, 0(0), 0.
- Levard, C., Hamdi-Alaoui, K., Baudin, I., Guillon, A., Borschneck, D., Campos, A., Bizi, M., Benoit, F., Chaneac, C., and Labille, J. (2021). "Silica-clay nanocomposites for the removal of antibiotics in the water usage cycle." *Environmental Science and Pollution Research*, 28(6), 7564–7573.
- Li, J., Hu, X., Zhou, Y., Zhang, L., Ge, Z., Wang, X., and Xu, W. (2019a). " β -Cyclodextrin-Stabilized Au Nanoparticles for the Detection of Butyl Benzyl Phthalate." *ACS Appl Nano Mater*, 2(5), 2743–2751.
- Li, L., Fan, L., Duan, H., Wang, X., and Luo, C. (2014). "Magnetically separable functionalized graphene oxide decorated with magnetic cyclodextrin as an excellent adsorbent for dye removal." *RSC Adv*, 4(70), 37114–37121.
- Li, X., Chen, A. Y., Yu, L. Y., Chen, X. X., Xiang, L., Zhao, H. M., Mo, C. H., Li, Y. W., Cai, Q. Y., Wong, M. H., and Li, H. (2019b). "Effects of B-cyclodextrin on phytoremediation of soil co-contaminated with Cd and BDE-209 by arbuscular mycorrhizal amaranth." *Chemosphere*, 220, 910–920.
- Liu, B., Zhang, B., Cui, Y., Chen, H., Gao, Z., and Tang, D. (2011). "Multifunctional gold-silica nanostructures for ultrasensitive electrochemical immunoassay of streptomycin residues." *ACS Appl Mater Interfaces*, 3(12), 4668–4676.
- Liu, G., Wang, H., Yang, X., and Li, L. (2009). "Synthesis of tri-layer hybrid microspheres with magnetic core and functional polymer shell." *Eur Polym J*, 45(7), 2023–2032.
- Liu, J. Y., Zhang, X., and Tian, B. R. (2020). "Selective modifications at the different positions of cyclodextrins: A review of strategies." *Turk J Chem*, 44(2), 261–278.
- Liu, X., Ma, Z., Xing, J., and Liu, H. (2004). "Preparation and characterization of amino-silane modified superparamagnetic silica nanospheres." *J Magn Magn Mater*, 270(1–2), 1–6.
- Liu, X., Yan, L., Yin, W., Zhou, L., Tian, G., Shi, J., Yang, Z., Xiao, D., Gu, Z., and Zhao, Y. (2014). "A magnetic graphene hybrid functionalized with beta-cyclodextrins for fast and efficient removal of organic dyes." *J Mater Chem A Mater*, 2(31), 12296–12303.
- López-Serna, R., Jurado, A., Vázquez-Suñé, E., Carrera, J., Petrović, M., and Barceló, D. (2013). "Occurrence of 95 pharmaceuticals and transformation products in urban groundwaters underlying the metropolis of Barcelona, Spain." *Environmental Pollution*, 174, 305–315.
- Lu, Y., Yao, G., Sun, K., and Huang, Q. (2014). " β -Cyclodextrin coated SiO₂@Au@Ag core-shell nanoparticles for SERS detection of PCBs." *Physical Chemistry Chemical Physics*, 17(33), 21149–21157.
- Maaz, K., Karim, S., Mumtaz, A., Hasanain, S. K., Liu, J., and Duan, J. L. (2009). "Synthesis and magnetic characterization of nickel ferrite nanoparticles prepared by co-precipitation route." *J Magn Magn Mater*, 321(12), 1838–1842.
- Mahdavi, M., Ahmad, M. Bin, Haron, M. J., Gharayebi, Y., Shamel, K., and Nadi, B. (2013). "Fabrication and Characterization of SiO₂/(3-Aminopropyl)triethoxysilane-Coated Magnetite Nanoparticles for Lead(II) Removal from Aqueous Solution." *J Inorg Organomet Polym Mater*, 23(3), 599–607.

Mahlambi, M. M., Malefetse, T. J., Mamba, B. B., and Krause, R. W. (2010). "β-Cyclodextrin-ionic liquid polyurethanes for the removal of organic pollutants and heavy metals from water: Synthesis and characterization." *Journal of Polymer Research*, 17(4), 589–600.

Mahmoodi, N. M. (2013). "Nickel ferrite nanoparticle: Synthesis, modification by surfactant and dye removal ability." *Water Air Soil Pollut*, 224(2).

Maiti, M., Sarkar, M., Xu, S., Das, S., Adak, D., and Maiti, S. (2019). "Application of silica nanoparticles to develop faujasite nanocomposite for heavy metal and carcinogenic dye degradation." *Environ Prog Sustain Energy*, 38(s1), S15–S23.

Mallard, I., Städe, L. W., Ruellan, S., Jacobsen, P. A. L., Larsen, K. L., and Fourmentin, S. (2015). "Synthesis, characterization and sorption capacities toward organic pollutants of new β-cyclodextrin modified zeolite derivatives." *Colloids Surf A Physicochem Eng Asp*, 482, 50–57.

Manzano, M., Aina, V., Areán, C. O., Balas, F., Cauda, V., Colilla, M., Delgado, M. R., and Vallet-Regí, M. (2008). "Studies on MCM-41 mesoporous silica for drug delivery: Effect of particle morphology and amine functionalization." *Chemical Engineering Journal*, 137(1), 30–37.

Marchlewicz, A., Guzik, U., and Wojcieszynska, D. (2015). "Over-the-Counter Monocyclic Non-Steroidal Anti-Inflammatory Drugs in Environment—Sources, Risks, Biodegradation." *Water Air Soil Pollut*, 226(10), 355.

Marques Fernandes, C., Ramos, P., Celta Falcão, A., and Baptista Veiga, F. J. (2003). "Hydrophilic and hydrophobic cyclodextrins in a new sustained release oral formulation of nifedipine: In vitro evaluation and bioavailability studies in rabbits." *Journal of Controlled Release*, 88(1), 127–134.

Medhat Bojnourd, F., and Pakizeh, M. (2018). "Preparation and characterization of a nanoclay/PVA/PSf nanocomposite membrane for removal of pharmaceuticals from water." *Appl Clay Sci*, 162(January), 326–338.

Mehmood, A., Saleem Ahmed Khan, F., Mujawar Mubarak, N., Hua Tan, Y., Rao Karri, R., Khalid, M., Walvekar, R., Chan Abdullah, E., Nizamuddin, S., and Ali Mazari, S. (2021). "Magnetic nanocomposites for sustainable water purification—a comprehensive review." *Environmental Science and Pollution Research*, 28, 19563–19588.

Menelaou, M., Georgoula, K., Simeonidis, K., and Dendrinou-Samara, C. (2014). "Evaluation of nickel ferrite nanoparticles coated with oleylamine by NMR relaxation measurements and magnetic hyperthermia." *Dalton Trans*, 43(9), 3626–36.

Meng, C., Zhikun, W., Qiang, L., Chunling, L., Shuangqing, S., and Songqing, H. (2018). "Preparation of amino-functionalized Fe₃O₄@mSiO₂ core-shell magnetic nanoparticles and their application for aqueous Fe³⁺ removal." *J Hazard Mater*, 341, 198–206.

Miranda, M. O., Cabral Cavalcanti, W. E., Barbosa, F. F., Antonio De Sousa, J., Ivan Da Silva, F., Pergher, S. B. C., and Braga, T. P. (2021). "Photocatalytic degradation of ibuprofen using titanium oxide: Insights into the mechanism and preferential attack of radicals." *RSC Adv*, 11(44), 27720–27733.

Mirgorod, Y. a, Borshch, N. a, Fedosyuk, V. M., and Yurkov, G. Y. (2013). "Magnetic properties of nickel ferrite nanoparticles prepared using flotation extraction." *Inorganic Materials*, 49(1), 109–114.

- Moeinpour, F., Alimoradi, A., and Kazemi, M. (2014). "Efficient removal of Eriochrome black-T from aqueous solution using NiFe₂O₄ magnetic nanoparticles." *J Environ Health Sci Eng*, 12(1), 112.
- Mohammad-Beigi, H., Yaghmaei, S., Roostaazad, R., Bardania, H., and Arpanaei, A. (2011). "Effect of pH, citrate treatment and silane-coupling agent concentration on the magnetic, structural and surface properties of functionalized silica-coated iron oxide nanocomposite particles." *Physica E Low Dimens Syst Nanostruct*, 44(3), 618–627.
- Mohapatra, S., Huang, C. H., Mukherji, S., and Padhye, L. P. (2016). "Occurrence and fate of pharmaceuticals in WWTPs in India and comparison with a similar study in the United States." *Chemosphere*, 159, 526–535.
- Mosquera, M. J., Los Santos, D. M. de, and Rivas, T. (2010). "Surfactant-synthesized ormosils with application to stone restoration." *Langmuir*, 26(9), 6737–6745.
- Moulahcene, L., Skiba, M., Senhadji, O., Milon, N., Benamor, M., and Lahiani-Skiba, M. (2015). "Inclusion and removal of pharmaceutical residues from aqueous solution using water-insoluble cyclodextrin polymers." *Chemical Engineering Research and Design*, 97, 145–158.
- Mourdikoudis, S., Menelaou, M., Fiuza-Maneiro, N., Zheng, G., Wei, S., Pérez-Juste, J., Polavarapu, L., and Sofer, Z. (2022). "Oleic acid/oleylamine ligand pair: a versatile combination in the synthesis of colloidal nanoparticles." *Nanoscale Horiz*, Royal Society of Chemistry.
- Mutiyar, P. K., Gupta, S. K., and Mittal, A. K. (2018). "Fate of pharmaceutical active compounds (PhACs) from River Yamuna, India: An ecotoxicological risk assessment approach." *Ecotoxicol Environ Saf*, 150(December 2017), 297–304.
- Nair, D. P., Podgórski, M., Chatani, S., Gong, T., Xi, W., Fenoli, C. R., and Bowman, C. N. (2014). "The Thiol-Michael addition click reaction: A powerful and widely used tool in materials chemistry." *Chemistry of Materials*, 26(1), 724–744.
- Nam, J., Kim, W. K., and Park, S. J. (2004). "Synthesis of nanocrystalline Ni ferrite as a superparamagnetic material." 1841(8), 1838–1841.
- Naseri, M. G., Saion, E. B., Ahangar, H. A., Hashim, M., and Shaari, A. H. (2011). "Simple preparation and characterization of nickel ferrite nanocrystals by a thermal treatment method." *Powder Technol*, 212(1), 80–88.
- Nasiri, S., and Alizadeh, N. (2021). "Hydroxypropyl- β -cyclodextrin-polyurethane/graphene oxide magnetic nanoconjugates as effective adsorbent for chromium and lead ions." *Carbohydr Polym*, 259.
- Nejati, K., and Zabihi, R. (2012). "Preparation and magnetic properties of nano size nickel ferrite particles using hydrothermal method." *Chem Cent J*, 6(1), 23.
- Nikolaou, A., Meric, S., and Fatta, D. (2007). "Occurrence patterns of pharmaceuticals in water and wastewater environments." *Anal Bioanal Chem*, 387(4), 1225–1234.
- Nunes, B., Antunes, S. C., Santos, J., Martins, L., and Castro, B. B. (2014). "Toxic potential of paracetamol to freshwater organisms: A headache to environmental regulators?" *Ecotoxicol Environ Saf*, 107, 178–185.

- Oliveira, A. M. D. de, Maniero, M. G., Rodrigues-Silva, C., and Guimarães, J. R. (2017). "Antimicrobial activity and acute toxicity of ozonated lomefloxacin solution." *Environmental Science and Pollution Research*, 24(7), 6252–6260.
- Ong, B. H., Chee, E. S. C., Abd Hamid, S. B. O. A., and Lim, K. P. (2012). "Synthesis and characterization of nickel ferrite magnetic nanoparticles by co-precipitation method." *AIP Conf Proc*, 1502(1), 221–229.
- Orgován, G., and Noszál, B. (2012). "NMR analysis and site-specific protonation constants of streptomycin." *J Pharm Biomed Anal*, 59(1), 78–82.
- Pape, P. G. (2011). "Adhesion Promoters: Silane Coupling Agents." *Applied Plastics Engineering Handbook*, Elsevier Inc., 503–517.
- Parashar, A., Sikarwar, S., and Jain, R. (2020). "Removal of pharmaceuticals from wastewater using magnetic iron oxide nanoparticles (IOPs)." *Int J Environ Anal Chem*, 00(00), 1–17.
- Parishani, M., Nadafan, M., Dehghani, Z., Malekfar, R., and Khorrami, G. H. H. (2017). "Optical and dielectric properties of NiFe₂O₄ nanoparticles under different synthesized temperature." *Results Phys*, 7, 3619–3623.
- Paul, S., Heng, P. W. S., and Chan, L. W. (2016). "PH-dependent complexation of hydroxypropyl-beta-cyclodextrin with chlorin e6: Effect on solubility and aggregation in relation to photodynamic efficacy." *Journal of Pharmacy and Pharmacology*, 68(4), 439–449.
- Petrie, B., Barden, R., and Kasprzyk-Hordern, B. (2015). "A review on emerging contaminants in wastewaters and the environment: Current knowledge, understudied areas and recommendations for future monitoring." *Water Res*, 72(0), 3–27.
- Pham, A. L. T., Sedlak, D. L., and Doyle, F. M. (2012). "Dissolution of mesoporous silica supports in aqueous solutions: Implications for mesoporous silica-based water treatment processes." *Appl Catal B*, 126, 258–264.
- Phan, T. N. T., Bacquet, M., Morcellet, M., and Morcellet, M. (2002). *The removal of organic pollutants from water using new silica-supported b-cyclodextrin derivatives. React Funct Polym.*
- Pindling, S., Azulai, D., Zheng, B., Dahan, D., and Perron, G. G. (2018). "Dysbiosis and early mortality in zebrafish larvae exposed to subclinical concentrations of streptomycin." *FEMS Microbiol Lett*, 365(18), 1–9.
- Pottker, W. E., Ono, R., Cobos, M. A., Hernando, A., Araujo, J. F. D. F., Bruno, A. C. O., Lourenço, S. A., Longo, E., and Porta, F. A. La. (2018). "Influence of order-disorder effects on the magnetic and optical properties of NiFe₂O₄nanoparticles." *Ceram Int*, (June).
- Qian, H., Li, J., Pan, X., Sun, Z., Ye, C., Jin, G., and Fu, Z. (2012). "Effects of streptomycin on growth of algae *Chlorella vulgaris* and *Microcystis aeruginosa*." *Environ Toxicol*, 27(4), 229–237.
- Quesada, H. B., Cusioli, L. F., O Bezerra, C. de, Baptista, A. T. A., Nishi, L., Gomes, R. G., and Bergamasco, R. (2019). "Acetaminophen adsorption using a low-cost adsorbent prepared from modified residues of *Moringa oleifera* Lam. seed husks." *Journal of Chemical Technology and Biotechnology*, 94(10), 3147–3157.
- Rabiet, M., Togola, A., Brissaud, F., Seidel, J. L., Budzinski, H., and Elbaz-Poulichet, F. (2006). "Consequences of treated water recycling as regards pharmaceuticals and drugs in surface and

ground waters of a medium-sized mediterranean catchment." *Environ Sci Technol*, 40(17), 5282–5288.

Rahman, N., and Nasir, M. (2020). "Effective removal of acetaminophen from aqueous solution using Ca (II)-doped chitosan/ β -cyclodextrin composite." *J Mol Liq*, 301.

Rajamanickam, D., and Shanthi, M. (2016). "Photocatalytic degradation of an organic pollutant by zinc oxide – solar process." *Arabian Journal of Chemistry*, 9, S1858–S1868.

Ramalingam, B., Khan, M. M. R., Mondal, B., Mandal, A. B., and Das, S. K. (2015). *Facile Synthesis of Silver Nanoparticles Decorated Magnetic-Chitosan Microsphere for Efficient Removal of Dyes and Microbial Contaminants*. *ACS Sustain Chem Eng*.

Ramimoghadam, D., Bagheri, S., and Hamid, S. B. A. (2014). "Progress in electrochemical synthesis of magnetic iron oxide nanoparticles." *J Magn Magn Mater*, Elsevier B.V.

Ranjan, B., Pillai, S., Permaul, K., and Singh, S. (2017). *A novel strategy for the efficient removal of toxic cyanate by the combinatorial use of recombinant enzymes immobilized on aminosilane modified magnetic nanoparticles Department of Biotechnology and Food Technology , Faculty of Applied Sciences , Durban U. Bioresour Technol*.

Rannug, U., Holme, J. A., Hongslo, J. K., and Srám, R. (1995). "An evaluation of the genetic toxicity of paracetamol." *Mutation Research - Fundamental and Molecular Mechanisms of Mutagenesis*, 327(1–2), 179–200.

Rawat, J., Rana, S., Srivastava, R., and Misra, R. D. K. (2007). "Antimicrobial activity of composite nanoparticles consisting of titania photocatalytic shell and nickel ferrite magnetic core." *Materials Science and Engineering C*, 27(3), 540–545.

Ren, C., Ding, X., Fu, H., Li, W., Wu, H., and Yang, H. (2017). "Core-shell superparamagnetic monodisperse nanospheres based on amino-functionalized CoFe₂O₄@SiO₂ for removal of heavy metals from aqueous solutions." *RSC Adv*, 7(12), 6911–6921.

Renard, E., Volet, G., and Amiel, C. (2005). "Synthesis of a novel linear water-soluble β -cyclodextrin polymer." *Polym Int*, 54(3), 594–599.

Repo, Z., Yin, D., Meng, Y., Jafari, S., and Sillanpää, M. (2015). *EDTA-Cross-Linked β -cyclodextrin: An 1 Environmentally Friendly Bifunctional Adsorbent 2 for Simultaneous Adsorption of Metals and Cationic 3 Dyes 4 Feiping*.

Reza, A. F. G. M., Kormoker, T., Idris, A. M., Shamsuzzoha, Md., Islam, Md. S., El-Zahhar, A. A., and Islam, Md. S. (2021). "Removal of arsenic(III) from aqueous media using amine functionalized-grafted styrene/maleic anhydride low-density polyethylene films." *Toxin Rev*, 1–8.

Robati, D. (2013). "Pseudo-second-order kinetic equations for modeling adsorption systems for removal of lead ions using multi-walled carbon nanotube." *J Nanostructure Chem*, 3(1), 55.

Rocha, L. S., Sousa, É. M. L., Gil, M. V., Oliveira, J. A. B. P., Otero, M., Esteves, V. I., and Calisto, V. (2021). "Producing magnetic nanocomposites from paper sludge for the adsorptive removal of pharmaceuticals from water—a fractional factorial design." *Nanomaterials*, 11(2), 1–20.

Rodrigues, A. R. O., Gomes, I. T., Almeida, B. G., Araújo, J. P., Castanheira, E. M. S., and Coutinho, P. J. G. (2015). "Magnetic liposomes based on nickel ferrite nanoparticles for biomedical applications." *Phys Chem Chem Phys*, 17(27), 18011–21.

- Sagadevan, S., Chowdhury, Z. Z., and Rafique, R. F. (2018). "Preparation and Characterization of Nickel ferrite Nanoparticles via Co-precipitation Method." *Materials Research*, 21(2), 1–5.
- Sahoo, B., Dutta, S., and Dhara, D. (2016). "Amine-functionalized magnetic nanoparticles as robust support for immobilization of Lipase." *Journal of Chemical Sciences*, 128(7), 1131–1140.
- Sahoo, J. K., Paikra, S. K., Baliarsingh, A., Panda, D., Rath, S., Mishra, M., and Sahoo, H. (2020). "Surface functionalization of graphene oxide using amino silane magnetic nanocomposite for Chromium (VI) removal and bacterial treatment." *Nano Express*, 1(1), 010062.
- Salavati-Niasari, M., Davar, F., and Mahmoudi, T. (2009). "A simple route to synthesize nanocrystalline nickel ferrite (NiFe₂O₄) in the presence of octanoic acid as a surfactant." *Polyhedron*, 28(8), 1455–1458.
- Sangeetha, J., and Philip, J. (2013). "Synthesis, characterization and antimicrobial property of Fe₃O₄-Cys-HNQ nanocomplex, with L-cysteine molecule as a linker." *RSC Adv*, 3(21), 8047.
- Santos, A. M., Wong, A., Prado, T. M., Fava, E. L., Fatibello-Filho, O., Sotomayor, M. D. P. T., and Moraes, F. C. (2021). "Voltammetric determination of ethinylestradiol using screen-printed electrode modified with functionalized graphene, graphene quantum dots and magnetic nanoparticles coated with molecularly imprinted polymers." *Talanta*, 224.
- Sapsford, K. E., and Ligler, F. S. (2004). "Real-time analysis of protein adsorption to a variety of thin films." *Biosens Bioelectron*, 19(9), 1045–1055.
- Schneiderman, E., and Stalcup, A. M. (2000). "Cyclodextrins: A versatile tool in separation science." *J Chromatogr B Biomed Sci Appl*, 745(1), 83–102.
- Sen, R., Jain, P., Patidar, R., Srivastava, S., Rana, R. S., and Gupta, N. (2015). "Synthesis and Characterization of Nickel Ferrite (NiFe₂O₄) Nanoparticles Prepared by Sol- Gel Method." *Mater Today Proc*, Elsevier Ltd, 3750–3757.
- Sezgin, N., Sahin, M., Yalcin, A., and Koseoglu, Y. (2013). "Synthesis, Characterization and, the Heavy Metal Removal Efficiency of MFe₂O₄ (M=Ni, Cu) Nanoparticles." *Ekoloji*, 96(November 2016), 89–96.
- Shafi, K. V. P. M., Kolytin, Y., Gedanken, A., Lendvai, J., and Felner, I. (1997). "Sonochemical Preparation of Nanosized Amorphous NiFe₂O₄ Particles." *Journal of Physical Chemistry B*, 5647(97), 6409–6414.
- Shahbazi, S., Ghasemzadeh, M. A., Shakib, P., Zolfaghari, M. R., and Bahmani, M. (2019). "Synthesis and antimicrobial study of 1,4-dihydropyrano[2,3-c]pyrazole derivatives in the presence of amino-functionalized silica-coated cobalt oxide nanostructures as catalyst." *Polyhedron*, 170, 172–179.
- Shanmugam, G., Sampath, S., Selvaraj, K. K., Larsson, D. G. J., and Ramaswamy, B. R. (2014). "Non-steroidal anti-inflammatory drugs in Indian rivers." *Environmental Science and Pollution Research*, 21(2), 921–931.
- Shen, S. C., Ng, W. K., Chia, L., Dong, Y. C., and Tan, R. B. H. (2011). "Sonochemical synthesis of (3-aminopropyl)triethoxysilane-modified monodispersed silica nanoparticles for protein immobilization." *Mater Res Bull*, 46(10), 1665–1669.

- Sheng, W., Wei, W., Li, J., Qi, X., Zuo, G., Chen, Q., Pan, X., and Dong, W. (2016). "Amine-functionalized magnetic mesoporous silica nanoparticles for DNA separation." *Appl Surf Sci*, 387, 1116–1124.
- Shi, Y., Ding, J., Liu, X., and Wang, J. (1999). "NiFe₂O₄ ultrafine particles prepared by co-precipitation / mechanical alloying." *J Magn Magn Mater*, 205, 249–254.
- Shraim, A., Diab, A., Alsuhaime, A., Niazy, E., Metwally, M., Amad, M., Sioud, S., and Dawoud, A. (2017). "Analysis of some pharmaceuticals in municipal wastewater of Almadinah Almunawarah." *Arabian Journal of Chemistry*, 10, S719–S729.
- Sikder, M. T., Mihara, Y., Islam, M. S., Saito, T., Tanaka, S., and Kurasaki, M. (2014). "Preparation and characterization of chitosan-caboxymethyl- β -cyclodextrin entrapped nanozero-valent iron composite for Cu (II) and Cr (IV) removal from wastewater." *Chemical Engineering Journal*, 236, 378–387.
- Singh, G., Diksha, Singh, A., Satija, P., Pawan, Mohit, González-Silvera, D., Espinosa-Ruíz, C., and Esteban, M. A. (2021). "Organosilanes and their magnetic nanoparticles as naked eye red emissive sensors for Ag⁺ ions and potent anti-oxidants." *New Journal of Chemistry*, 45(12), 5517–5525.
- Sinha, A., and Jana, N. R. (2015). "Separation of microcystin-LR by cyclodextrin-functionalized magnetic composite of colloidal graphene and porous silica." *ACS Appl Mater Interfaces*, 7(18), 9911–9919.
- Sinniah, S., Mohamad, S., and Manan, N. S. A. (2015). "Magnetite nanoparticles coated with β -cyclodextrin functionalized-ionic liquid: Synthesis and its preliminary investigation as a new sensing material." *Appl Surf Sci*, 357, 543–550.
- Sivakumar, P., Ramesh, R., Ramanand, A., Ponnusamy, S., and Muthamizhchelvan, C. (2011a). "Synthesis and characterization of nickel ferrite magnetic nanoparticles." *Mater Res Bull*, 46(12), 2208–2211.
- Sivakumar, P., Ramesh, R., Ramanand, A., Ponnusamy, S., and Muthamizhchelvan, C. (2011b). "Preparation and properties of nickel ferrite (NiFe₂O₄) nanoparticles via sol–gel auto-combustion method." *Mater Res Bull*, 46(12), 2204–2207.
- Sivakumar, P., Ramesh, R., Ramanand, A., Ponnusamy, S., and Muthamizhchelvan, C. (2012). "A simple wet chemical route to synthesize ferromagnetic nickel ferrite nanoparticles in the presence of oleic acid as a surfactant." *Journal of Materials Science: Materials in Electronics*, 23(5), 1041–1044.
- Smith, E. A., and Chen, W. (2008). "How to prevent the loss of surface functionality derived from aminosilanes." *Langmuir*, 24(21), 12405–12409.
- Springer, V., Pecini, E., and Avena, M. (2016). "Magnetic nickel ferrite nanoparticles for removal of dipyrone from aqueous solutions." *J Environ Chem Eng*, 4(4), 3882–3890.
- Srinivasan, B., and Huang, X. (2008). "Functionalization of magnetic nanoparticles with organic molecules: Loading level determination and evaluation of linker length effect on immobilization." *Chirality*, 20(3–4), 265–277.

- Srivastava, M., Chaubey, S., and Ojha, A. K. (2009a). "Investigation on size dependent structural and magnetic behavior of nickel ferrite nanoparticles prepared by sol-gel and hydrothermal methods." *Mater Chem Phys*, 118(1), 174–180.
- Srivastava, M., Ojha, A. K., Chaubey, S., and Materny, A. (2009b). "Synthesis and optical characterization of nanocrystalline NiFe₂O₄ structures." *J Alloys Compd*, 481(1–2), 515–519.
- S.S. Yattinahalli, S. B. Kaparkar, H. H. Ayachit, and S. N. M. (2013). "Synthesis and structural characterization of nano-sized nickel ferrite." *International Journal of Self-Propagating High-Temperature Synthesis*, 22(3), 147–150.
- Stoia, M., Barvinschi, P., Barbu-Tudoran, L., and Bunoiu, M. (2016). "Influence of polyols on the formation of nanocrystalline nickel ferrite inside silica matrices." *J Cryst Growth*.
- Streckova, M., Hadraba, H., Bures, R., Faberova, M., Roupkova, P., Kubena, I., Medvecký, L., Girman, V., Kollar, P., Fuzer, J., and Cizmar, E. (2015). "Chemical synthesis of nickel ferrite spinel designed as an insulating bilayer coating on ferromagnetic particles." *Surf Coat Technol*, 270, 66–76.
- Stuparu, M. C., and Khan, A. (2016). "Thiol-epoxy 'click' chemistry: Application in preparation and postpolymerization modification of polymers." *J Polym Sci A Polym Chem*, 54(19), 3057–3070.
- Subedi, B., Balakrishna, K., Sinha, R. K., Yamashita, N., Balasubramanian, V. G., and Kannan, K. (2015). "Mass loading and removal of pharmaceuticals and personal care products, including psychoactive and illicit drugs and artificial sweeteners, in five sewage treatment plants in India." *J Environ Chem Eng*, 3(Part 4A), 2882–2891.
- Sugimoto, M. (n.d.). *The Past, Present, and Future of Ferrites*.
- Šulek, F., Drofenik, M., Habulin, M., and Knez, Ž. (2010a). "Surface functionalization of silica-coated magnetic nanoparticles for covalent attachment of cholesterol oxidase." *J Magn Magn Mater*, 322(2), 179–185.
- Šulek, F., Drofenik, M., Habulin, M., and Knez, Ž. (2010b). "Surface functionalization of silica-coated magnetic nanoparticles for covalent attachment of cholesterol oxidase." *J Magn Magn Mater*, 322(2), 179–185.
- Sun, S., Zeng, H., Robinson, D. B., Raoux, S., Rice, P. M., Wang, S. X., and Li, G. (2004). "Monodisperse MFe₂O₄ (M = Fe, Co, Mn) Nanoparticles." *J Am Chem Soc*, 126(1), 273–279.
- Swain, S. K., Sahoo, A., Swain, S. K., Tripathy, S. K., and Phaomei, G. (2020). "Synthesis of a novel β-cyclodextrin-functionalized Fe₃O₄/BaMoO₄:Dy³⁺+magnetic luminescent hybrid nanomaterial and its application as a drug carrier." *Dalton Transactions*, 49(41), 14605–14612.
- Tahir, M. B., Iqbal, T., Hassan, A., and Ghazal, S. (2017). "Wet Chemical Co-precipitation Synthesis of Nickel Ferrite Nanoparticles and Their Characterization." *J Inorg Organomet Polym Mater*, 27(5), 1430–1438.
- Teijon, G., Candela, L., Tamoh, K., Molina-Díaz, A., and Fernández-Alba, A. R. (2010). "Occurrence of emerging contaminants, priority substances (2008/105/CE) and heavy metals in treated wastewater and groundwater at Depurbaix facility (Barcelona, Spain)." *Science of the Total Environment*, 408(17), 3584–3595.

- Tejabhram, Y., Pradeep, R., Helen, A. T., Gopalakrishnan, C., and Ramasamy, C. (2014). "Ferrous sulfate based low temperature synthesis and magnetic properties of nickel ferrite nanostructures." *Mater Res Bull*, 60(1), 778–782.
- Tiringer, U., Milošev, I., Durán, A., and Castro, Y. (2018a). "Hybrid sol–gel coatings based on GPTMS/TEOS containing colloidal SiO₂ and cerium nitrate for increasing corrosion protection of aluminium alloy 7075-T6." *J Solgel Sci Technol*, 85(3), 546–557.
- Tiringer, U., Milošev, I., Durán, A., and Castro, Y. (2018b). "Hybrid sol–gel coatings based on GPTMS/TEOS containing colloidal SiO₂ and cerium nitrate for increasing corrosion protection of aluminium alloy 7075-T6." *J Solgel Sci Technol*, 85(3), 546–557.
- Topuz, F., and Uyar, T. (2017). "Cyclodextrin-functionalized mesostructured silica nanoparticles for removal of polycyclic aromatic hydrocarbons." *J Colloid Interface Sci*, 497, 233–241.
- Vakili, M., Amouzgar, P., Wang, B., Guo, X., Mojiri, A., Zeimaran, E., and Salamatinia, B. (2019). "Ultrasound-Assisted Preparation of Chitosan/Nano-Activated Carbon Composite Beads Aminated with (3-Aminopropyl)Triethoxysilane for Adsorption of Acetaminophen from Aqueous Solutions Aqueous Solutions." *Polymers (Basel)*, 11, 1701.
- Valle, E. M. M. del. (2004). "Cyclodextrins and their uses: A review." *Process Biochemistry*.
- Varganici, C. D., Durdureanu-Angheluta, A., Rosu, D., Pinteala, M., and Simionescu, B. C. (2012). "Thermal degradation of magnetite nanoparticles with hydrophilic shell." *J Anal Appl Pyrolysis*, 96, 63–68.
- Vasudevan, R., Ramalinga Chandra Sekar, A., Sundarakannan, B., and Velkennedy, R. (2012). "A technique to dispose waste plastics in an ecofriendly way - Application in construction of flexible pavements." *Constr Build Mater*, 28(1), 311–320.
- Villa, S., Riani, P., Locardi, F., and Canepa, F. (2016). "Use of Amine (APTES) and Thiol (MPTMS) Silanes and Their Physical Characterization." *Materials*, 9(10), 826.
- Wang, J., Ren, F., Yi, R., Yan, A., Qiu, G., and Liu, X. (2009). "Solvothermal synthesis and magnetic properties of size-controlled nickel ferrite nanoparticles." *J Alloys Compd*, 479(1–2), 791–796.
- Wang, J., Yang, J., Li, X., Wei, B., Wang, D., Song, H., Zhai, H., and Li, X. (2015a). "Synthesis of Fe₃O₄@SiO₂@ZnO-Ag core-shell microspheres for the repeated photocatalytic degradation of rhodamine B under UV irradiation." *J Mol Catal A Chem*, 406, 97–105.
- Wang, J., Zheng, S., Shao, Y., Liu, J., Xu, Z., and Zhu, D. (2010). "Amino-functionalized Fe₃O₄@SiO₂ core-shell magnetic nanomaterial as a novel adsorbent for aqueous heavy metals removal." *J Colloid Interface Sci*, 349(1), 293–299.
- Wang, N., Zhou, L., Guo, J., Ye, Q., Lin, J. M., and Yuan, J. (2014). "Adsorption of environmental pollutants using magnetic hybrid nanoparticles modified with β -cyclodextrin." *Appl Surf Sci*, 305, 267–273.
- Wang, P., Wang, X., Yu, S., Zou, Y., Wang, J., Chen, Z., Alharbi, N. S., Alsaedi, A., Hayat, T., Chen, Y., and Wang, X. (2016). "Silica coated Fe₃O₄ magnetic nanospheres for high removal of organic pollutants from wastewater." *Chemical Engineering Journal*, 306, 280–288.

- Wang, S., Li, Y., Fan, X., Zhang, F., and Zhang, G. (2015b). "β-cyclodextrin functionalized graphene oxide: an efficient and recyclable adsorbent for the removal of dye pollutants." *Front Chem Sci Eng*, 9(1), 77–83.
- Wang, Z., Cui, F., Pan, Y., Hou, L., Zhang, B., Li, Y., and Zhu, L. (2019). "Hierarchically micro-mesoporous β-cyclodextrin polymers used for ultrafast removal of micropollutants from water." *Carbohydr Polym*, 213, 352–360.
- Wang, Z., Zhang, P., Hu, F., Zhao, Y., and Zhu, L. (2017). "A crosslinked β-cyclodextrin polymer used for rapid removal of a broad-spectrum of organic micropollutants from water." *Carbohydr Polym*, 177, 224–231.
- Wong, S., Lim, Y., Ngadi, N., Mat, R., Hassan, O., Inuwa, I. M., Mohamed, N. B., and Low, J. H. (2018a). "Removal of acetaminophen by activated carbon synthesized from spent tea leaves: equilibrium, kinetics and thermodynamics studies." *Powder Technol*, 338, 878–886.
- Wong, S., Lim, Y., Ngadi, N., Mat, R., Hassan, O., Inuwa, I. M., Mohamed, N. B., and Low, J. H. (2018b). "Removal of acetaminophen by activated carbon synthesized from spent tea leaves: equilibrium, kinetics and thermodynamics studies." *Powder Technol*, 338, 878–886.
- Xiao, P., Dudal, Y., Corvini, P. F. X., and Shahgaldian, P. (2011). "Polymeric cyclodextrin-based nanoparticles: Synthesis, characterization and sorption properties of three selected pharmaceutically active ingredients." *Polym Chem*, 2(1), 120–125.
- Xiao, P., Weibel, N., Dudal, Y., Corvini, P. F. X., and Shahgaldian, P. (2015). "A cyclodextrin-based polymer for sensing diclofenac in water." *J Hazard Mater*, 299, 412–416.
- Yadav, R. S., Kuřitka, I., Vilcakova, J., Havlica, J., Masilko, J., Kalina, L., Tkacz, J., Enev, V., and Hajdúchová, M. (2017). "Structural, magnetic, dielectric, and electrical properties of NiFe₂O₄ spinel ferrite nanoparticles prepared by honey-mediated sol-gel combustion." *Journal of Physics and Chemistry of Solids*, 107, 150–161.
- Yadav, S., Asthana, A., Singh, A. K., Chakraborty, R., Vidya, S. S., Susan, M. A. B. H., and Carabineiro, S. A. C. (2021). "Adsorption of cationic dyes, drugs and metal from aqueous solutions using a polymer composite of magnetic/β-cyclodextrin/activated charcoal/Na alginate: Isotherm, kinetics and regeneration studies." *J Hazard Mater*, 409.
- Yamaura, M., Camilo, R. L., Sampaio, L. C., Macêdo, M. A., Nakamura, M., and Toma, H. E. (2004). "Preparation and characterization of (3-aminopropyl)triethoxysilane-coated magnetite nanoparticles." *J Magn Magn Mater*, 279(2–3), 210–217.
- Yan, H., Li, H., Yang, H., Li, A., and Cheng, R. (2013). "Removal of various cationic dyes from aqueous solutions using a kind of fully biodegradable magnetic composite microsphere." *Chemical Engineering Journal*, 223, 402–411.
- Yattinahalli, S. S., Kapatkar, S. B., and Mathad, S. N. (2014). "Structural and Mechanical Properties of a Nano Ferrite." *Advanced Science Focus*, 2(1), 42–46.
- Yin, H., Too, H. P., and Chow, G. M. (2005). "The effects of particle size and surface coating on the cytotoxicity of nickel ferrite." *Biomaterials*, 26(29), 5818–5826.
- Yu, L., Xue, W., Cui, L., Xing, W., Cao, X., and Li, H. (2014). "Use of hydroxypropyl-β-cyclodextrin/polyethylene glycol 400, modified Fe₃O₄ nanoparticles for congo red removal." *Int J Biol Macromol*, 64, 233–239.

- Yu, Z., Chen, Q., Lv, L., Pan, Y., Zeng, G., and He, Y. (2017). "Attached β -cyclodextrin/ γ -(2,3-epoxypropoxy) propyl trimethoxysilane to graphene oxide and its application in copper removal." *Water Science and Technology*, 75(10), 2403–2411.
- Yuan, C., Liu, B., and Liu, H. (2015). "Characterization of hydroxypropyl- β -cyclodextrins with different substitution patterns via FTIR, GC-MS, and TG-DTA." *Carbohydr Polym*, 118, 36–40.
- Yuan, Q., Chi, Y., Yu, N., Zhao, Y., Yan, W., Li, X., and Dong, B. (2014). "Amino-functionalized magnetic mesoporous microspheres with good adsorption properties." *Mater Res Bull*, 49(1), 279–284.
- Zalite, I., Heidemane, G., Kodols, M., Grabis, J., and Maiorov, M. (2012). "The synthesis, characterization and sintering of nickel and cobalt ferrite nanopowders." *Medziagotyra*, 18(1), 3–7.
- Zeinali, S., Abdollahi, M., and Sabbaghi, S. (2016). "Carboxymethyl- β -cyclodextrin Modified Magnetic Nanoparticles for Effective Removal of Arsenic from Drinking Water: Synthesis and Adsorption Studies." *J. Water Environ. Nanotechnol*, 1(2), 104–115.
- Zhang, F., Sautter, K., Larsen, A. M., Findley, D. A., Davis, R. C., Samha, H., and Linford, M. R. (2010). "Chemical vapor deposition of three aminosilanes on silicon dioxide: Surface characterization, stability, effects of silane concentration, and cyanine dye adsorption." *Langmuir*, 26(18), 14648–14654.
- Zhang, L., and Jiao, W. (2015). "The effect of microstructure on the gas properties of NiFe₂O₄ sensors: Nanotube and nanoparticle." *Sens Actuators B Chem*, 216, 293–297.
- Zhang, Y., Gao, F., Wanjala, B., Li, Z., Cernigliaro, G., and Gu, Z. (2016). "High efficiency reductive degradation of a wide range of azo dyes by SiO₂-Co core-shell nanoparticles." *Appl Catal B*, 199(June), 504–513.
- Zhang, Y., Shen, S., Wang, S., Huang, J., Su, P., Wang, Q., and Zhao, B. (2014). "A dual function magnetic nanomaterial modified with lysine for removal of organic dyes from water solution." *CHEMICAL ENGINEERING JOURNAL*, 239, 250–256.
- Zhang, Y., Wang, S., Shen, S., and Zhao, B. (2013). "A novel water treatment magnetic nanomaterial for removal of anionic and cationic dyes under severe condition." *Chemical Engineering Journal*, 233, 258–264.
- Zhou, C. G., Gao, Q., Wang, S., Gong, Y. S., Xia, K. S., Han, B., Li, M., and Ling, Y. (2016a). "Remarkable performance of magnetized chitosan-decorated lignocellulose fiber towards biosorptive removal of acidic azo colorant from aqueous environment." *React Funct Polym*, 100, 97–106.
- Zhou, J., and Ritter, H. (2010). "Cyclodextrin functionalized polymers as drug delivery systems." *Polym Chem*, 1(10), 1552.
- Zhou, L., Gao, C., and Xu, W. (2010). "Magnetic dendritic materials for highly efficient adsorption of dyes and drugs." *ACS Appl Mater Interfaces*, 2(5), 1483–1491.
- Zhou, Y., Cheng, G., Chen, K., Lu, J., Lei, J., and Pu, S. (2019). "Adsorptive removal of bisphenol A, chloroxylenol, and carbamazepine from water using a novel β -cyclodextrin polymer." *Ecotoxicol Environ Saf*, 170, 278–285.

- Zhou, Y., Ping, T., Maitlo, I., and Wang, B. (2016b). "Regional selective construction of nano-Au on Fe₃O₄ @ SiO₂ @ PEI nanoparticles by photoreduction." *Nanotechnology*, 27(21), 1–9.
- Zhou, Y., Sun, L., Wang, H., Liang, W., Yang, J., Wang, L., and Shuang, S. (2016c). "Investigation on the uptake and release ability of β -cyclodextrin functionalized Fe₃O₄ magnetic nanoparticles by methylene blue." *Mater Chem Phys*, 170, 83–89.
- Zhu, Z., Li, X., Zhao, Q., Li, H., Shen, Y., and Chen, G. (2010). "Porous 'brick-like' NiFe₂O₄ nanocrystals loaded with Ag species towards effective degradation of toluene." *Chemical Engineering Journal*, 165(1), 64–70.
- Żur, J., Piński, A., Marchlewicz, A., Hupert-Kocurek, K., Wojcieszynska, D., and Guzik, U. (2018). "Organic micropollutants paracetamol and ibuprofen—toxicity, biodegradation, and genetic background of their utilization by bacteria." *Environmental Science and Pollution Research*, 25(22), 21498–21524.

LIST OF PUBLICATIONS AND CONFERENCES

Publication in Peer-Reviewed International Journals (IF-Impact Factor)

1. Adsorption of fluoroquinolones by cysteine modified silane magnetic nanocomposite from the aqueous phase. Thivani Senathiraja, Sai Abhishek Lolla, Yushmita Singh, **Smitha Chandrashekar Kollarahithlu**, Raj Mohan Balakrishnan. *International Journal of Environmental Science and Technology*. (Accepted) IF 2.86
2. Adsorption of pharmaceuticals pollutants, Ibuprofen, Acetaminophen, and Streptomycin from the Aqueous Phase using Amine Functionalized Superparamagnetic Silica Nanocomposite. **Smitha Chandrashekar Kollarahithlu**, & Raj Mohan B (2021). *Journal of Cleaner Production*, 126155. IF-11.2
3. Adsorption of ibuprofen using cysteine functionalized silane coated nanocomposites. **Smitha Chandrashekar Kollarahithlu**, Raj Mohan B (2019). *Environmental science and Pollution research*. IF-3.05

Papers Presented in Conference/Symposium but not Published

1. Seenivasaperumal Alagarsamy, **Smitha Chandrashekar Kollarahithlu**, Raj Mohan Balakrishnan. “Biosynthesis of nickel ferrite nanoparticles via an endophytic fungus *Lasiodiplodia theobromae* isolated from *Plectranthus amboinicus*”. International Conference in challenges in environmental science and engineering -2017.Kunming, China [Oral Presentation].
2. Raj Mohan Balakrishnan and **Smitha Chandrashekar Kollarahithlu**, “Triethanolamine and Oleic acid assisted synthesis of nickel ferrite nanoparticles for degradation of pollutants in aqueous systems” 5th International Symposium on Environmental Analytical Chemistry (ISEAC 5 ASIA) May 16-20, Ho Chin Min City, Vietnam [Oral Presentation].
3. **Smitha Chandrashekar Kollarahithlu**, Raj Mohan Balakrishnan, “Selenium Doped Fe₂O₃ nanocomposites for adsorption of chromium from aqueous systems” In: Rene, E.R., Balakrishnan, R.M., Kiran, M.G., Behera, R.N. and Lens, P.N.L (eds.), In: Abstract book from the 5th International Conference on Research Frontiers in Chalcogen Cycle Science & Technology, December 19-21, 2016, Goa, India [Oral Presentation].

BIO DATA

SMITHA C K

Shashanka

Urwa store, Mangalore-575006

Educational Profile

Doctor of Philosophy (2015 – Present)

Chemical Engineering | CGPA: 7.67

NITK Surathkal | Mangalore, India

Thesis title: Hydroxypropyl- β -cyclodextrin modified nickel ferrite nanocomposites for removal of pharmaceutical pollutants

• **Master of Technology** (2012 – 2014)

Nanotechnology |CGPA: 7.34

SRM University | Chennai, India

Thesis title: Samarium doped TiO_2 - SnO_2 nanocomposites.

• **Bachelor of Engineering** (2008 – 2012)

Biotechnology |Percentile: 72 %

P.A College of Engineering | Mangalore, India

Thesis title: Comparative Study of Synthesis of Silver Nanoparticles Using Different Organisms.

Professional Profile

• **Assistant Professor**

Department of Nanotechnology,

Srinivas University, Mangalore, India

Declaration:

I hereby declare that all the above given information is true and correct to best of my knowledge and belief.

DATE: 3-10-2022

(SMITHA C K)

PLACE: MANGALORE